

Doctor Dissertation

固有ひずみ理論と弾性有限要素法を用いた船体構造の溶接プロセスの改善に関する研究

**(Study on Improvement of Welding Process of Ship Grillage Structure using Elastic Finite Element Method with Inherent Strain Theory)**

September 2020

Graduate School of Engineering

Hiroshima University

**Donghan Woo**

**D184300**



## Summary

The design concept of most merchant ships and offshore structures focuses on economic and safe sailing and building them with the reduction of the overall weight by incorporating lighter and thinner steel structures, which can reduce the fuel consumption. Thus, the improvement in accuracy management of products is one of the most crucial factors for heavy building industries to meet the trend of consumers. It is practically impossible to completely constrain welding distortion; however, with the accurate estimation and effective assembly process, it could be reduced as much as possible. The main factor that causes welding distortion is local shrinkage, as illustrated in Figure 1 (longitudinal shrinkage, transverse shrinkage, and angular distortion), which is mainly caused by the rapid change in welding temperature from heating to cooling along the welding line and is also regarded as an inherent deformation. In the study, elastic Finite Element Method (FEM) using inherent strain theory was introduced to numerically validate proposed methods reducing welding displacements.

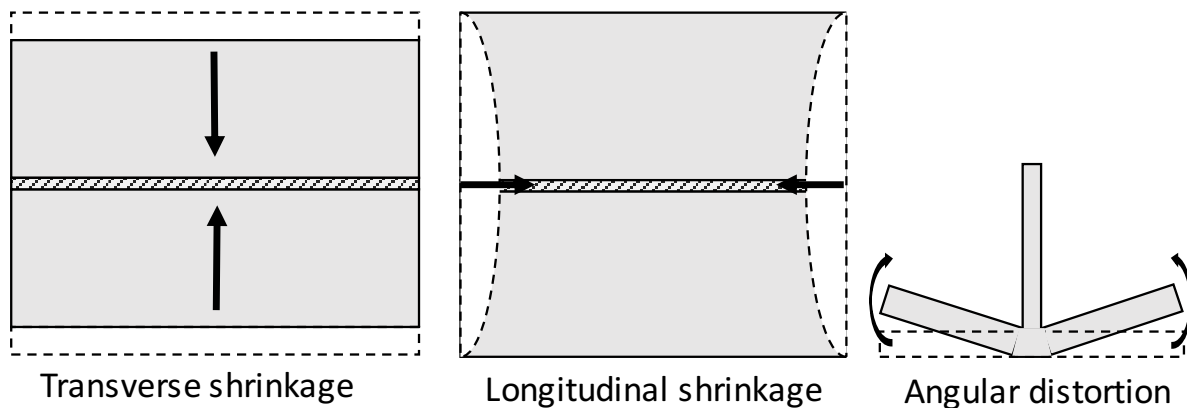


Figure 1 Classification of welding distortion

The optimization of the assembly sequence to obtain the lowest deformation for huge steel structures, such as ships and offshore structures, is crucial. The objective of the first study is to introduce an efficient method to systemically determine the optimal welding sequence for the lowest deformation of a general ship side panel, which is widely employed to design vessels and offshore structures. In this study, numerical simulation with a finite element method based on the inherent strain, interface element, and multipoint constraint function (MPC) is used as a precise computational approach to analyze the welding deformation. The employed numerical simulation obviously validated proposed systemic method to efficiently decide the optimal welding sequence for minimizing welding displacement.

Secondly, the optimal simultaneous welding to minimize welding deformation of a general ship grillage structure was studied. Most previous studies on the optimized welding sequence for the reducing welding displacements have focused on one welding line at each order. However, in heavy industries, several welders or robotic welding machines generally work together to efficiently spend work time. Herein, Inherent strain theory is introduced to calculate the complex mechanical behavior during a

welding operation using the elastic FEM. MPC and the interface element theory are employed to consider the relationship of the different welded parts. The impact of the optimal simultaneous welding in the sequence on the reduction of welding displacement is validated by using proposed numerical method in the study.

The third study validated the effect of the gravity force on numerical prediction of the optimal welding sequence of a general ship grillage structure was validated with the introduction of a new boundary condition in which the structure is placed over rails. Additionally, the direction of the gravity force of welded structures could be changed at the final assembly process according to the production plan. The effect of the gravitational orientation on the final welding displacements was also investigated herein. The elastic finite element method using the inherent strain, interface element and multipoint constraint function was introduced to analyze the welding deformation. This study validated the influence of the gravity force on the numerical prediction of welding displacements in a general ship grillage structure.

Lastly, the fourth study proposed the systematic method for positioning clamps and strongbacks based on their influence on welding displacements. To control welding displacements, mitigation methods such as clamps and strongbacks are widely used in heavy industries. It can be easily concluded that providing for as many clamps and strongbacks as feasible on welded structures to minimize welding displacements is common knowledge, but this may not always be feasible due to restrictive work environments as well as cost factors and interference from other portions of the structure. Currently there is not a distinct system to efficiently position clamps and strongbacks at welded structures. Based on understanding of how clamps and strongbacks effect on the reduction of welding displacements, a systematic method to efficiently position them will enable improvements to the welding process. In the study, several cases which have differently positioned clamps and strongbacks at welded structures were numerically simulated by the elastic FEM using inherent strain theory to investigate the influence of clamps and strongbacks on the reduction of welding distortions. According to the simulation data, the applicable systematic method for efficiently positioning clamps and strongbacks for minimizing welding deformations is proposed herein.

## List of Publication

1. Method to Systemically Order Welding Sequence to Efficiently Mitigate Welding Displacement of a General Ship Grillage Structure. Donghan Woo, Mitsuru Kitamura, Akihiro Takezawa, Journal of Ships and Offshore Structures (2019)
2. Systematic Method for Positioning Clamps and Strongbacks Based on their Influence on Welding Displacements. Donghan Woo, Mitsuru Kitamura, Akihiro Takezawa, Journal of Ocean Engineering (2020)
3. Numerical prediction of welding distortion considering gravity force on general ship grillage structure by elastic FEM using Inherent Strain. Donghan Woo, Mitsuru Kitamura , Journal of Marine Science and Engineering (2020)

# Thesis Structure

This thesis comprises seven chapters and briefly explained the description of each chapter as below.

**Chapter 1: Introduction**, this chapter explicitly explains the mechanism of welding displacements and theory of inherent strain and displacement. Additionally, the concept of the introduction of inherent strain theory to numerical simulation and additional numerical functions such as MPC and interface element method to be able to realize sequential simulations are explained in this chapter.

**Chapter 2: Literature review**, this chapter provides the previous studies regarding numerical prediction of welding displacements using inherent strain theory under various conditions.

**Chapter 3: Method to systemically order welding sequence to efficiently mitigate welding displacement of a general ship grillage structure**, this chapter provides an efficient method to systemically determine the optimal welding sequence for the lowest deformation of a general ship side panel, which is widely employed to design vessels and offshore structures. In order to validate proposed method, simulation results of various welding sequences which were assembled according to the rule of this study are compared in this chapter.

**Chapter 4: Optimal simultaneous welding to minimize welding deformation of a general ship grillage structure**, this chapter provides optimally grouping welding sequences which was proposed in the previous chapter for the optimal simultaneous welding for minimizing welding displacements.

**Chapter 5: Numerical prediction of welding distortion considering gravity force on general ship grillage structure by elastic FEM using Inherent Strain**, this chapter validates the effect of the gravity force on the numerical prediction of the optimal welding sequence of the general ship grillage structure and the effect of the gravitational orientation on the final welding displacements.

**Chapter 6: Systematic method for positioning clamps and strongbacks based on their influence on welding displacements**, this chapter provides applicable systemic method for optimally positioning clamps and strongbacks to be able to maximize their efficiency for minimizing welding displacements under restrictive work environments as well as cost factors and interference from other portions of the structure.

**Chapter 7: Conclusion and recommendation**, this chapter summarizes the new findings obtained in this thesis. Finally, the recommendation for improvement of newly proposed methods is proposed.

# Contents

Summary .....	1
List of Publication.....	3
Thesis Structure .....	4
Contents .....	5
List of Figures.....	8
List of Tables .....	11
Nomenclature.....	12
1. Introduction.....	14
1.1 Method of analysis.....	14
1.2 Concept of inherent displacement and inherent strain .....	14
1.2.1 Generation mechanism of inherent displacement .....	14
1.2.2 Calculation of inherent displacement.....	16
1.2.3 Inherent strain approach.....	17
1.2.4 Calculation of inherent strain.....	18
1.2.5 Application of inherent strain with elastic analysis .....	18
1.3 Multipoint constraint function .....	19
1.4 Interface element approach .....	21
2. Literature review .....	23
3. Method to systemically order welding sequence to efficiently mitigate welding displacement of a general ship grillage structure .....	25
3.1 Introduction.....	25
3.2 Analysis logic in the elastic FEM .....	25
3.3 Analysis model.....	26
3.4 Welding sequence cases.....	26
3.5 Results and discussion .....	29
3.5.1 Category A .....	30
3.5.2 Category B .....	33
3.5.3 Comparison between Category A and B.....	36
3.6 Conclusion .....	37
4. Optimal simultaneous welding to minimize welding deformation of a general ship grillage structure .....	38
4.1 Introduction.....	38
4.2 Analysis logic in the elastic FEM .....	38
4.3 Analysis model.....	39
4.4 Simulation scenario of simultaneous welding.....	39
4.4.1 Sequence of one by one welding lines .....	39

4.4.2 Sequence of grouped welding lines.....	39
4.5 Results and discussion .....	40
4.5.1 Process of <b>Adistance</b> at each step of the optimal welding sequence .....	40
4.5.2 Effect of the simultaneous welding process.....	41
4.6 Optimal group of the welding sequence .....	45
4.7 Discussion of the risk magnitude of welding displacement.....	47
4.8 Conclusion .....	48
5. Numerical prediction of welding distortion with considering gravity force on general ship grillage structure by elastic FEM using inherent strain.....	49
5.1 Introduction.....	49
5.2 Analysis model.....	49
5.3 Boundary condition of the rails with considering the gravity force.....	50
5.4 Effect of the gravity force under the rail boundary condition on welding sequence .....	52
5.4.1 Effect of each welding line on the bottom plate .....	52
5.4.2 Welding sequence .....	52
5.4.3 Results and discussion of effect of gravity force under the rail boundary condition on welding sequence .....	54
5.5 Effect of the change of gravity direction on the numerical prediction of welding displacements .....	58
5.5.1 Results and discussion of effect of the change of gravity direction on the numerical prediction of welding displacements.....	58
5.6 Conclusion .....	60
6. Systematic method for positioning clamps and strongbacks based on their influence on welding displacements.....	61
6.1 Introduction.....	61
6.2 Analysis logic in the elastic FEM .....	61
6.3 Analysis model.....	61
6.4 Effect of Additional Clamps and Efficient Positioning of Clamps to reduce Welding Displacements of the Square-Shaped Grillage Structure.....	63
6.4.1 Results and Discussion of the Effect of Clamping on the Square-Shaped Grillage Structure .....	64
6.5 The Effect of Strongbacks and Efficient Positioning of Strongbacks to Minimize Welding Displacements of the Square-Shaped Grillage Structure.....	69
6.5.1 Results and Discussion of the Effect of Strongbacks on the Square-Shaped Grillage Structure .....	69
6.6 The Effect of Additional Clamping along Strongbacks on the Square-Shaped Grillage Structure .....	74
6.7 Validation of Systematic Method to Efficiently Position Clamps for the reduction of Welding Displacements of the General Ship Grillage Structure under Limited Work Environment.....	74
6.7.1 Results and Discussion of the Effect of Clamping on the General Ship Grillage Structure .....	75

6.8 Validation of Systematic Method to Efficiently Position Strongbacks for the reduction of Welding Displacements of the General Ship Grillage Structure under Limited Work Environment.....	78
6.8.1 Results and Discussion of the Effect of Strongbacks on the General Ship Grillage Structure	
79	
6.9 Validation of the effect of additional clamping along strongbacks on the General Ship Grillage Structure .....	81
6.10 Conclusion .....	82
7. Conclusion and Future Works.....	84
7.1 Conclusions.....	84
7.2 Future Works .....	85
References.....	86

# List of Figures

Figure 1 Classification of welding distortion.....	1
Figure 1.1 Truss model constrained by a spring .....	14
Figure 1.2 Response history in thermal cycle .....	15
Figure 1.3 Application of inherent strain along welding line .....	17
Figure 1.4 Application of inherent strain at the welding line .....	19
Figure 1.5 Application of multipoint constraint function .....	19
Figure 1.6 MPC physical explanation (Attaching two plane plate, 500 mm x 250 mm).....	20
Figure 1.7 Concept of interface element.....	21
Figure 3.1 Analysis procedure logic by the sequence of elastic FEM .....	25
Figure 3.2 General Ship Grillage Structure (3000 mm × 2000 mm) .....	26
Figure 3.3 Measuring line for the displacement distribution .....	29
Figure 3.4 Category A z-axis distance average.....	30
Figure 3.5 Z-axis displacement distribution of Line 1 .....	31
Figure 3.6 Z-axis displacement distribution of Line 2.....	31
Figure 3.7 Z-axis displacement distribution of Line 3 .....	31
Figure 3.8 Z-axis displacement distribution of Line 4.....	32
Figure 3.9 Z-axis displacement of Category A-2.....	32
Figure 3.10 Z-axis displacement of Category A-8.....	32
Figure 3.11 Category B z-axis distance average.....	33
Figure 3.12 Distribution of z-axis displacement of Line 1 of Category B-6, B-10 and B-12.....	34
Figure 3.13 Distribution of z-axis displacement of Line 2 of Category B-6, B-10 and B-12.....	34
Figure 3.14 Distribution of z-axis displacement of Line 3 of Category B-6, B-10 and B-12.....	34
Figure 3.15 Distribution of z-axis displacement of Line 2 of Category B-6, B-10 and B-12.....	35
Figure 3.16 Z-axis displacement of Category B-6.....	35
Figure 3.17 Z-axis displacement of Category B-10.....	35
Figure 3.18 Z-axis displacement of Category B-12 .....	36
Figure 3.19 Comparing results of z-axis displacement of Category A-8 and Category B-10 .....	36
Figure 4.1 Analysis procedure logic by the sequence of elastic FEM .....	38
Figure 4.2 Progress of <i>Adistance</i> at each step of the welding sequence .....	41
Figure 4.3 <i>Adistance</i> of the simultaneous welding process by the different number of welders.....	42

Figure 4.4 Maximum z-axis displacement of the simultaneous welding process by the different number of welders.....	42
Figure 4.5 z-axis displacement of Cases 1, 10, 20 and 29 .....	43
Figure 4.6 Measuring lines for the displacement distribution.....	43
Figure 4.7 z-axis displacement distribution curve along Line T (Cases 1, 10, 20 and 29) .....	44
Figure 4.8 z-axis displacement distribution curve along Line L (Cases 1, 10, 20 and 29) .....	44
Figure 4.9 z-axis displacement distribution curve along Line T (Case 10, and Optimal group) .....	46
Figure 4.10 z-axis displacement distribution curve along Line L (Case 10, and Optimal group) .....	46
Figure 4.11 Magnitude of the stress with welding displacement.....	47
Figure 5.1 Change of the effect of the gravitational orientation on welded structures .....	49
Figure 5.2 Effect of gravity force on the bottom plate under the simple boundary condition .....	50
Figure 5.3 Welding work environment in heavy industries .....	51
Figure 5.4 Effect of gravity on the bottom plate under the rail boundary condition .....	51
Figure 5.5 Total gap between the welding lines and plate, after welding each line.....	52
Figure 5.6 Measuring lines for the z-axis displacement distribution .....	55
Figure 5.7 <i>Adistance</i> of Category A under two different boundary condition .....	56
Figure 5.8 <i>Adistance</i> of Category B under two different boundary condition.....	56
Figure 5.9 Z-axis displacement distribution along line T of Sequence B-10 in three different boundary conditions.....	57
Figure 5.10 Z-axis displacement distribution along line L of Sequence B-10 in three different boundary conditions.....	57
Figure 5.11 Welding work process of a hatch cover.....	58
Figure 5.12 <i>Adistance</i> with the change of the gravitational orientation .....	59
Figure 5.13 Z-axis displacement of Rail boundary condition + Gravitational orientation .....	59
Figure 6. 1 Square Shape Grillage Structure (400 mm × 400 mm) .....	62
Figure 6.2 General Ship Grillage Structure (3000 mm × 2000 mm) .....	62
Figure 6.3 Z-axis displacement of the bottom plate of Case A-1 .....	63
Figure 6.4 Additional clamping cases (Square shape grillage structure 400 mm × 400 mm) .....	64
Figure 6.5 Measuring line for the displacement distribution of the square-shaped grillage structure ..	64
Figure 6.6 <i>Zaverage</i> of Cases A-1, A-2, A-3 and A-4.....	65
Figure 6.7 Z-axis displacement of the bottom plate of Case A-1, A-2, A-3 and A-4 .....	65
Figure 6.8 Z-axis displacement distribution of ST.....	66
Figure 6.9 Z-axis displacement distribution of SL.....	66

Figure 6.10 Displacement reduction efficiency of comp position with respect to displacement measured line .....	67
Figure 6.11 Z-axis displacement distribution of TS.....	68
Figure 6.12 Z-axis displacement distribution of LS.....	68
Figure 6.13 Systematic method to optimally position clamps under limited work environment .....	68
Figure 6.14 Lines positioning strongbacks of the square shaped grillage structure .....	69
Figure 6.15 Positions of strongbacks and z-axis displacement curves of SL in Cases B-1, B-2 and B-3 .....	70
Figure 6.16 <i>Zaverage</i> of the square-shaped grillage structure with differently positioned strongbacks .....	71
Figure 6.17 Effect of strongback on z-axis displacement curves in Case B-2 and B-3 .....	71
Figure 6.18 Angle of each section (40 ~ 140 mm) of the displacement distribution curve without strongbacks .....	72
Figure 6.19 <i>Zaverage</i> for the square shape grillage structure obtained for each of the five strongbacks positions based on the angle of the displacement curve .....	72
Figure 6.20 Position of strongbacks and z-axis displacement curve of ST in Case B-4.....	73
Figure 6.21 Systematic method to optimally position strongbacks under limited work environment..	73
Figure 6.22 Combining clamps and strongbacks in Case B-3+ and <i>Zaverage</i> .....	74
Figure 6.23 Z-axis displacement of the bottom plate of Case C-1.....	75
Figure 6.24 Additional clamping cases (General ship grillage structure 3000 mm × 2000 mm) .....	75
Figure 6.25 Measuring line for the displacement distribution of the general ship grillage structure GT and GL1 .....	76
Figure 6.26 <i>Zaverage</i> of the general ship grillage structures.....	77
Figure 6.27 Z-axis displacement of the bottom plate of Case C-2 and C-3 .....	77
Figure 6.28 Z-axis displacement distribution of GT.....	77
Figure 6.29 Z-axis displacement distribution of GL1 .....	78
Figure 6.30 Lines positioning strongbacks of the general ship grillage structure.....	79
Figure 6.31 Strongbacks positioning in Cases D-1 and D-2.....	79
Figure 6.32 Measuring line for the displacement distribution of the general ship grillage structure GT and GL2 .....	80
Figure 6.33 <i>Zaverage</i> of the general ship grillage structures with differently positioned strongbacks .....	80
Figure 6.34 Positions of strongbacks and z-axis displacement curve of Cases D-1 and D-2 along GT	81
Figure 6.35 Positions of strongbacks and z-axis displacement curve of Cases D-1 and D-2 along GL2 .....	81
Figure 6.36 Combining clamps and strongback and z-axis displacement curves of Case D-2+ along GL2 .....	82

## List of Tables

Table 1.1 Arc butt welding Conditions .....	16
Table 1.2 Mechanical property of HT50 steel .....	17
Table 3.1 Total gap between the welding lines and plate, after welding each line .....	27
Table 3.2 Welding sequences.....	27
Table 4.1 Optimized sequence of one by one welding lines.....	39
Table 4.2 Result of each step of Case 19 and Case 20 for simultaneous welding processes .....	45
Table 4.3 Result of each step of optimally grouped simultaneous welding processes .....	46
Table 5. 1 Welding sequences of Category A.....	52
Table 5. 2 Welding sequences of Category B.....	53

## Nomenclature

<b>Abbreviation</b>	
FEM	Finite element method
FE	Finite element
MPC	Multipoint constraint function
HT	High strength steel
<b>Symbols</b>	
$Z_{average}$	Z-axis displacement average (mm)
$A_{distance}$	Z-axis distance average (mm)
$a$	Area of cross-section of the truss
$b$	Width of the element along the welding line [mm]
$b_p$	Width of the plate [mm]
$c$	Specific heat [J/kg/K]
$C_t(L)$	Welding length compensation coefficient for lateral shrinkage
$C_a(L)$	Welding length compensation coefficient for angular deformation
$E$	Young's modulus [MPa]
$F_T$	Contraction force [N]
$h$	Plate thickness [mm]
$k^*$	Rigidity of the spring
$L$	Welding length [mm]
$n$	Total number of nodes of a bottom plate
$Q^*$	Heat input [J/mm <sup>3</sup> ]
$Q_{net}$	Net heat input [J/mm]
$S$	Transverse shrinkage [mm]
$S_0$	Transverse shrinkage at a welding length of 200 mm [mm]
$\nu$	Poisson's ratio
$z_k$	Z-axis displacement of a node of a bottom plate [mm]
$\alpha$	Linear expansion coefficient [1/K]
$\alpha_L$	coefficient that express the magnitude level of the initial deflection
$\sigma$	linear expansion coefficient
$\sigma_Y$	Yield stress [MPa]

$\beta$	Plate slenderness parameter
$\rho$	Density [kg/mm <sup>3</sup> ]
$\theta$	Angular deformation
$\theta_0$	Angular deformation at a welding length of 200 mm [mm]
$\varepsilon^{total}$	Total strain
$\varepsilon^{elastic}$	Elastic strain
$\varepsilon^{thermal}$	Thermal strain
$\varepsilon^{plastic}$	Plastic strain
$\varepsilon^{creep}$	Creep strain
$\varepsilon^{phase}$	Phase transformation
$\varepsilon^* = \varepsilon^{inherent}$	Inherent strain
$\varepsilon_l^*$	Inherent strain of longitudinal shrinkage
$\varepsilon_t^*$	Inherent strain of transverse shrinkage
$\varepsilon_a^*$	Inherent strain of angular distortion

# 1. Introduction

## 1.1 Method of analysis

The thermal elastic plastic method is a useful method to precisely analyze the welding distortion for a small and simple structure. However, its disadvantage is that analyses of large and complex structures require considerable calculation effort (Ueda et al., 1993). To reduce significant calculation time and be able to realize the sequence based analysis, in-house developed code which based on elastic FEM with the application of inherent strains is employed. Additionally, MPC and interface element are assigned along welding line to consider the effect of gap and misalignment in the welding sequence.

## 1.2 Concept of inherent displacement and inherent strain

### 1.2.1 Generation mechanism of inherent displacement

In the welding operation, the thermal expansion of the welding line is restrained by the low temperature part of a structure where the rigidity is high. Inherent strain does not directly appear with the thermal source. In other words, plastic strain occurs following the disappearance of the thermal strain along with the cooling process, and it mainly causes residual stress and welding deformation (Ueda et al., 2012). A simple example of this theory is the model of a truss constrained by a spring, as shown in Figure 1.1.

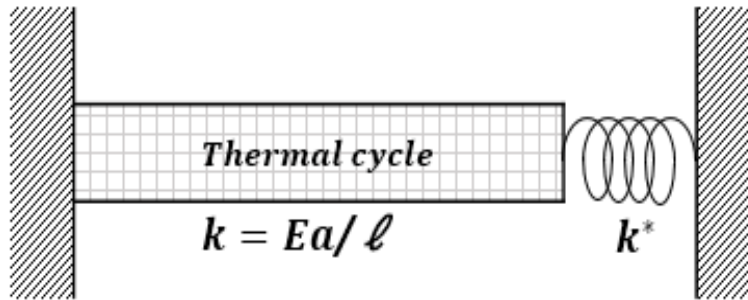


Figure 1.1 Truss model constrained by a spring

The simple truss can be defined by the following equations:

$$\beta = \frac{k^*}{k+k^*} : \text{Constraint parameter indicating relative strength of the spring}$$

$$k = \frac{Ea}{l} : \text{Rigidity of the truss}$$

The following equation represents the actual stress of the bar with the restraint of the spring under elastic behaviour.

$$\sigma = -\beta\alpha TE$$

When  $\sigma_Y$  is the yield stress of the material, the maximum thermal stress in the heating process is the compressive stress of the yield stress. The overheat temperature can be defined as  $T_1$  as given below:

$$T_1 = \frac{\sigma_Y}{\beta\alpha E} \quad (1.1)$$

At the cooling stage, the stress reaches the yield stress. This process leads to the displacement of the truss model; thus, it pulls the spring.

The heating temperature can be defined as

$$T_2 = 2T_1 \quad (1.2)$$

The behavior of the truss at  $T_2$  can be described by the temperature from the standpoint of plastic deformation, as shown in Figure 1.2.

$$1) T_{max} < T_1$$

In the O-A-O cycle, when the maximum temperature is less than  $T_1$ , the thermal response at the end of the heating process is lower than the yield stress. Thus, there is no plastic deformation.

$$2) T_1 < T_{max} < T_2$$

In the O-B-C-D cycle, when the maximum temperature reaches the middle of  $T_1$  and  $T_2$ , the thermal stress reaches the yield stress, leading to plastic deformation. However, the cooling process does not reach the yield stress. This implies the elastic process and thus, cannot cause plastic deformation.

$$2) T_2 < T_{max}$$

In the O-B-G-H-F cycle, the heating and cooling processes reach the yield stress. Hence, both the processes produce plastic deformation.

According to the above theory, the two main causes of inherent strain are the maximum temperature of heating and strength of the constraint.

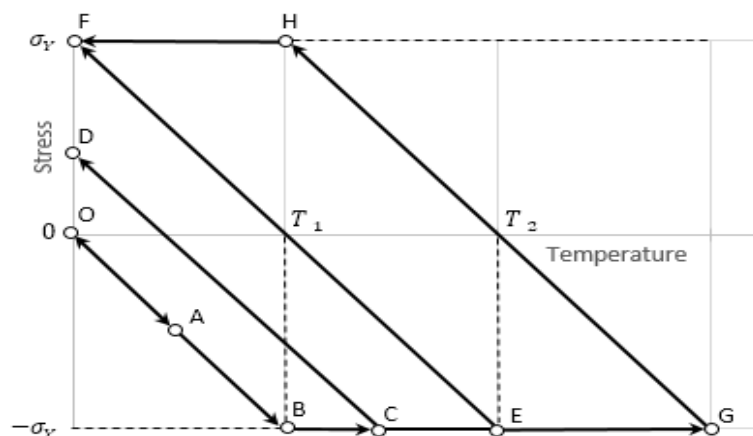


Figure 1.2 Response history in thermal cycle

## 1.2.2 Calculation of inherent displacement

(Japan Shipbuilding Research Association, 2000) used arc butt welding as Table 1.1 to experimentally measure welding displacement of the simple plane structure (200 mm × 200 mm × 10 mm) using HT50 steel as Table 1.2. Based on measured database, equations as Eqs. 1.3-1.5 were derived to be able to calculate inherent displacements such as transverse shrinkage  $S$ , longitudinal shrinkage  $F_T$  and angular distortion  $\theta$  as Figure 1. According to the amount of the heat input  $Q^*$  the magnitude of welding displacement is decided in these equations. (Kunihiko et al., 1976) demonstrated that the amount of the net heat  $Q_{net}$  in the welding process is related with the thickness  $h$  of the welded steel plate as  $Q^* = Q_{net}/h^2$ . In terms of determining the resulting stress field by conventional elastic analysis, the longitudinal shrinkage is derived as the tendon force  $F_T$  (White et al., 1980).

1) Transverse shrinkage

$$S = C_t(L)S_0 \quad (1.3)$$

$$S_0 = \begin{cases} 1.16 \times 10^{-3} Q_{net}/h & (Q^* \leq 6.27) \\ h\{1.44 \times 10^{-4}[(Q^*)^2 - Q^*] + 2.5 \times 10^{-3}\} & (6.27 < Q^* \leq 20) \\ 2.85 \times 10^{-3} Q_{net}/h & (20 < Q^*) \end{cases}$$

$$C_t(L) = [4\tan^{-1}(L/200) + (L/100) \times \log(1 + 40000/L^2)]/3.74$$

2) Angular deformation

$$\theta = C_a(L)\theta_0 \quad (1.4)$$

$$\theta_0 = \begin{cases} 1.44 \times 10^{-3} Q^* & (Q^* \leq 6.27) \\ 1.06 \times 10^{-1} Q^*/\{(Q^* - 6.16)^2 + 73.6\} & (6.27 < Q^*) \end{cases}$$

$$C_a(L) = [8\tan^{-1}(L/120) + (1 + \nu)(L/60) \times \log(1 + 14400/L^2)]/8.84$$

3) Longitudinal shrinkage (contraction force)

$$F_T = 0.2Q_{net} \quad (1.5)$$

Table 1.1 Arc butt welding Conditions

Current [A]	Voltage [V]	Travel speed [mm/s]	Heat efficiency	Net heat [J/mm <sup>2</sup> ]
230	23	5	0.77	500

Table 1.2 Mechanical property of HT50 steel

Density [kg/m <sup>3</sup> ]	Young's Modulus [MPa]	Specific heat [J/kg/°C]	Yield stress [MPa]	Poisson's ratio
7720	$2.0 \times 10^5$	659.4	440	0.3

### 1.2.3 Inherent strain approach

Based on thermal elastic-plastic FEM and experimental observation, Ueda et al. (1993) pointed out that the inherent strain  $\varepsilon^{inherent}$  causes welding distortions and residual stress along welding line. During the heating and cooling cycle of welding process, the component of the total strain  $\varepsilon^{total}$  is given as Eq. 1.6. When the welding heat finally disappears, the inherent strain is the sum of inelastic strain components as Eq. 1.7. In particular, the plastic strain  $\varepsilon^{plastic}$  is the representative of the inherent strain because the creep strain  $\varepsilon^{creep}$  and the phase transformation  $\varepsilon^{phase}$  are negligibly small (Murakawa et al., 2012). As Figure 1.3, the inherent strain produces welding deformations which are clarified into transverse shrinkage  $S$ , angular distortion  $\theta$  and longitudinal shrinkage which results in a contraction force  $F_t$  that can be used in elastic simulation to improve results. The inherent strain could be considered as existing in a limited portion near the welding line, thus inherent strain is constantly applied to limited elements which are positioned along welding lines (Murakawa et al., 2012).

$$\varepsilon^{total} = \varepsilon^{elastic} + \varepsilon^{thermal} + \varepsilon^{plastic} + \varepsilon^{creep} + \varepsilon^{phase} \quad (1.6)$$

$$\varepsilon^* = \varepsilon^{inherent} = \varepsilon^{total} - \varepsilon^{elastic} = \varepsilon^{thermal} + \varepsilon^{plastic} + \varepsilon^{creep} + \varepsilon^{phase} \quad (1.7)$$

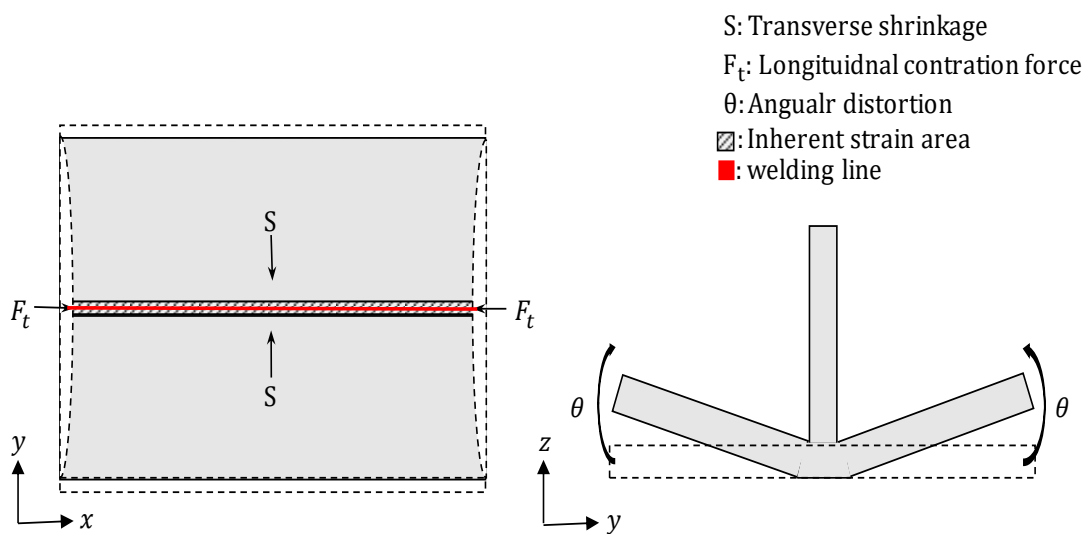


Figure 1.3 Application of inherent strain along welding line

## 1.2.4 Calculation of inherent strain

Strain remains uniformly distributed toward the surface and out-of-plane deformation (Ueda et al., 1993). Bending strain is linearly distributed against the direction of thickness to be formed. Regarding the width of the element that produced the equivalent inherent strain, the width of the deformation source is caused by the welding process. It is desirable to establish the correlation here. If the maximum temperature is  $T = \sigma_Y/E\alpha$  ( $\alpha$ : linear expansion coefficient) and the heat source is approximated to the instantaneous line heat source, the width  $b$  is defined as Eq 1.8, (Kenichi et al., 1997).

$$b = \sqrt{0.117(\alpha/c\rho)(E/\sigma_Y)Q_{net}} \quad (1.8)$$

### 1. Inherent strain of longitudinal shrinkage

When the element width is  $b$ , inherent strain of the longitudinal shrinkage can be defined as Eq 1.9.

$$\varepsilon_l^* = 0.5(F_T/(Ehb)) \quad (1.9)$$

### 2. Inherent strain of transverse shrinkage

To simply analyze the inherent strain, assume the width distribution of strain has uniform value

$$\varepsilon_t^* = 0.5(S/b) \quad (1.10)$$

### 3. Inherent strain of angular deformation

Angular deformation is defined as the bending stress to elements that the inherent strain is applied. The progress of the angular deformation changes the inherent strain

$$\varepsilon_a^* = -hk \quad (1.11)$$

$k$  is the curvature of the deformation.

$$k = \theta/b \quad (1.12)$$

## 1.2.5 Application of inherent strain with elastic analysis

In the case of welding, the source of welding residual stress (inherent strain) is considered to be produced only in a limited portion near the welding line (Murakawa et al., 2012). The inherent transverse shrinkage and angular distortion under constraint and after the release of the constraint are almost identical because the plastic strain produced in welding thermal cycles becomes stable at lower temperature (Ma and Huang, 2017). Therefore, a constant inherent strain obtained from non-constraint weldment is applicable in the constraint condition of a similar type of steel and welding.

The inherent strain calculated by Eqs (1.9–1.11) is applied along both sides of the welding line, and it leads to an inherent deformation, such as longitudinal shrinkage, transverse shrinkage, and angular

deformation at the assigned area. During this simulation, because inherent strain is applied, it is important to point out the uniform distribution of thermal history and deformation, except at both ends of the welding line, as shown in Figure 1.4. In terms of the simulation of the welding sequence, the influence of thermal history of the first welding process that is proximate or intersect the second welding line is not considered.

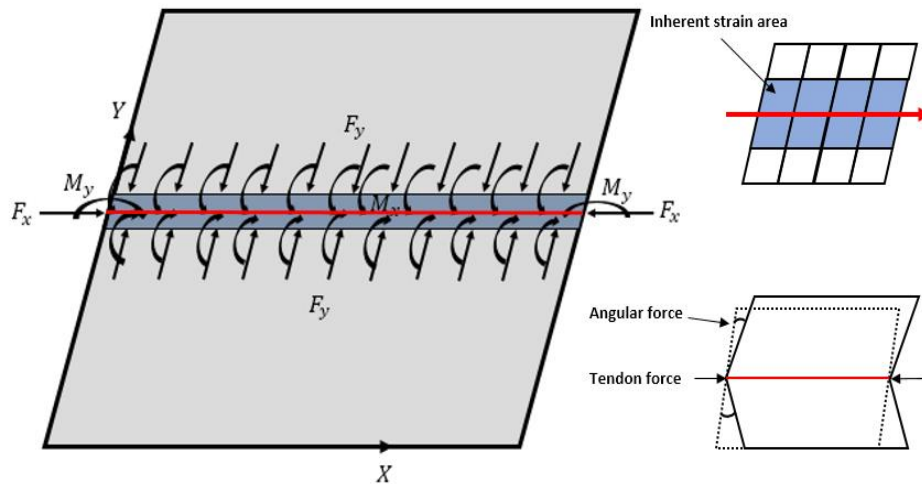


Figure 1.4 Application of inherent strain at the welding line

### 1.3 Multipoint constraint function

A strategy for the definition of the relationship of the different welded parts is based on the application of multipoint constraint function (MPC) along the welding lines. MPC is an advanced method for combined FEM analysis to connect different nodes and degrees of freedom. In Figure 1.5, Nodes 1 and 2 are originally positioned at two different elements. By using MPC, these two nodes are connected to each other, and can be defined as attached elements. MPC can change the state of one node to work as a master or slave.

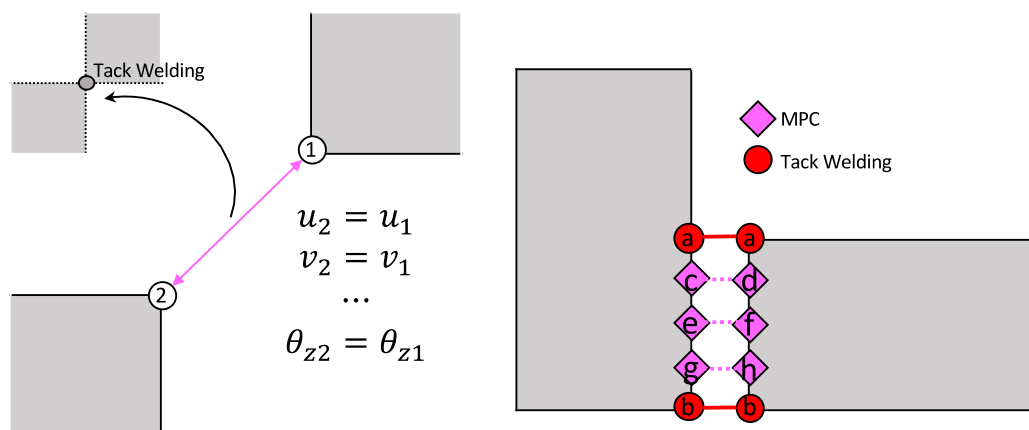
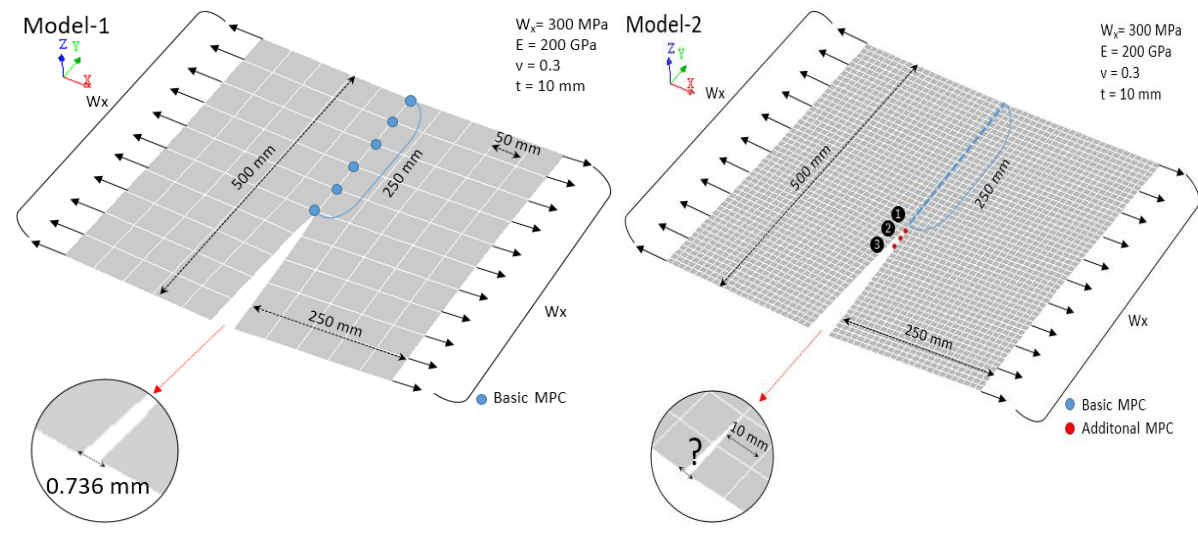


Figure 1.5 Application of multipoint constraint function

In this study, tack welding (to temporarily attach plates) is employed to model the initial analysis model. As shown in Figure 1.5, Nodes a and b are initially connected using MPC as tack welding. In addition, Nodes (c, d), (e, f) and (g, h) install MPC to be activated at assigned welding order.



**Plate dimension (500 mm x 500 mm), Element size ( 50mm)**

Basic MPC (250 mm)	Distance = 0.736 mm
--------------------	---------------------

**Plate dimension (500 mm x 500 mm), Element size ( 10 mm)**

Additional MPC ① (250 mm + 10 mm)	Distance = 0.830 mm
Additional MPC ①+② (250 mm + 20 mm)	Distance = 0.748 mm
Additional MPC ①+②+③ (250 mm + 30 mm)	Distance = 0.669 mm

Figure 1.6 MPC physical explanation (Attaching two plane plate, 500 mm x 250 mm)

In the present study, a tack welding is just expressed by connecting two nodes using MPC. In order to validate the physical effect of the tack welding presented by MPC on the constraint of the displacements in the numerical simulation, simple cases are simulated as Figure 1.6. In Model-1 (Left in Figure 1.6), two plane plates (500 mm x 250 mm) are partly attached with basic MPC and pulled each other sides by the uniformly distributed load in x direction. In this condition, the distance of the two points of the not attached edge is measured. In the case of element size of 50 mm, the distance is 0.0736 mm. In order to validate the specific range of the effect of MPC on the displacement, with changing the size of the element to 10 mm and adding additional MPC in Model-2 (Right in Figure 1.6), the distance of the two points is measured. The additional two MPC (①+②) in Model-2 produces the similar distance to Model-1. Hence, in the numerical simulation with the model basically using element size of 50mm, an MPC is assumed to be the tack welding of 20 mm under the assumption that a tack welding joins

members with the same rigidity as the base metal. Thus, introducing MPC to express a tack welding is reasonable in this study.

## 1.4 Interface element approach

To improve the result of welding sequence simulation, the definition of the relationship between the newly welded part and originally welded part is essential because it leads to the gap and misalignment of a structure (Deng and Murakawa, 2008).

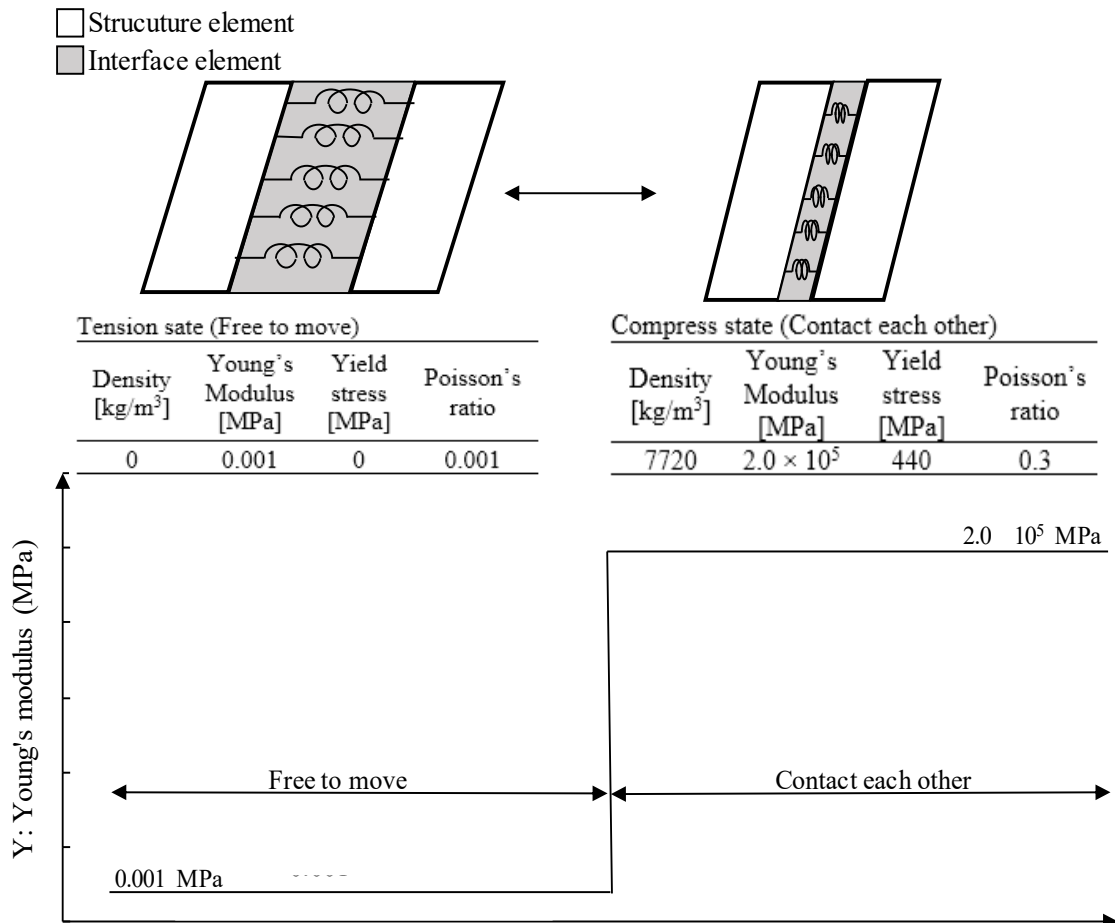


Figure 1.7 Concept of interface element

The method of interface element is used to tackle this problem in the elastic FEM. The interface element has negligibly small size. It is assigned between two different structure parts which will be welded according to the sequence to define their mechanical relationship. Meanwhile, prior to welding those two parts their relationship is basically touching each other. While processing the numerical simulation for the welding sequence, each step involved checks the state of stress of all the assigned interface elements, to distinguish whether tension or compress case. In the state of tension case, the material property of interface element changed as air to freely move different parts without mechanically impacting each other. This indicates the gap between two parts. In the state of compress case, the material property of interface element changed as mild steel to allow different parts push each other.

When the joint is completely attached following the welding process, with activation of MPC, interface elements positioned along the welded lines are inactivated as non-existent elements. In order to check and change the state of interface element in the process of the numerical simulation, there is two step iteration in the elastic FEM. This iteration could be considered as the nonlinear simulation. Thus, interface element is defined as a nonlinear spring as Figure 1.7.

## 2. Literature review

According to the welding mechanism, residual stress and deformation are strongly related to the nonlinear characteristics, such as material nonlinearity, geometric nonlinearity, and contact nonlinearity (Liang and Deng, 2018). Therefore, to obtain precise analysis results of the nonlinear numerical simulation, the nonlinearity characteristic of welding should be carefully considered. Thermal elastic plastic element method can estimate the result of welding operation on a structure; however, owing to the disadvantage of increased time-consumption, most of the recent studies employed inherent strain theory using elastic analysis. The theory of inherent strain defines the residual plastic strain along the welding line. This is a practical and effective approach to calculate the amount of welding deformation of a large structure without involving excessive hours of calculation. With the improvement in the prediction method for welding deformation, a variety of techniques to mitigate the total deformation have been developed over the decades. One of the most important parameters to reduce the welding deformation value is the sequence that strongly affects the final stress. (Ueda and Yuan, 2008) employed inherent strain in typical welding joints to predict the welding residual stress. (Luo et al., 1997) estimated the welding deformation and residual stress based on the inherent strain method using a multi-pass welding process. (Michaleris and Debiccari, 1997) proposed a thermomechanical welding simulation that was performed to calculate welding residual stresses. The value of welding distortion could be obtained by introducing the data to an elastic analysis. (Jung, 2004) developed plasticity-based distortion to analyze the relationship between six cumulative plastic strain components and angular distortion in detail. (Deng et al., 2004) assigned the interface element along the welding lines of the welded structure to consider the effect of gap between the complex welded structures. (Liang et al., 2005) improved the inverse analysis method with the help of a cutting technique to overcome the analysis of thin-plate based on the inherent strain theory. Based on the introduction of inherent strain, elastic FEM is used to predict welding distortion of a large structure during the assembly process with considering the influence of initial gap, then predicted data was validated with experimental results (Deng et al., 2007). (Wang et al., 2013) employed linear heat to reduce out of plane distortion in the finite element simulation based on the inherent strain for a large panel. (Ma et al., 2015) investigated the effect of jig constraint on welding deformation with comparing both results of numerical simulation and experimental measurement. (Ninshu Ma et al., 2016) proposed the method of line heating for the reduction of welding distortion with combined computational approach, which has thermal elastic plastic finite element and elastic finite element analysis. (Wang et al., 2016) validated the effect of zigzag welding procedure on the reduction of welding distortion caused bucking behavior of large and complex welded structures with using elastic FE analysis with inherent deformation and interface element. (N. Ma et al., 2016) investigated the influence of temporary tacking on the welding distortion. The temporary tack welding is able to mitigate displacement during assembly process. (Ma et al., 2017) demonstrated the efficiency and validity of the elastic FEM solver which introduced inherent

deformation database to be able to quickly predict welding deformation. The effect of jig constraint on the reduction of welding displacement was clarified with using numerical computation (Ma and Huang, 2017). (Wang et al., 2017) demonstrated the crucial effect of the welding sequence for a structure. The optimal welding sequence could significantly influence the final dimensional accuracy through straightening in the fitting procedure. (Liang and Deng, 2018) investigated the welding deformation of an asymmetrical curved structure based on inherent strain by conducting a numerical study on the effect of different welding sequences and external restraint. The study suggested the necessity of tack welding to reduce the deformation caused by the asymmetrical curve and different welding sequence. (Shadkam et al., 2018) studied the effect of the welding sequence for the overall deformation of a structure; however, they found that L-stiffener induced the lowest deformation as a result of the simulation of various stiffeners.

### 3. Method to systemically order welding sequence to efficiently mitigate welding displacement of a general ship grillage structure

#### 3.1 Introduction

The optimization of the assembly sequence to obtain the lowest deformation for huge steel structures, such as ships and offshore structures, is crucial. The objective of this study is to introduce an efficient method to systemically determine the optimal welding sequence for the lowest deformation of a general ship side panel, which is widely employed to design vessels and offshore structures. In this study, numerical simulation with a finite element method based on the inherent strain, interface element, and multipoint constraint function (MPC) is used as a precise computational approach to analyze the welding deformation. The employed numerical simulation obviously validated proposed systemic method to efficiently decide the optimal welding sequence for minimizing welding displacement.

#### 3.2 Analysis logic in the elastic FEM

In-house developed code based on the elastic FEM with the application of inherent strains, MPC and interface element method is employed, besides, has iteration logic system to realize the sequence based analysis as Figure 3.1.

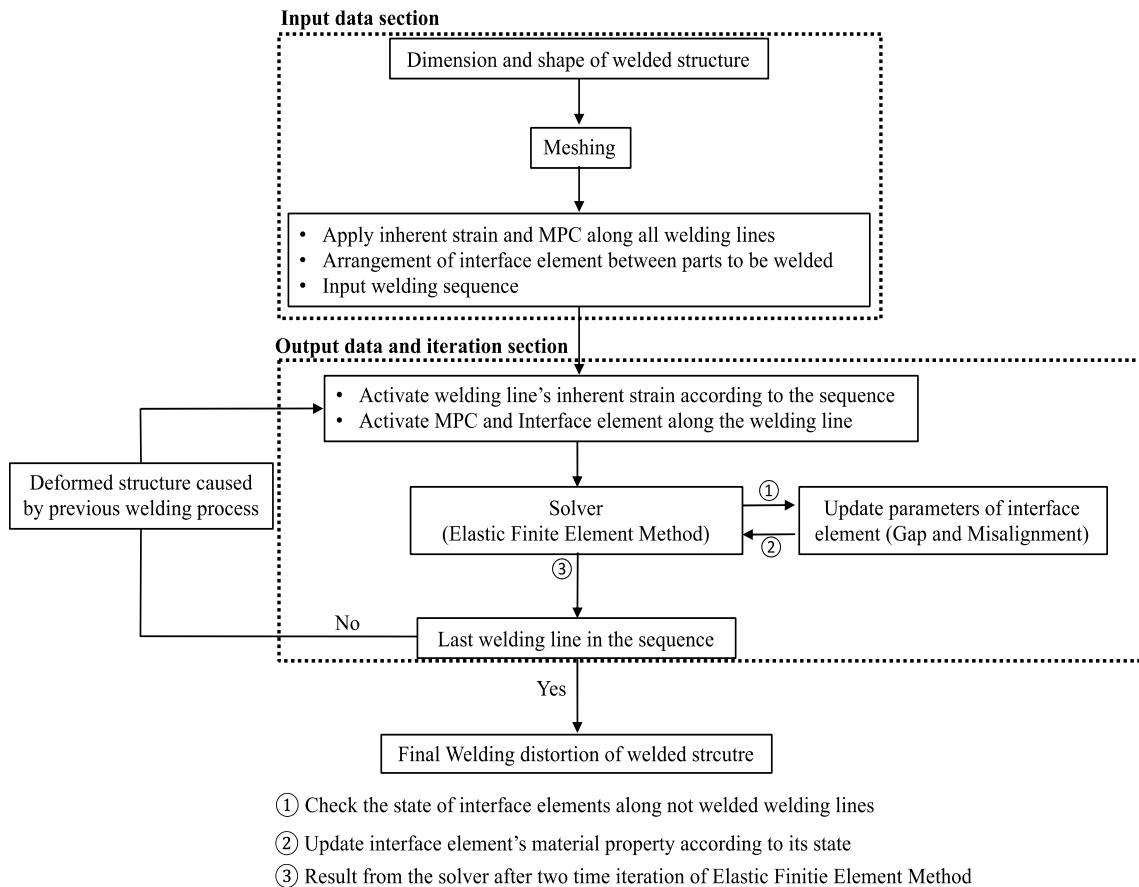


Figure 3.1 Analysis procedure logic by the sequence of elastic FEM

### 3.3 Analysis model

A general ship grillage is selected for this study. The thickness of each part is 10 mm. The material is HT50 steel (TMCP steel), which is commonly employed to build a marine structure as Table 1.2. The details of the dimensions of the objective structure are shown in Figure 3.2. All cross points at both ends of the welding line are tack welded prior to the complete connection. A CO<sub>2</sub> metal arc is employed, and the condition of all welding lines is assumed to be constant, as summarized in Table 1 (Japan Shipbuilding Research Association, 2000). To improve the result of the numerical simulation by using the inherent strain method, primarily fine mesh is introduced for the structure.

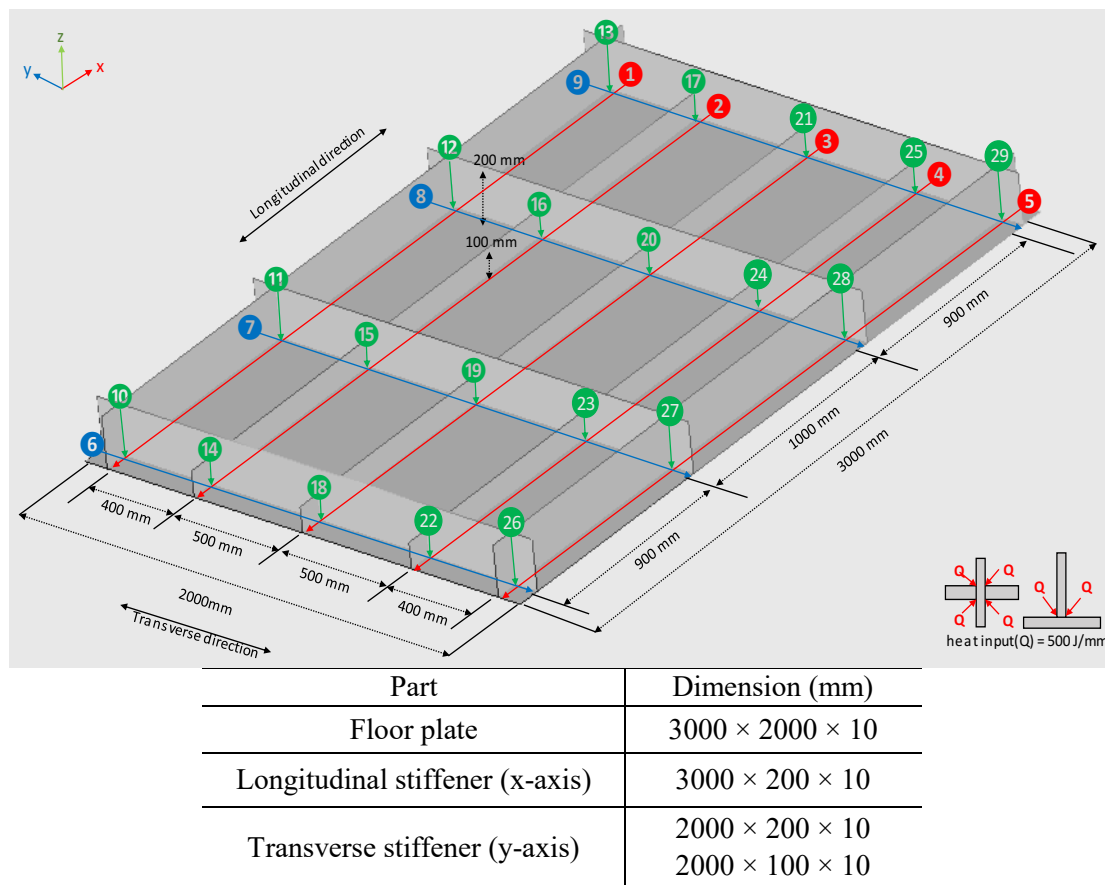


Figure 3.2 General Ship Grillage Structure (3000 mm × 2000 mm)

### 3.4 Welding sequence cases

Figure 3.2 shows the numbering of each welding line. There are three categories, namely, longitudinal (1-5), transverse (6-9), and vertical (10-21) welding lines. This study mainly focuses on the lowest deformation of the plate. Therefore, the relationship between final displacement of the plate and gap, misalignment while processing welding sequence is considerable. Considering this fact, prior to creating welding sequences, all welding lines are respectively welded alone. Then, the gap between the stiffeners (frames) and plate is measured and aggregated, as shown in Table 3.1. It indicates the effect of each welding line on the structure.

Table 3.1 Total gap between the welding lines and plate, after welding each line

	Number	Overall gap (mm)
Longitudinal	1	0.02052
	2	0.04745
	3	0.12125
	4	0.04740
	5	0.02067
Transverse	6	0.13221
	7	0.126824
	8	0.126824
	9	0.132216
Vertical	10	0.004424
	11	0.008546
	12	0.008546
	13	0.004424
	14	0.054773
	15	0.067253
	16	0.067253
	17	0.054773
	18	0.053096
	19	0.071685
	20	0.071685
	21	0.053096
	22	0.054562
	23	0.067291
	24	0.067291
	25	0.054562
	26	0.006481
	27	0.009451
	28	0.009451
29	0.006481	

Table 3.2 Welding sequences

	Number	Welding sequence preference		Welding sequence
Category A	1	Bottom (Plate)	Vertical	H 6→9→7→8→3→2→4→5→1→20→19→24→23→15→16→14→17→22→25→18→21→27→28→11→12→26→29→10→13
	2			L 6→9→7→8→3→2→4→5→1→10→13→26→29→11→12→27→28→18→21→22→25→14→17→15→16→23→24→19→20
	3			H 1→5→4→2→3→7→8→6→9→20→19→24→23→15→16→14→17→22→25→18→21→27→28→11→12→26→29→10→13
	4			L 1→5→4→2→3→7→8→6→9→10→13→26→29→11→12→27→28→18→21→22→25→14→17→15→16→23→24→19→20
	5	Vertical	Bottom (Plate)	H 20→19→24→23→15→16→14→17→22→25→18→21→27→28→11→12→26→29→10→13→6→9→7→8→3→2→4→5→1
	6			L 20→19→24→23→15→16→14→17→22→25→18→21→27→28→11→12→26→29→10→13→1→5→4→2→3→7→8→6→9

7		L	H	10→13→26→29→11→12→27→28→18→21→22→25→14→17 →15→16→23→24→19→20→6→9→7→8→3→2→4→5→1
8		L	L	10→13→26→29→11→12→27→28→18→21→22→25→14→17 →15→16→23→24→19→20→1→5→4→2→3→7→8→6→9

Number	Welding sequence preferences				Welding sequence	
	Vertical	Longitudinal (Plate)	Transverse (Plate)	Direction	Sequence	
Category B	1	H	H	H	20→19→24→23→15→16→14→17→22→25→18→21→27→28→11→12→26→29→10→13→3→2→4→5→1→6→9→7→8	
	2	H	H	L	20→19→24→23→15→16→14→17→22→25→18→21→27→28→11→12→26→29→10→13→3→2→4→5→1→7→8→6→9	
	3	H	L	H	20→19→24→23→15→16→14→17→22→25→18→21→27→28→11→12→26→29→10→13→1→5→4→2→3→6→9→7→8	
	4	H	L	L	20→19→24→23→15→16→14→17→22→25→18→21→27→28→11→12→26→29→10→13→1→5→4→2→3→7→8→6→9	
	5	L	H	H	10→13→26→29→11→12→27→28→18→21→22→25→14→17→15→16→23→24→19→20→3→2→4→5→1→6→9→7→8	
	6	L	H	L	10→13→26→29→11→12→27→28→18→21→22→25→14→17→15→16→23→24→19→20→3→2→4→5→1→7→8→6→9	
	7	L	L	H	10→13→26→29→11→12→27→28→18→21→22→25→14→17→15→16→23→24→19→20→1→5→4→2→3→6→9→7→8	
	8	L	L	L	10→13→26→29→11→12→27→28→18→21→22→25→14→17→15→16→23→24→19→20→1→5→4→2→3→7→8→6→9	
Category B	9	H	H	H	20→19→24→23→15→16→14→17→22→25→18→21→27→28→11→12→26→29→10→13→6→9→7→8→3→2→4→5→1	
	10	H	H	L	20→19→24→23→15→16→14→17→22→25→18→21→27→28→11→12→26→29→10→13→6→9→7→8→1→5→4→2→3	
	11	H	L	H	20→19→24→23→15→16→14→17→22→25→18→21→27→28→11→12→26→29→10→13→7→8→6→9→3→2→4→5→1	
	12	H	L	L	20→19→24→23→15→16→14→17→22→25→18→21→27→28→11→12→26→29→10→13→7→8→6→9→1→5→4→2→3	
	13	L	H	H	10→13→26→29→11→12→27→28→18→21→22→25→14→17→15→16→23→24→19→20→6→9→7→8→3→2→4→5→1	
	14	L	H	L	10→13→26→29→11→12→27→28→18→21→22→25→14→17→15→16→23→24→19→20→6→9→7→8→1→5→4→2→3	
	15	L	L	H	10→13→26→29→11→12→27→28→18→21→22→25→14→17→15→16→23→24→19→20→7→8→6→9→3→2→4→5→1	
	16	L	L	L	10→13→26→29→11→12→27→28→18→21→22→25→14→17→15→16→23→24→19→20→7→8→6→9→3→2→4→5→1	

According to these results, this study conducted 24 different welding sequences, as listed in Table 3.2. There are two categories: category A, which divides the bottom (longitudinal and transverse) and vertical welding lines, and category B, which has three divisions (longitudinal, transverse, and vertical). In Table 3.2, ‘H’ denotes the preference of the first order of the welding line, which leads to the high value of the gap and ‘L’ is opposite.

### 3.5 Results and discussion

A total of 24 cases of two categories (A and B) were considered to suggest the new standard to determine the optimal welding sequence for the lowest deformation of the plate. The representative reference value to discuss the effect of additional clamps is z-axis distance average that the average of the z-axis distance of all the bottom plate nodes from z-axis displacement average value to their original values as below. Additionally, the z-axis distance between the lowest and the highest node positions of the bottom plate was measured herein. To compare the distribution curves of the displacement of the plate, values of two lines, such as Line 1 (Transverse) and Line 2 (Longitudinal) are measured, as shown in Figure 3.3.

$$Z_{average} = \frac{\sum_{k=1}^n z_k}{n} \quad (3.1)$$

$$A_{distance} = \frac{\sum_{k=1}^n (z_k - A_{displacement})}{n} \quad (3.2)$$

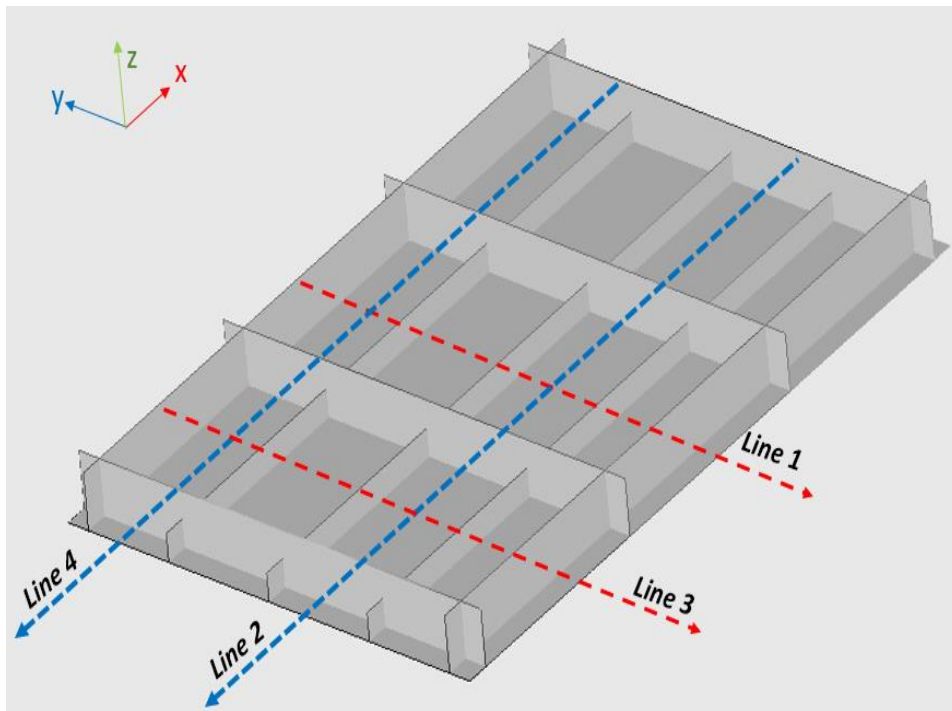


Figure 3.3 Measuring line for the displacement distribution

### 3.5.1 Category A

The result of Category A demonstrates two points. Initially, in terms of considering the priority between the vertical welding line and plate welding line (longitudinal, transverse), the vertical welding line is immensely effective in causing small distortion, as shown in Figure 3.4. Comparing to the result of Category A-2 (0.6397 mm), the sequence of Category A-8 (0.4552 mm) has 28.8% reduction for the mitigation of welding displacements. Figures 3.6-3.9 show the distribution of the z-axis displacement of Line 1-4.

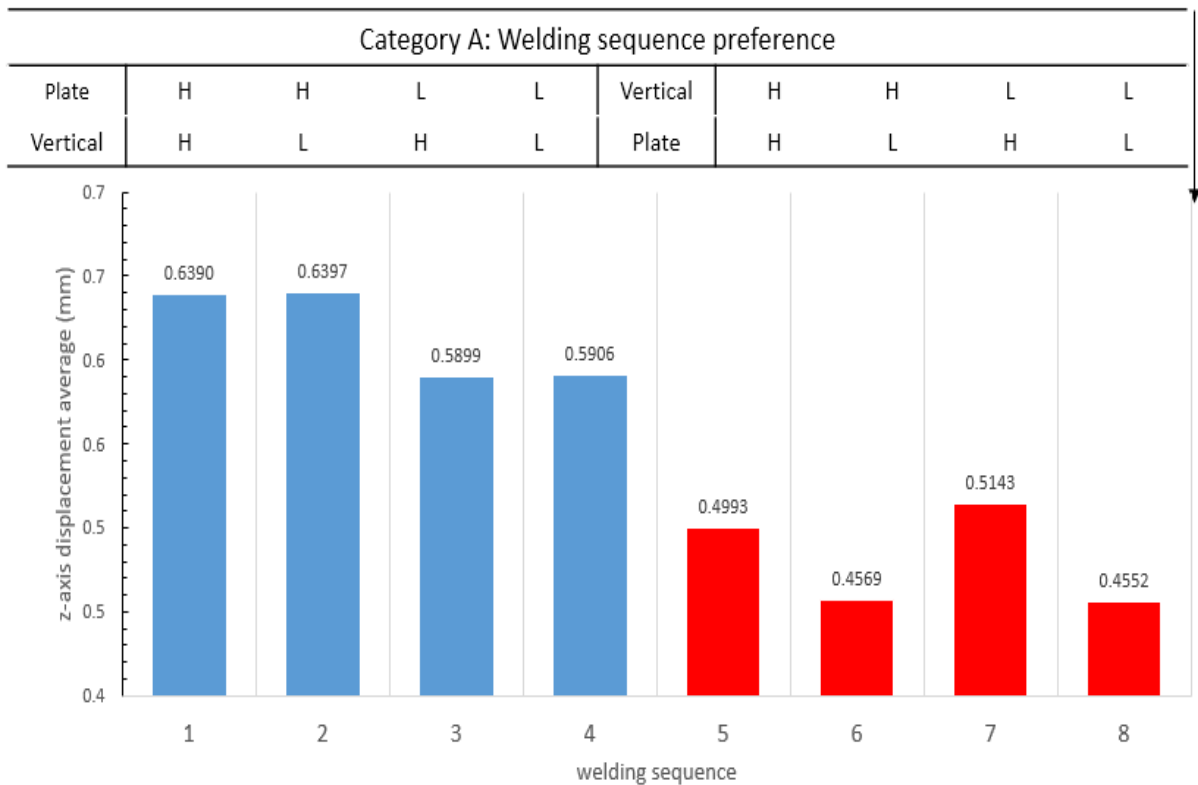


Figure 3.4 Category A z-axis distance average

In Figure 3.5 and Figure 3.6, the z-axis displacement distribution curves of Line 1 and Line 2 of Category A-8 have the lowest values comparing to other welding sequences. In Figure 3.7 and Figure 3.8, although the z-axis displacement distribution curves of Line 3 and Line 4 of Category A-8 have not the lowest values, it leads to the reduction of z-axis distance average. Furthermore, while comparing Figure 3.9 with Figure 3.10, it is evident that the deformation of the plane plate of (Category A-2) is significantly larger than (Category A-8). Comparing Figure 3.9 and 3.10 clearly demonstrate the effect of the optimal welding sequence (Category A-8) to mitigate the distortion of the objective structure.

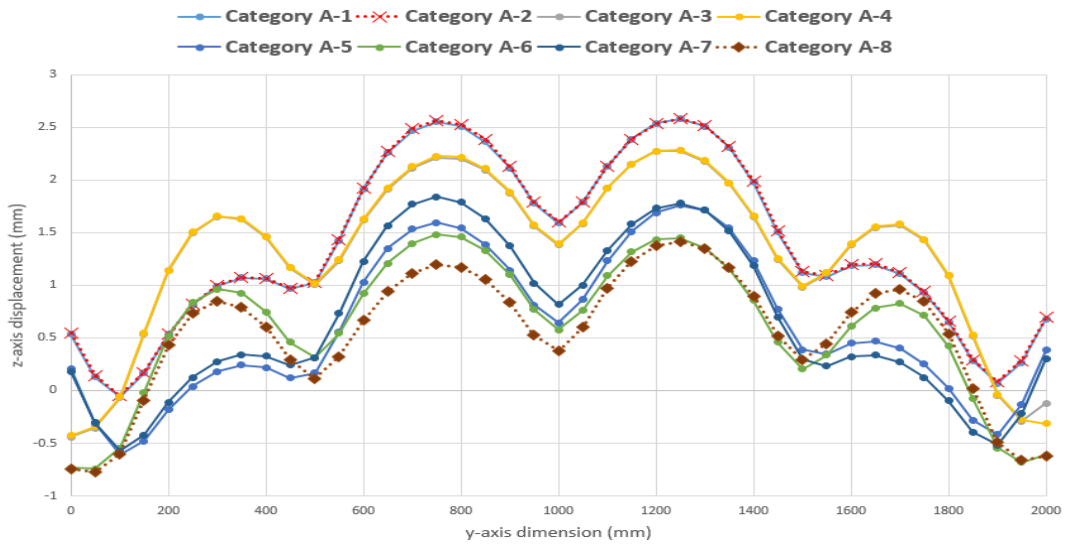


Figure 3.5 Z-axis displacement distribution of Line 1

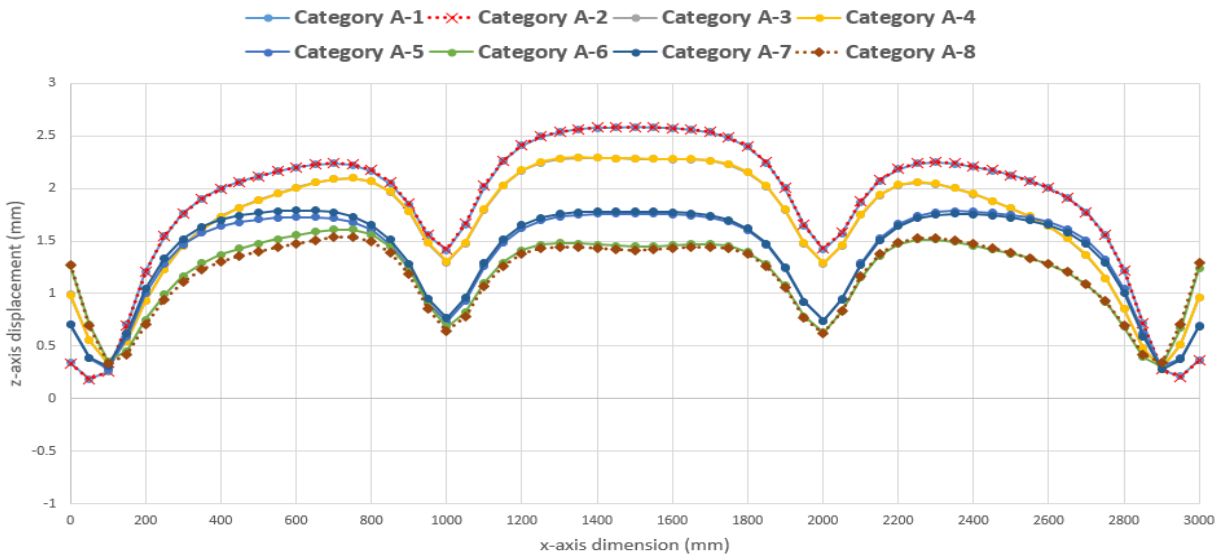


Figure 3.6 Z-axis displacement distribution of Line 2

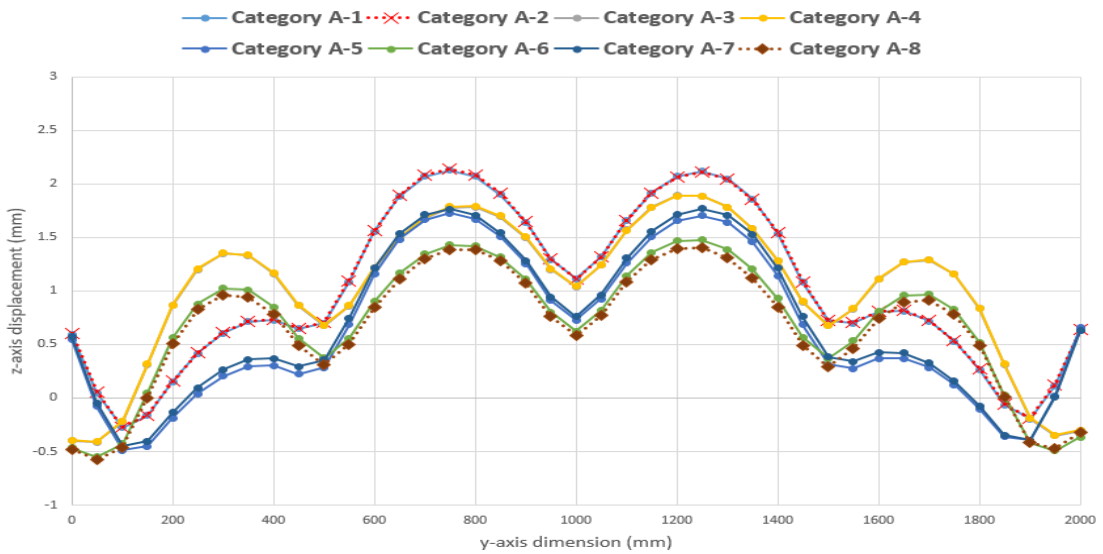


Figure 3.7 Z-axis displacement distribution of Line 3

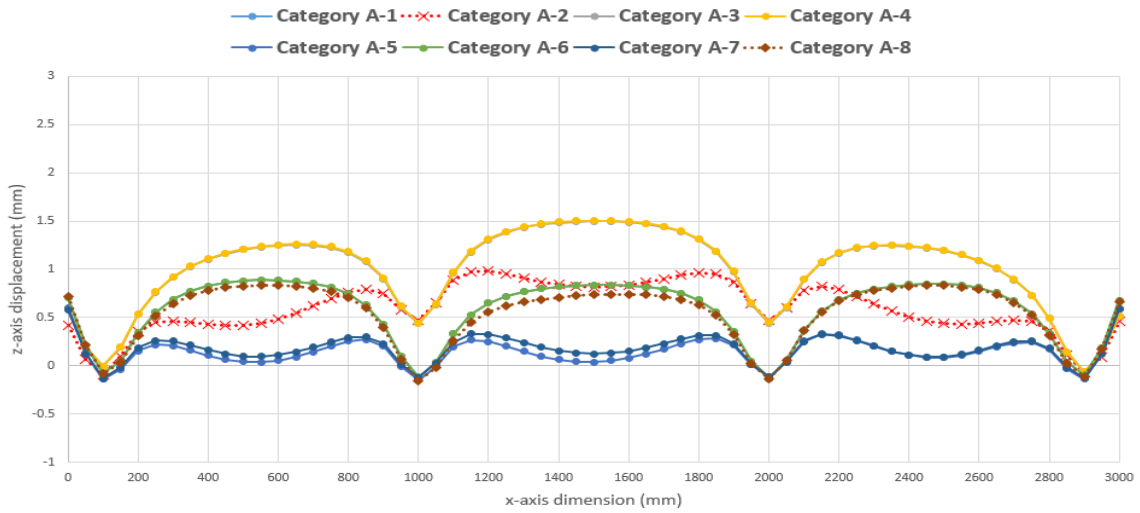


Figure 3.8 Z-axis displacement distribution of Line 4

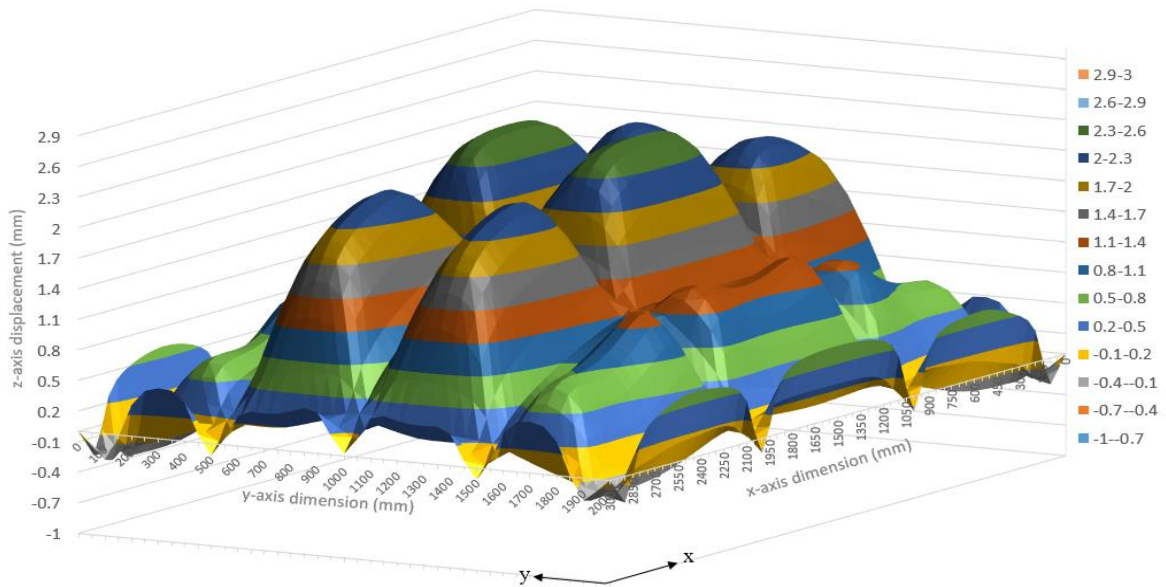


Figure 3.9 Z-axis displacement of Category A-2

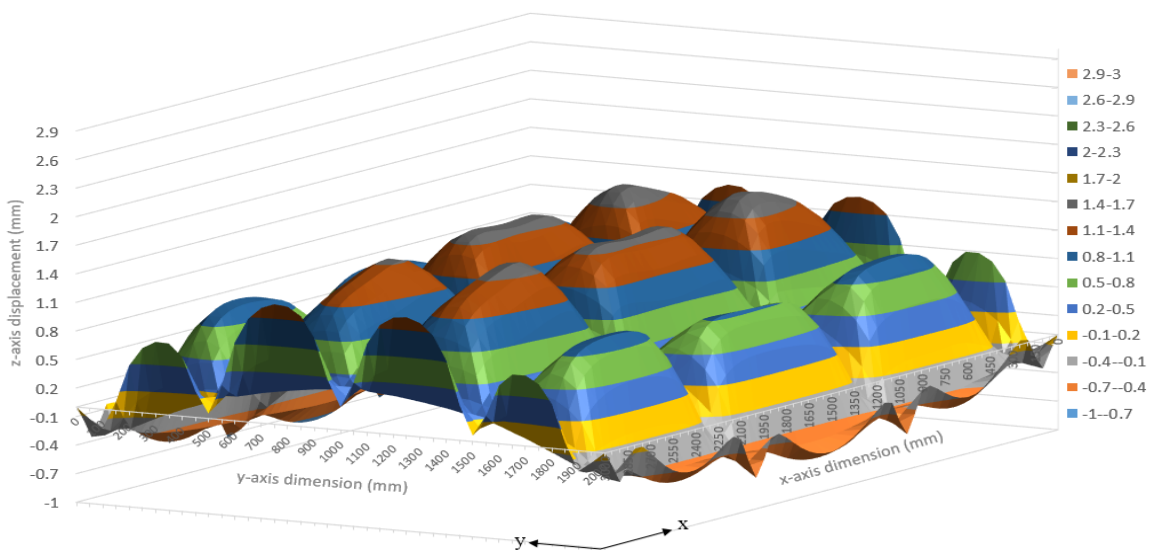


Figure 3.10 Z-axis displacement of Category A-8

### 3.5.2 Category B

According to the results of Category A, initially, the vertical welding lines are ordered in the welding sequences of Category B. Additionally, the welding lines positioned on the plane plate are divided into two groups as Transverse and Longitudinal to study in-depth the various standards to systemically order welding sequence that lead to different complex displacements. In Figure 3.11, comparing Category B (1-8) and (9-16), it has limited scope to explain the consistency in the roles of two different groups for the displacement of the structure. Therefore, it is inadequate to determine the priority between transverse and longitudinal welding lines in the sequence. Category B-3, B-7, B-10, and B-14 welding sequences show the relatively low result values. In the view of the composition of welding sequences of 4 cases, the opinion that the priority of welding lines leading to a small gap in the sequence (in the view of results of Category A) is not applicable for all simulations. However, the common point of these 4 cases is the priority of the highest gap of transverse in their respective welding sequences. This tendency can be explained as following the reason that Table 3.2 displays welding lines of transverse flame, causing much higher values of the overall gap than longitudinal and vertical. Therefore, in order to preferentially improve the rigidity of the structure, welding lines which lead to relatively high gap are initially welded following the vertical welding operation.

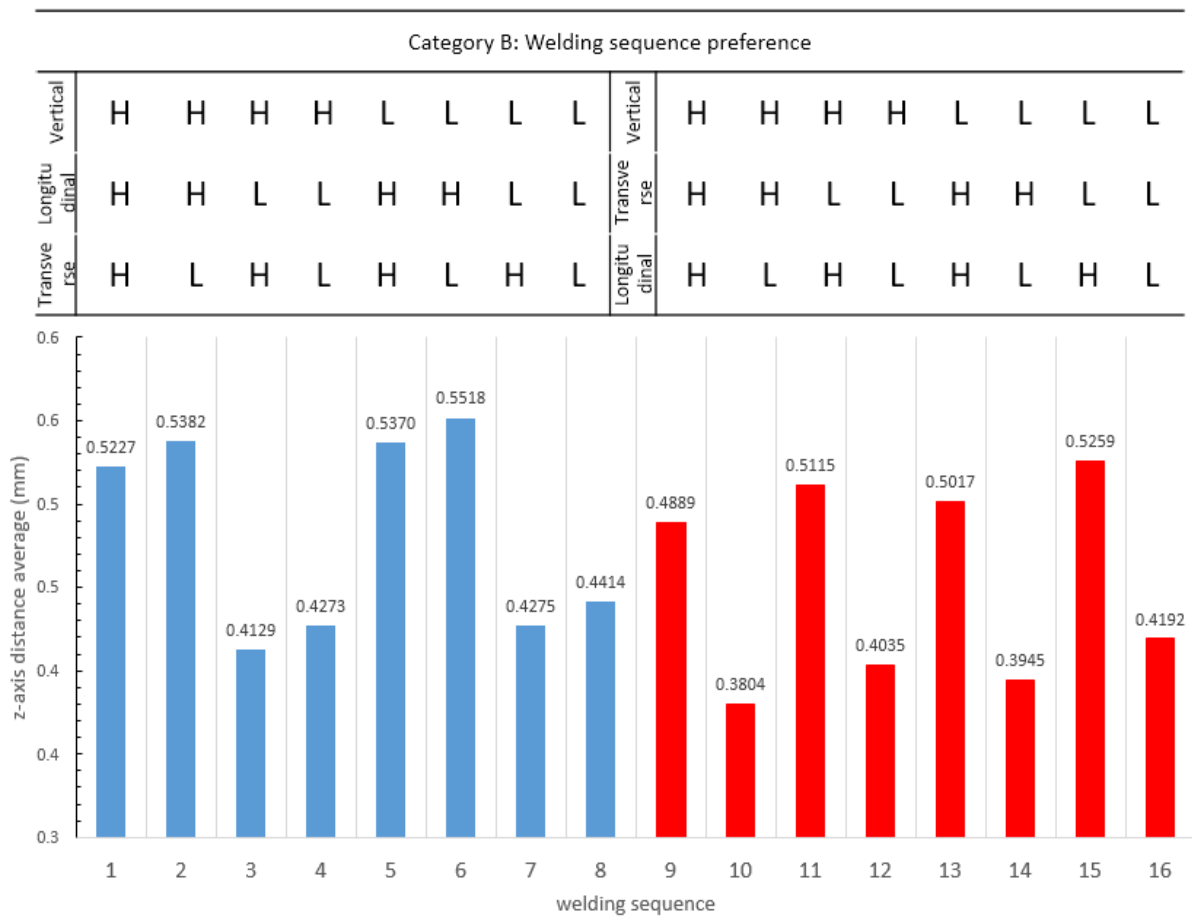


Figure 3.11 Category B z-axis distance average

Figure 3.12-3.18 show the influence of referred tendency in the simulation. Comparing Category B-10 with Category B-12, although the preference standard for welding sequence for vertical (H) and longitudinal (L) except transverse, the result of distribution of z-axis displacement reveals the important role of the priority of high gap transverse lines in welding sequence.

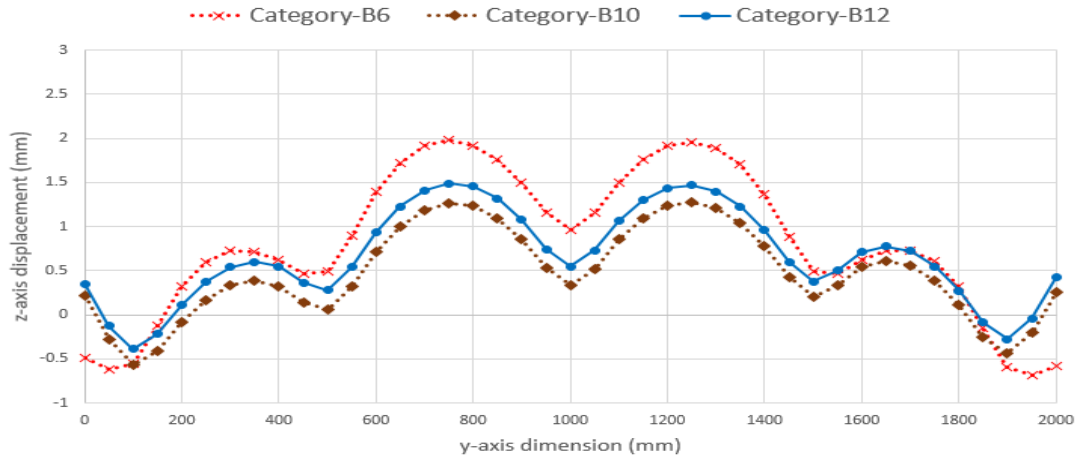


Figure 3.12 Distribution of z-axis displacement of Line 1 of Category B-6, B-10 and B-12

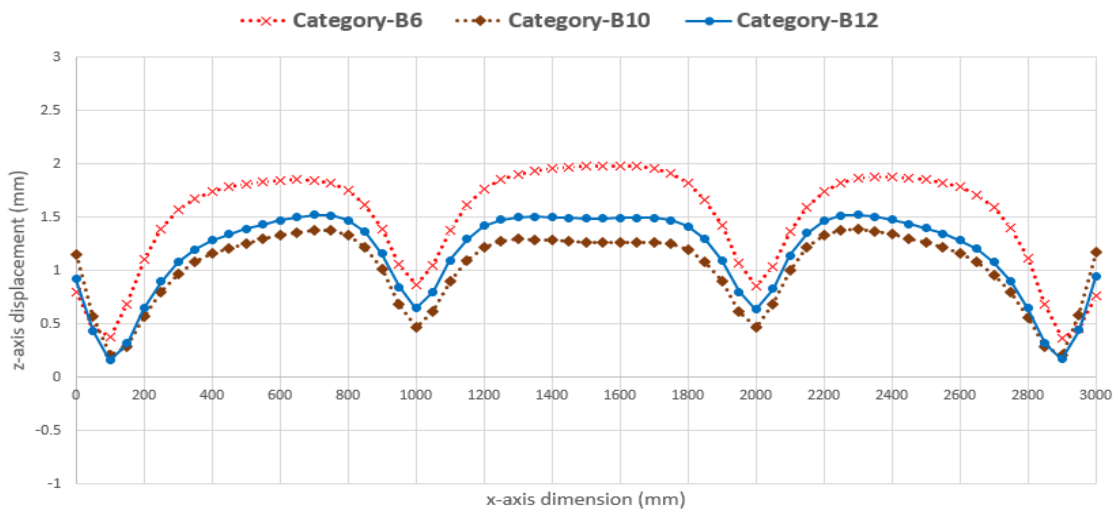


Figure 3.13 Distribution of z-axis displacement of Line 2 of Category B-6, B-10 and B-12

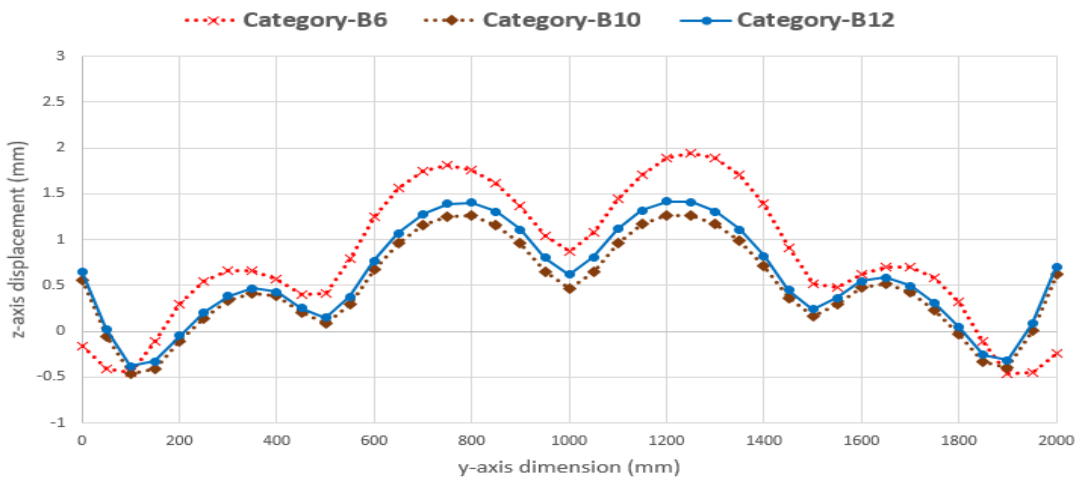


Figure 3.14 Distribution of z-axis displacement of Line 3 of Category B-6, B-10 and B-12

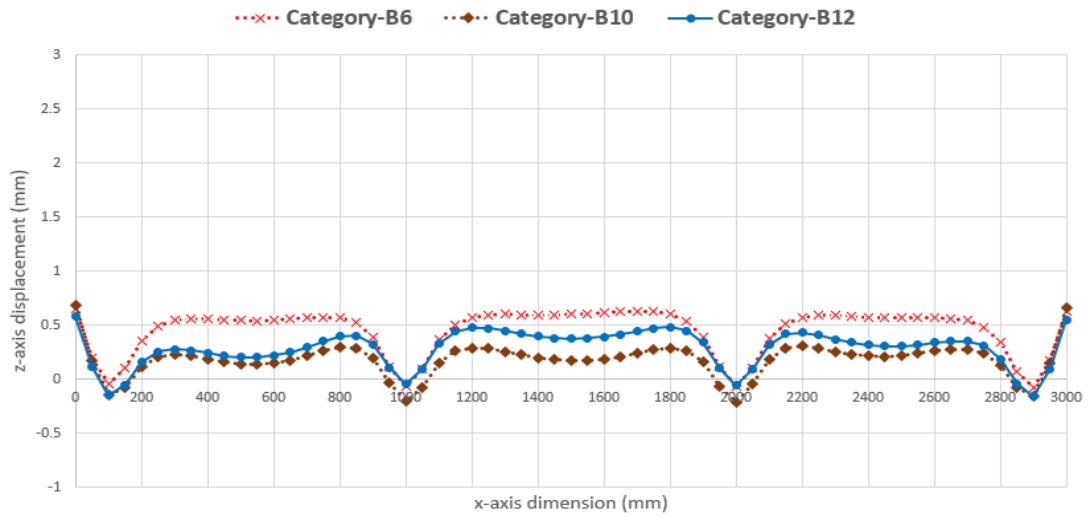


Figure 3.15 Distribution of z-axis displacement of Line 2 of Category B-6, B-10 and B-12

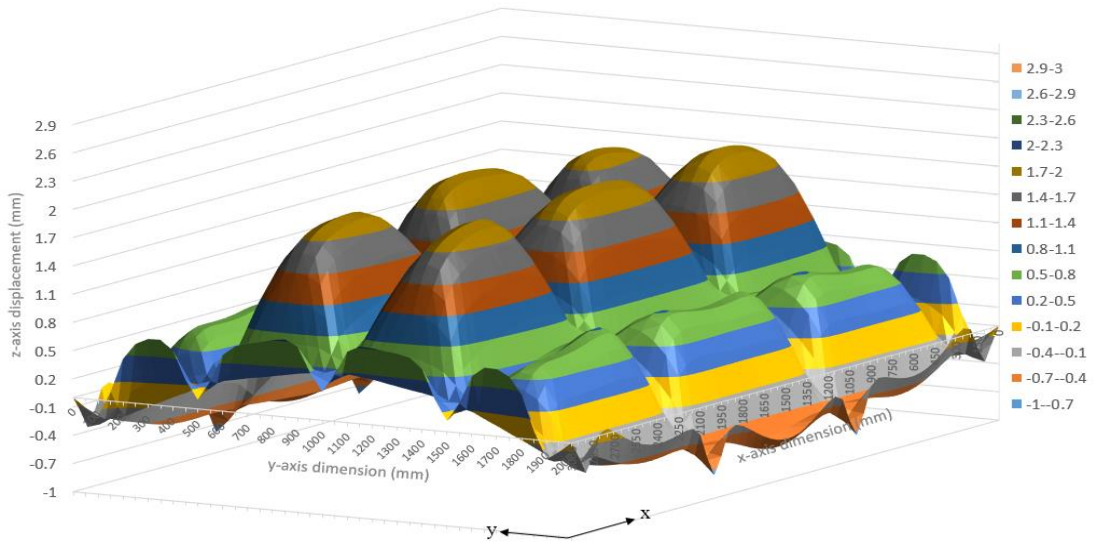


Figure 3.16 Z-axis displacement of Category B-6

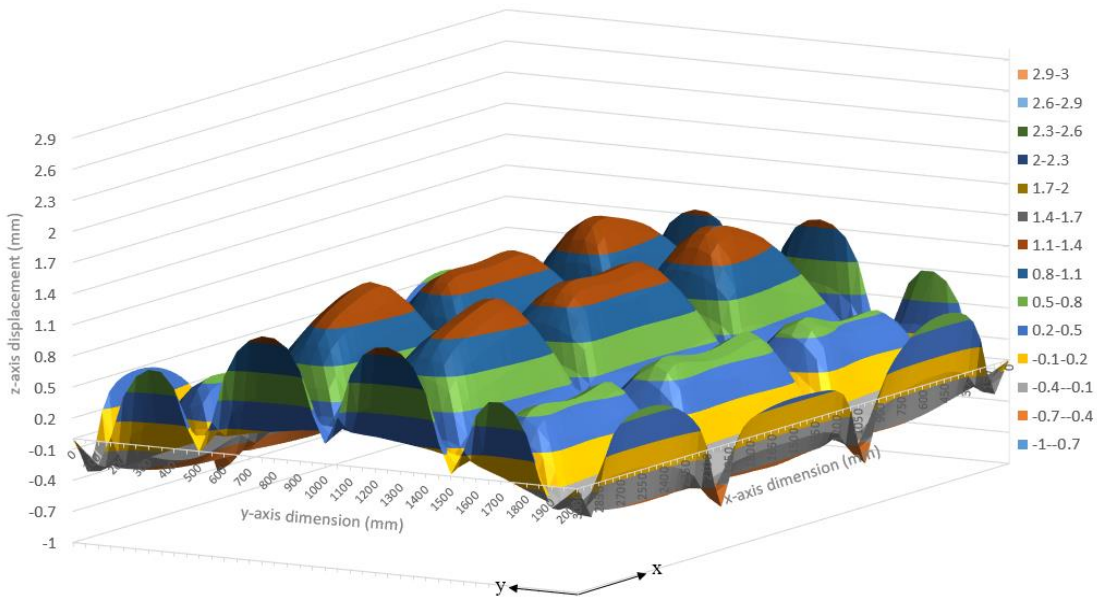


Figure 3.17 Z-axis displacement of Category B-10

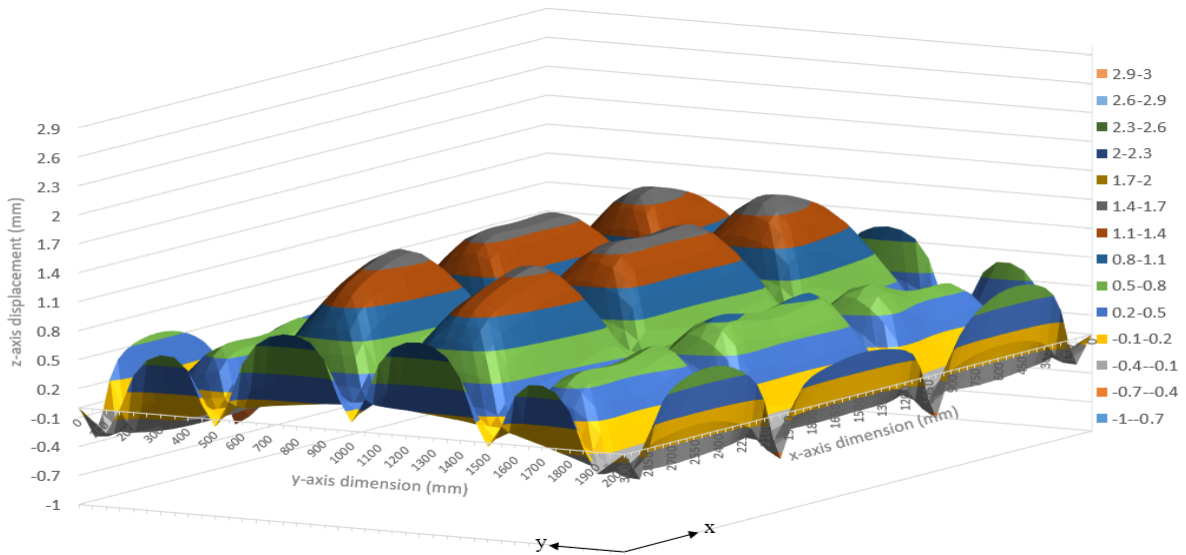


Figure 3.18 Z-axis displacement of Category B-12

### 3.5.3 Comparison between Category A and B

The incremental number of groups to categorize welding lines such as three groups in Category B facilitates improvement in the method to find the optimal welding sequence to reduce the distortion of the structure. The lowest value of z-axis distance average of Category A-8 is 0.4552 mm. The lowest value of z-axis distance average of Category B-10 is 0.3804 mm. Although the difference between two values is 0.0748 mm, the reduction is 16.43% and Figure 3.19 demonstrates the reduction of the displacement and different bucking tendency.

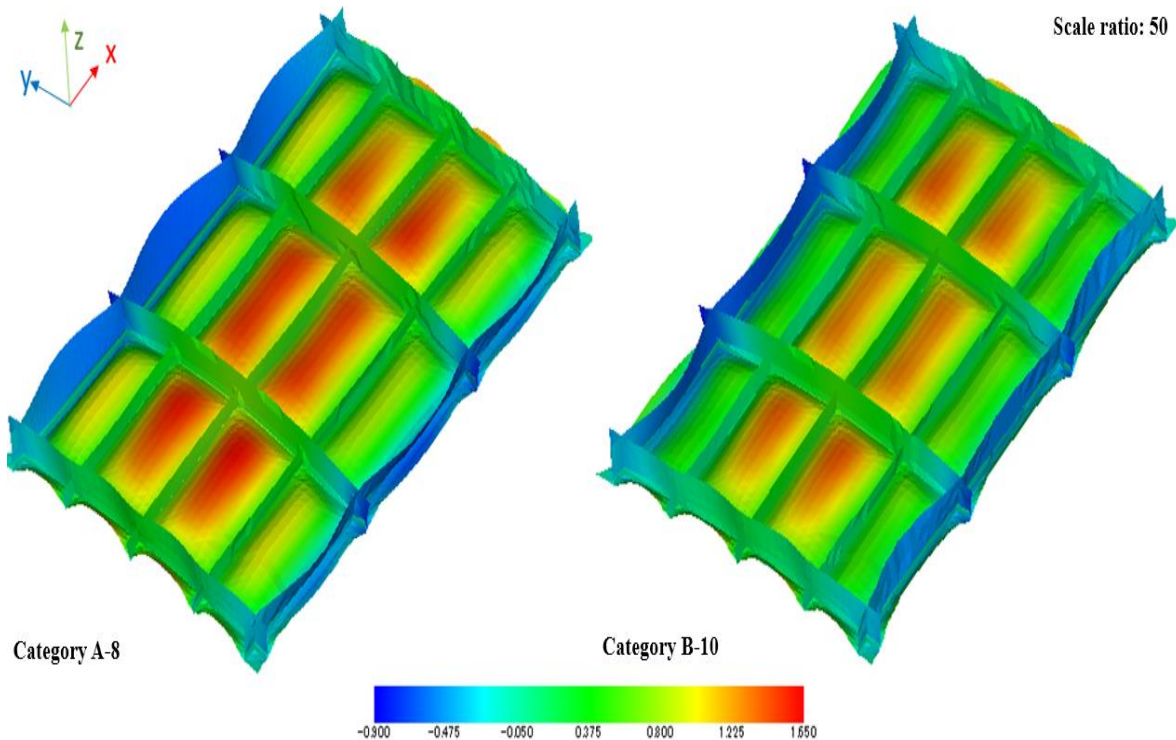


Figure 3.19 Comparing results of z-axis displacement of Category A-8 and Category B-10

### 3.6 Conclusion

In this study, to suggest the new standard to develop the optimal welding sequence to mitigate the distortion of a general ship grillage structure, the FEM approach is introduced with inherent strain and interface element methods. This research demonstrates the necessity of studying various standards to systemically order welding lines depending on a structure. The conclusions of this research and suggestions are as follows:

1. Although each vertical welding line produces a relatively smaller gap between the plane plate and stiffeners, initially welding them in a particular order can significantly reduce the final displacement of the structure. Owing to the role of the previously welded vertical lines, the total strength of the structure is substantially improved.
2. The priority for a weld sequence between the longitudinal and transverse welding lines which require heat effect directly on the bottom plate; the welding group of transverse welding lines that produce a relatively higher gap prior to the longitudinal welding lines are beneficial in mitigating distortion.

Depending on increased number of groups to categorize welding lines, this procedure positively improves the method to find the optimal welding sequence to reduce the distortion of the structure. Although the difference between Category A and B is fairly small in this study, the increase of the number of standard to systemically order welding sequence would be able to significantly reduce the total displacement for a huge complex structure. Therefore, the study of various standards of welding lines to characterize different structures is essential to develop the widely applicable system.

## 4. Optimal simultaneous welding to minimize welding deformation of a general ship grillage structure

### 4.1 Introduction

This study validated the effect of the optimal simultaneous welding on the mitigation of welding displacements. Most previous studies on the optimized welding sequence for the reducing welding displacements have focused on one welding line at each order. However, in heavy industries, several welders or robotic welding machines generally work together to efficiently spend work time. Herein, Inherent strain theory is introduced to calculate the complex mechanical behavior during a welding operation using the elastic FEM. MPC and the interface element theory are employed to consider the relationship of the different welded parts. The impact of the optimal simultaneous welding in the sequence on the reduction of welding displacement is validated by using proposed numerical method in the present study.

### 4.2 Analysis logic in the elastic FEM

In order to save computation time and realize the sequence based analysis, in-house developed code based on finite element elastic method with the application of the inherent strain theory, MPC and interface element method is employed herein. The analysis logic is expressed as Figure 4.1.

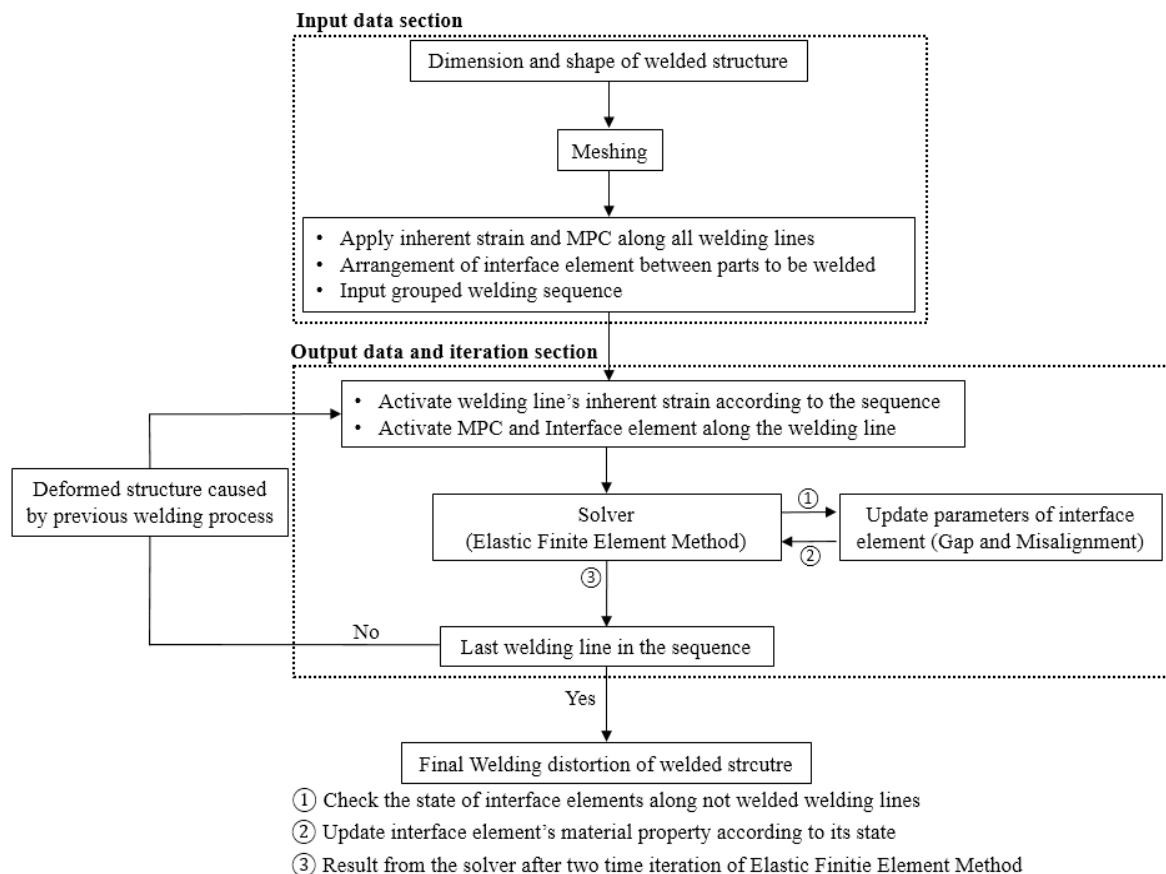


Figure 4.1 Analysis procedure logic by the sequence of elastic FEM

### 4.3 Analysis model

A representative shape of a general ship's side panel is introduced herein. The structure with a dimension similar to that in a previous study of the chapter 3 is introduced to investigate of the effect of the simultaneous welding. Figure 3.2 illustrates the analysis model with its dimension. MPC's are applied to the upper and bottom points of all the cross-sections for expressing tack welding such that the whole structure is shaped before being in a fully welding operation. The four corner points of the panel are clamped. Arc butt welding condition shown in Table 1.1 is used for all the welding lines. The numbers in circles indicate individual welding line in Figure 3.2. A total of 29 welding lines exist and are organized into three groups categorized as longitudinal lines (1–5), transverse lines (6–9) and vertical lines (10–29).

### 4.4 Simulation scenario of simultaneous welding

#### 4.4.1 Sequence of one by one welding lines

The chapter 3 proposed the optimal sequence of one by one welding lines for the model structure introduced above. The study validated the optimized welding sequence under the assumption that one worker welds all welding lines by himself. So, no more than one welding line can be taken care of simultaneously. It was recommended that the vertical welding lines are treated first to improve the total stiffness of the structure at the early stage. Each transverse line is welded just after welding vertical lines. Finally, the longitudinal welding lines are handled resulting in the minimum welding displacement. The welding sequence by one worker giving the minimum welding displacement is shown in Table 4.1.

Table 4.1 Optimized sequence of one by one welding lines

Welding sequence Preference (Vertical–transverse –longitudinal)
20 → 19 → 24 → 23 → 15 → 16 → 14 → 17 → 22 → 25 → 18 → 21 → 27 → 28 → 11 → 12 → 26 → 29 → 10 → 13 → 6 → 9 → 7 → 8 → 1 → 5 → 4 → 2 → 3

#### 4.4.2 Sequence of grouped welding lines

In general, several welders and/or robotic welding machines process the welding work for a structure together in heavy industries to increase the productivity. So, several lines are welded simultaneously. Simultaneously welding of several lines leads to a different welding deformation of the structure from the one by one welding. Therefore, grouping welding sequences is highly important and investigated here.

The number of welders is focused on in this study. Specifically, one group of welding lines is offered for each number of welders. The welding lines are grouped by the following steps.

1. Set the number of welders for a simultaneously welding.
2. Select as many welding lines as workers from top of the welding sequence listed in Table 3 as the members in the same group such that each welder can handle one welding line.
3. Remove the welding lines selected in step 2 from the welding sequence.
4. Repeat steps 2 and 3 until all welding lines are selected.

For example, if 10 welders work together, the welding lines are grouped as

- The first group: lines 20, 19, 24, 23, 15, 16, 14, 17, 22, 25 (10 lines)
- The second group: lines 18, 21, 27, 28, 11, 12, 26, 29, 10, 13 (10 lines)
- The third group: lines 6, 9, 7, 8, 1, 5, 4, 2, 3 (9 lines)
- ❖ If 29 welders work together, all welding lines are welded simultaneously.

## 4.5 Results and discussion

A total of 29 cases of different welding processes depending on the number of welders were simulated herein to investigate the effect of a simultaneous welding process on the model structure. The z-axis distance average  $A_{distance}$  is used as the representative reference value to discuss the effect of different simultaneous welding sequences.  $A_{distance}$  given by Eq. 3.2 is the average of the z-axis distance of all the bottom plate nodes from z-axis displacement average  $Z_{average}$  of Eq. 3.1 to their original values. Additionally, the z-axis maximum displacement between the lowest and the highest node positions of the bottom plate is measured.

### 4.5.1 Process of $A_{distance}$ at each step of the optimal welding sequence

Prior to discussing the results of differently grouped welding sequence for the simultaneous welding process, understanding the effect of each welding line on  $A_{distance}$  of the structure is important. Figure 4.2 illustrates the progress of  $A_{distance}$  at each step of the welding sequence expected be to the optimal in the chapter 3.  $A_{distance}$  continuously increases from welding steps 1 to 20 in which vertical lines are welded. Moreover, a highly increases of  $A_{distance}$  is observed in the welding steps from 25 to 29 in which longitudinal welding lines are treated. However, the welding of transverse lines whose steps are from 21 to 24 highly reduces  $A_{distance}$ . So, welding the transverse lines has the effect of amending the displacement of the bottom plate.

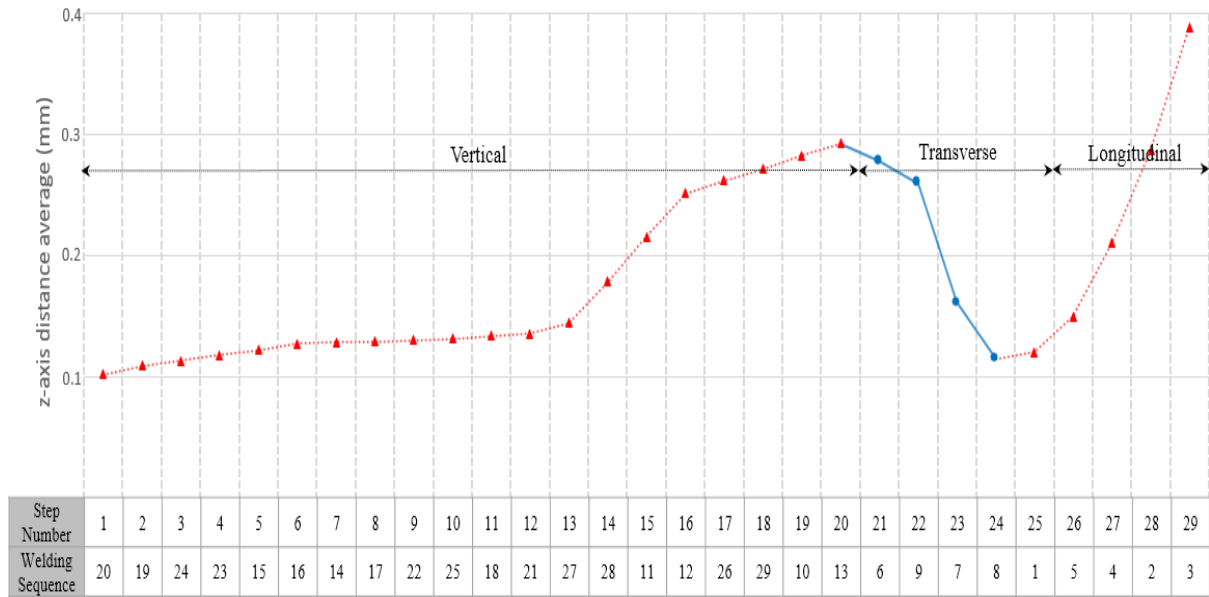


Figure 4.2 Progress of  $A_{distance}$  at each step of the welding sequence

## 4.5.2 Effect of the simultaneous welding process

Figures 4.3 and 4.4 show  $A_{distance}$  and the maximum z-axis displacement of the simultaneous welding process by the different number of welders in 29 cases. Case  $n$  shows the result of  $n$  welders are assigned so that the digit after “Case” indicates the number of workers in the simultaneous welding. According to this notation, Case 1 indicates the welding by 1 welder resulting in the sequence of one by one welding lines, while Case 29 is for that all lines are welded at once. A comparison of the results of Cases 1 and 29 demonstrates that welding all lines at once leads to 11.3 % increase of  $A_{distance}$  from one by one welding. This result shows the fact that simultaneous welding by many welders isn’t always better than the less welders. Case 10 has the smallest  $A_{distance}$  of 0.343 mm which is 9.7 % reduction from Case 1 and 21.0% from Case 29, respectively. In terms of minimizing welding displacements, the value of 21.0 % is not ignorable efficiency.

There are two local minimums exist at Cases 10 and 20 in  $A_{distance}$  which decreases almost monotonically from Case 2 to Case 10 and from Case 13 to Case 20.  $A_{distance}$  keeps nearly constant after increasing sharply from Cases 21 to 23. The maximum z-axis displacement shown in Figure 4.4 has the similar tendency to  $A_{distance}$ .

Figure 4.5 is a bird's eye view of the deformed structure in Cases 1, 10, 20 and 29. It is noted that buckled features mainly appear at the center of the structure. In Cases 10 and 20, the buckled displacements at the center of the bottom plate of the structure are highly mitigated from Case 1. However, Case 29 leads to the increase of the magnitude of the buckled features at the center of the structure.

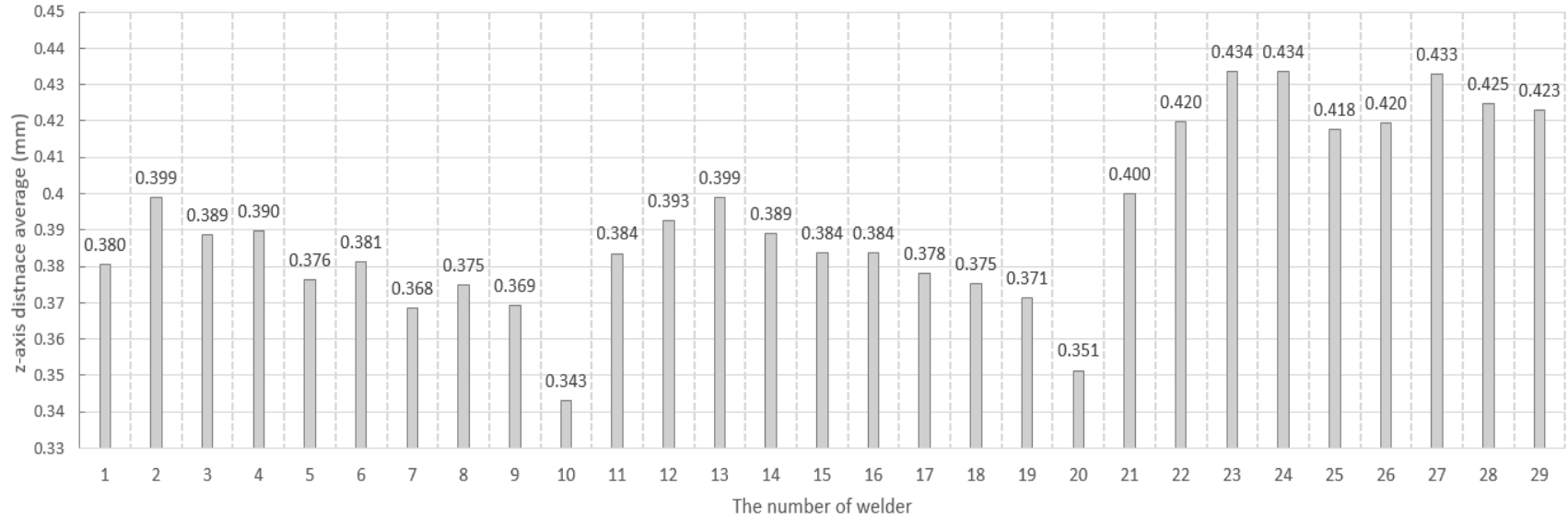


Figure 4.3  $A_{distance}$  of the simultaneous welding process by the different number of welders

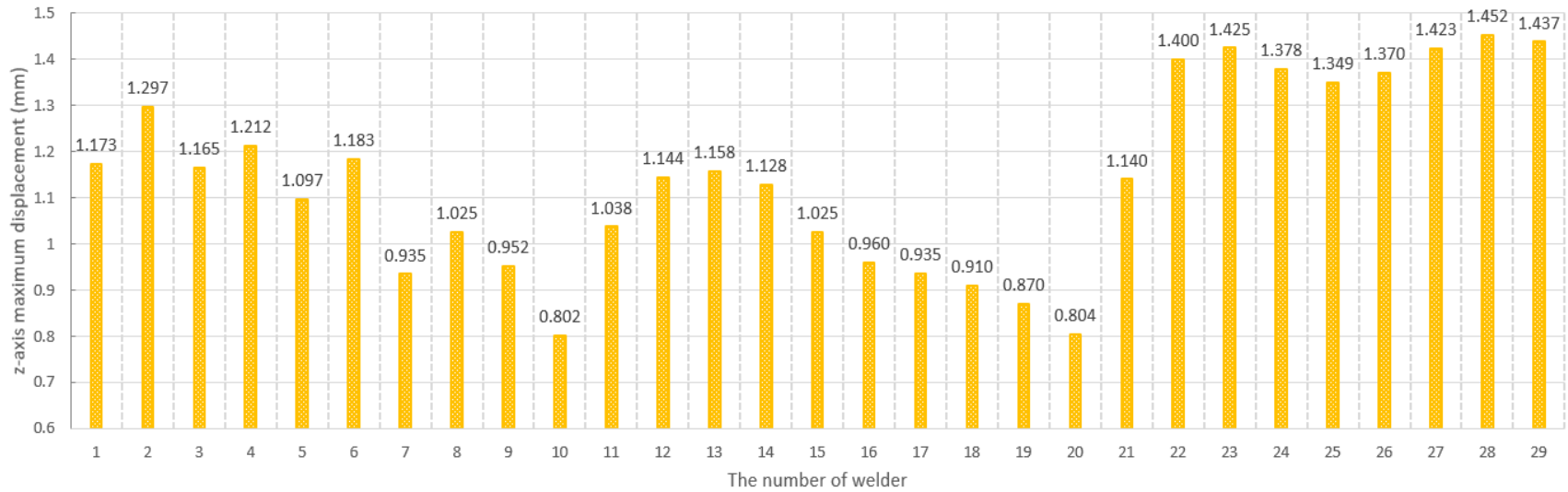


Figure 4.4 Maximum z-axis displacement of the simultaneous welding process by the different number of welders

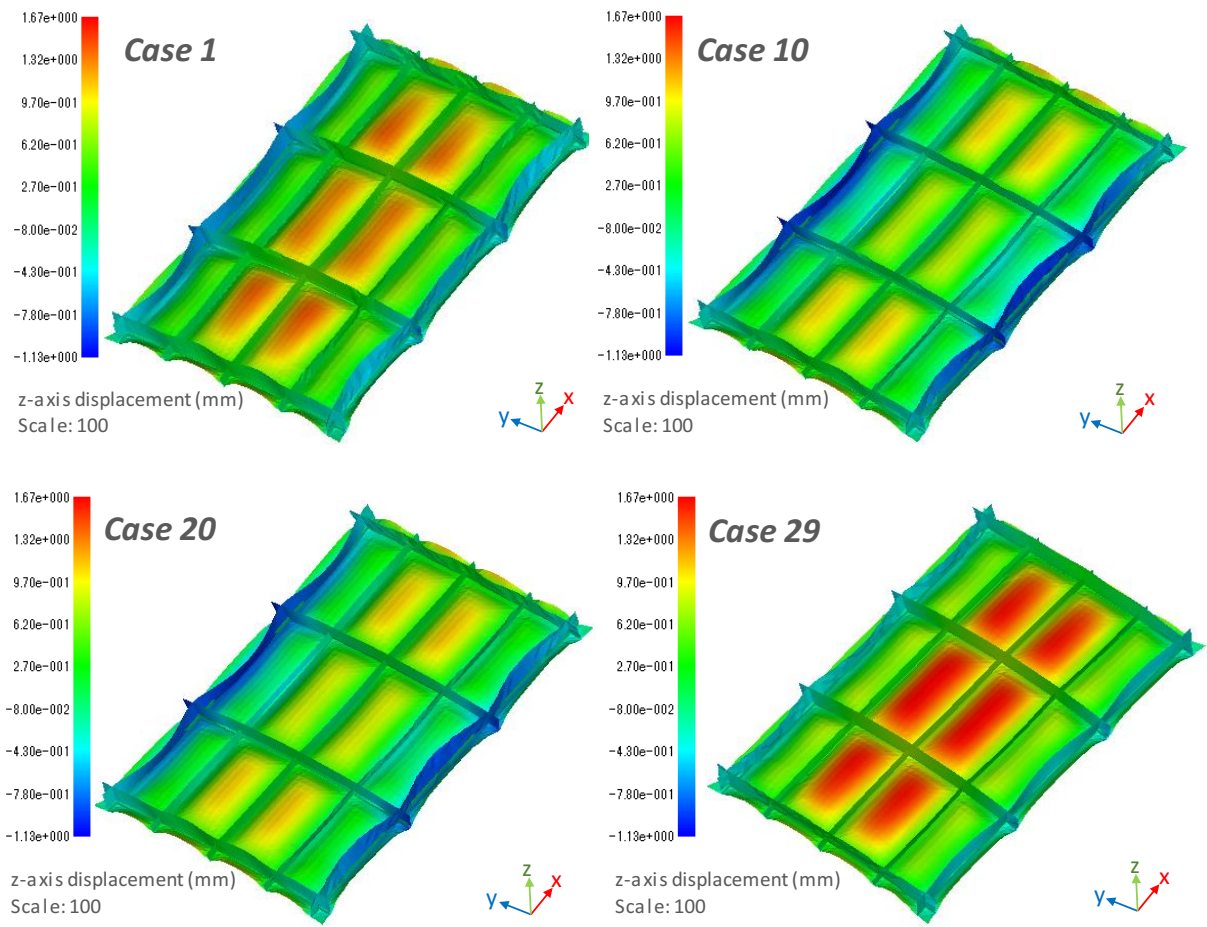


Figure 4.5 z-axis displacement of Cases 1, 10, 20 and 29

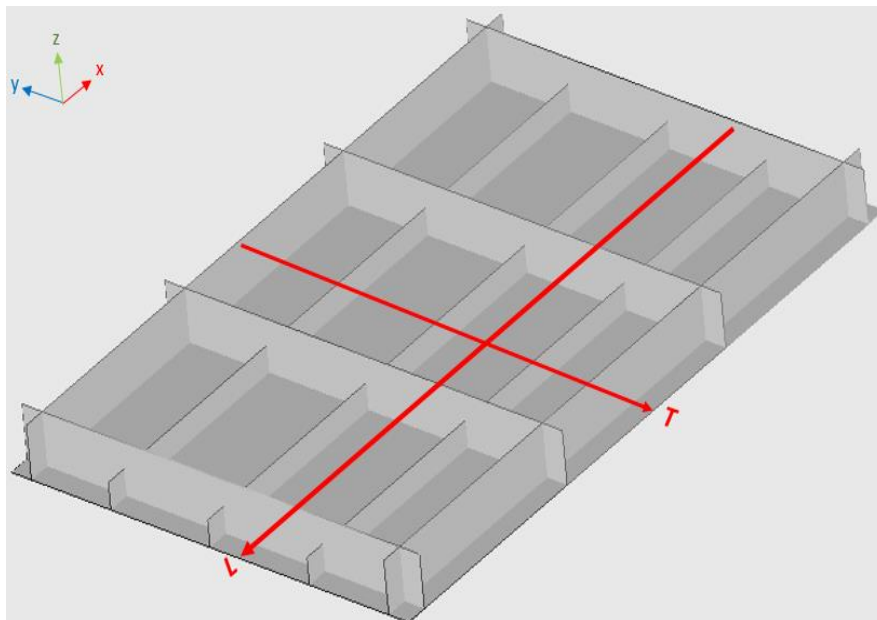


Figure 4.6 Measuring lines for the displacement distribution

The values of two lines as lines T (transverse) and L (longitudinal) shown in Figure 4.6 are measured to compare the distribution curves of the floor plate displacement. Figures 11 and 12 show that the optimal number of welders for the simultaneous welding process mitigates the overall z-axis distribution of the welding displacement. Comparing to z-axis displacement distribution of Cases 10 and 20, although both cases have the similar value of  $A_{distance}$ , Case 10 has smaller buckled deformations than Case 20 in Figures 4.7 and 4.8.

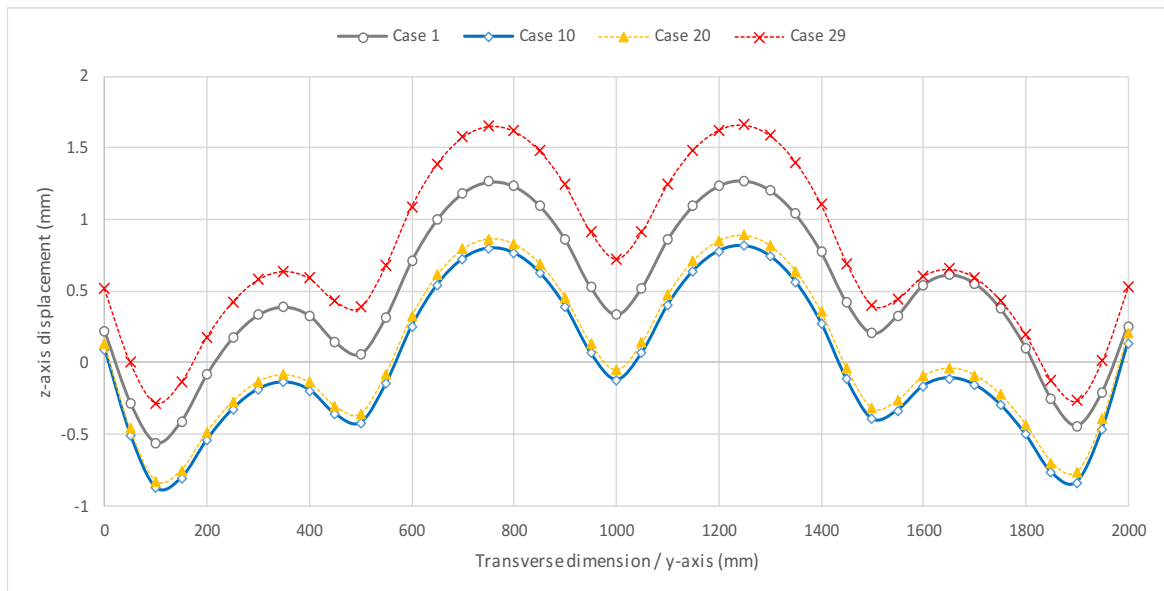


Figure 4.7 z-axis displacement distribution curve along Line T (Cases 1, 10, 20 and 29)

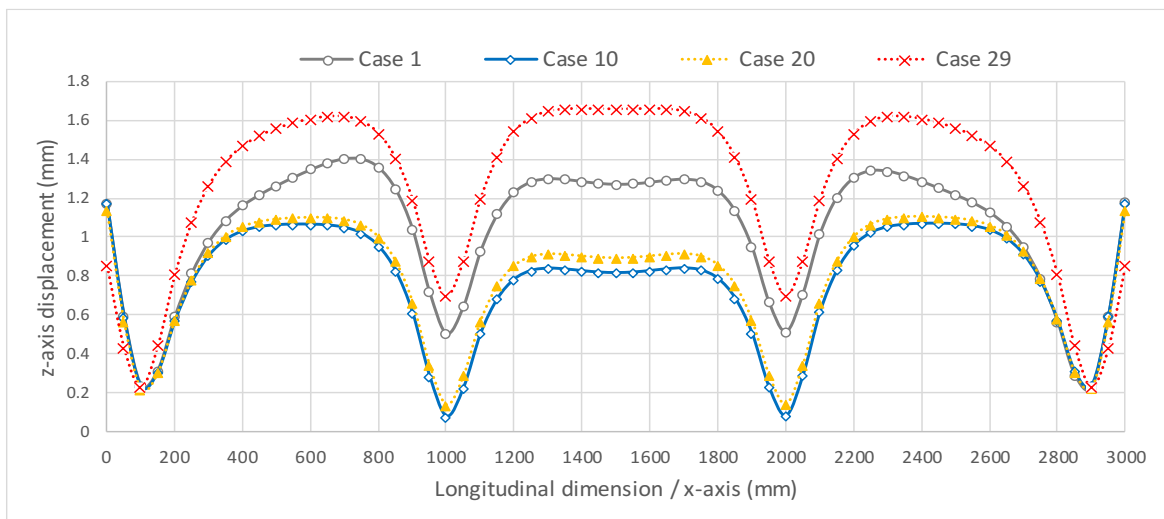


Figure 4.8 z-axis displacement distribution curve along Line L (Cases 1, 10, 20 and 29)

Table 4.2 Result of each step of Case 19 and Case 20 for simultaneous welding processes

Case 10	Simultaneous welding part	Step 1 Vertical (10)	Step 2 Vertical (10)	Step 3 Transvers (4) + Longitudinal (5)
	Grouped welding lines	20 + 19 + 24 + 23 + 15 + 16 + 14 + 17 + 22 + 25	18 + 21 + 27 + 28 + 11 + 12 + 26 + 29 + 10 + 13	6 + 9 + 7 + 8 + 1 + 5 + 4 + 2 + 3
	$A_{distance}$ at end of step	0.1357	0.2957	0.3431
Case 20	Simultaneous welding part	Step 1 Vertical (20)		Step 2 Transvers (4) + longitudinal (5)
	Grouped welding lines	20 + 19 + 24 + 23 + 15 + 16 + 14 + 17 + 22 + 25 + 18 + 21 + 27 + 28 + 11 + 12 + 26 + 29 + 10 + 13		6 + 9 + 7 + 8 + 1 + 5 + 4 + 2 + 3
	$A_{distance}$ at end of step	0.3127		0.3513

The result of  $A_{distance}$  at each step of differently grouped simultaneous welding process of Cases 10 and 20 is shown in Table 4.2. Comparing to Case 20, Case 10 has the two steps for welding total vertical lines of the structure. After finishing welding all vertical lines, Case 10 has lower  $A_{distance}$  than Case 20 in Table 4.2. In Case 10, vertical welding lines which are positioned at the center of the structure are welded before welding side vertical lines. Thus, prior to obtaining the sufficient stiffness of the center of the structure, simultaneously welding excessive number of parts leads to higher welding displacements.

## 4.6 Optimal group of the welding sequence

According to above results, two points are noted for optimally grouping welding sequence. At first, simultaneously welding vertical lines which are positioned at the center of the structure improves the stiffness of the center of the structure prior to causing excessive welding displacements. Secondly, welding transverse and longitudinal lines together after finishing the vertical welding lines produce a palliative effect on reducing the final welding displacement. Complying with those two points, optimal group of the welding sequence is proposed as Table 4.3. Comparing to Case 10, this grouped welding sequence leads to 5.7 % reduction of  $A_{distance}$  from Case 10 which is the best in the previous 29 Cases. In Figures 4.9 and 4.10, the proposed optimal group of the welding sequence leads to the mitigation of the distribution curve of welding displacements.

Table 4.3 Result of each step of optimally grouped simultaneous welding processes

Simultaneous welding part	Step 1 Vertical (6)	Step 2 Vertical (14)	Step 3 Transvers (4) + longitudinal (5)
Grouped welding lines	20 + 19 + 24 + 23 + 15 + 16	14 + 17 + 22 + 25 + 18 + 21 + 27 + 28 + 11 + 12 + 26 + 29 + 10 + 13	6 + 9 + 7 + 8 + 1 + 5 + 4 + 2 + 3
$A_{distance}$ at end of step	0.1331	0.2897	0.3234

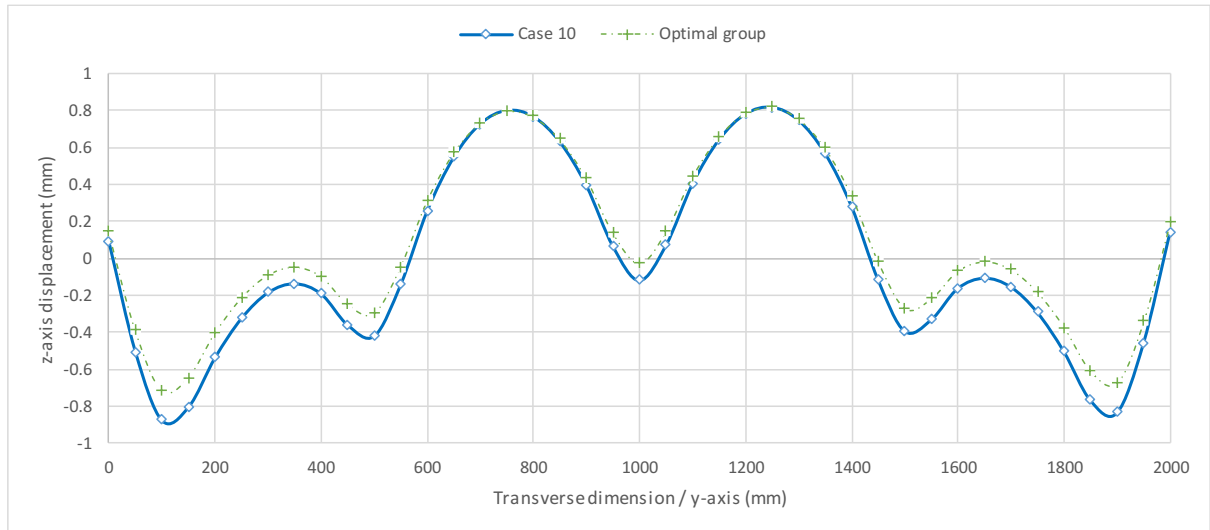


Figure 4.9 z-axis displacement distribution curve along Line T (Case 10, and Optimal group)

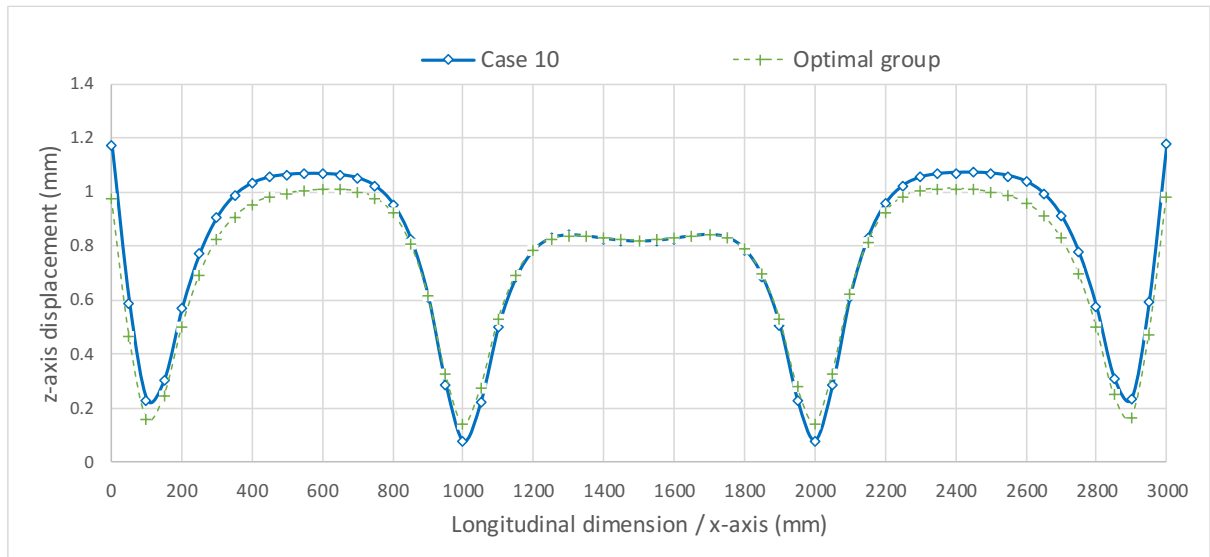


Figure 4.10 z-axis displacement distribution curve along Line L (Case 10, and Optimal group)

## 4.7 Discussion of the risk magnitude of welding displacement

There is no officially allowable welding deformation in the field. Generally, even small welding displacements of separately welded huge block structures could lead high misalignment in the assembling process which results in the reduction of structural safety and the increase of work time to revise the displacements in heavy industries. Thus, many previous studies have been focusing on minimizing welding displacement as much as possible to improve the quality of welded structure and save working time for revising welding displacements.

In Figure 4.4, the z-axis maximum displacement is 1.452 mm as Case 28. Its magnitude of deformation could be considered as very small in the view of the total dimension of the floor plate (2000 mm × 3000 mm × 10 mm). However, when supposed to have 1.452 mm displacement at the end of the cantilever model which looks like the corner of the floor plate as Figure 4.11, the maximum stress is 435.6 MPa. In the assembling process of welded structure blocks, these stresses could lead to the unfavorable accumulation of the high stress.

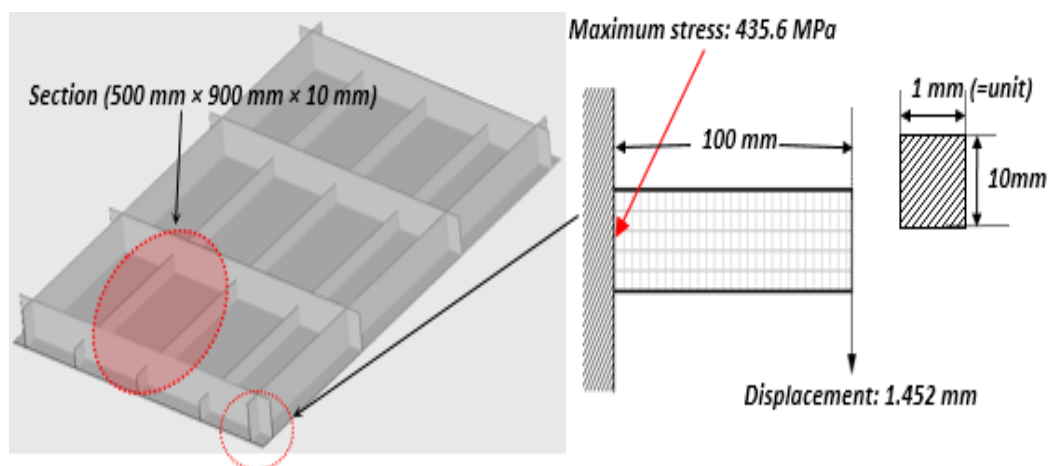


Figure 4.11 Magnitude of the stress with welding displacement

With regard to the maximum initial deflection, (SMITH et al., 1988) approximated the maximum measured initial deflection as Eqs 4.1 and 4.2.

$$w_{max}/h = \alpha_L \beta^2 \quad (4.1)$$

$$\beta = b_p/h\sqrt{\sigma_Y/E} \quad (4.2)$$

Based on the statistical investigation of the measurement values, (SMITH et al., 1988) proposed the reference value for the coefficient that express the magnitude level of the intimal deflection as follow:

$\alpha = 0.025$  : slight

$\alpha = 0.1$  : average

$\alpha = 0.3$  : severe

The coefficient of initial deflection due to welding of the section (500 mm × 900 mm × 10 mm) of the general ship grillage structure as Figure 4.11 is calculated. In the calculation, the maximum displacement is supposed to be 1.452 mm as the result of Case 28 in the paper. According to the result of the calculation, the value of the coefficient ( $\alpha_L$ ) is 0.06. Thus, the initial deflection (1.452 mm) of the general ship grillage structure could not be considered as ignorable dangerous factor for the structural safety.

Based on the above aspect, comparing the z-axis maximum displacement of Cases 10 and 28, although those difference is 0.65 mm, the efficiency for the reduction of the risk magnitude of initial deflection due to welding is 44.8% with using optimal simultaneous welding.

## 4.8 Conclusion

In principle, many welders and robotic welding machines working together for a huge block steel structure generally reduce the work time in heavy industries. However, this general knowledge should carefully be considered in fabricating huge steel structures because a wrongly grouped optimized welding sequence could cause a high displacement, which then leads to the increase of the re-work time.

The conclusion of this research and suggestions are as follows:

1. Even if the number of welders is enough to simultaneously weld all welding lines, vertical welding lines should first be welded before welding transverse and longitudinal welding lines. The role of vertical welding lines limits the displacement caused by the direct heat operation on the bottom plate. Additionally, firstly welding group of vertical lines which are positioned at the center of the structure is preferred for obtaining sufficient stiffness of the center area.
2. Welding transverse and longitudinal lines together after finishing the vertical welding lines produce a palliative effect on reducing the final welding displacement. Hence, based on understanding the role of each welding line, an optimally grouped welding sequence is helpful in improving building ships and offshore structures.
3. Even if the optimized welding sequence is employed to build a structure, a wrongly grouped simultaneous welding sequence leads to a higher displacement for the structure. Therefore, a further study to efficiently use human resource to make optimally grouped welding sequence is essential.

## 5. Numerical prediction of welding distortion considering gravity force on general ship grillage structure by elastic FEM using inherent strain

### 5.1 Introduction

The accurate numerical prediction of welding deformation is important to improve the structural safety of ships and offshore structures in heavy industries. The precise reflection of the real working condition in the numerical prediction is an essential factor to improve its result. In the present study, the effect of the gravity force on numerical prediction of the optimal welding sequence of a general ship grillage structure was validated with the introduction of a new boundary condition in which the structure is placed over rails. Additionally, the direction of the gravity force of welded structures could be changed at the final assembly process according to the production plan as Figure 5.1. The effect of the gravitational orientation on the final welding displacements was also investigated herein. The elastic finite element method using the inherent strain, interface element and multipoint constraint function was introduced to analyze the welding deformation. This study validated the influence of the gravity force on the numerical prediction of welding displacements in a general ship grillage structure.

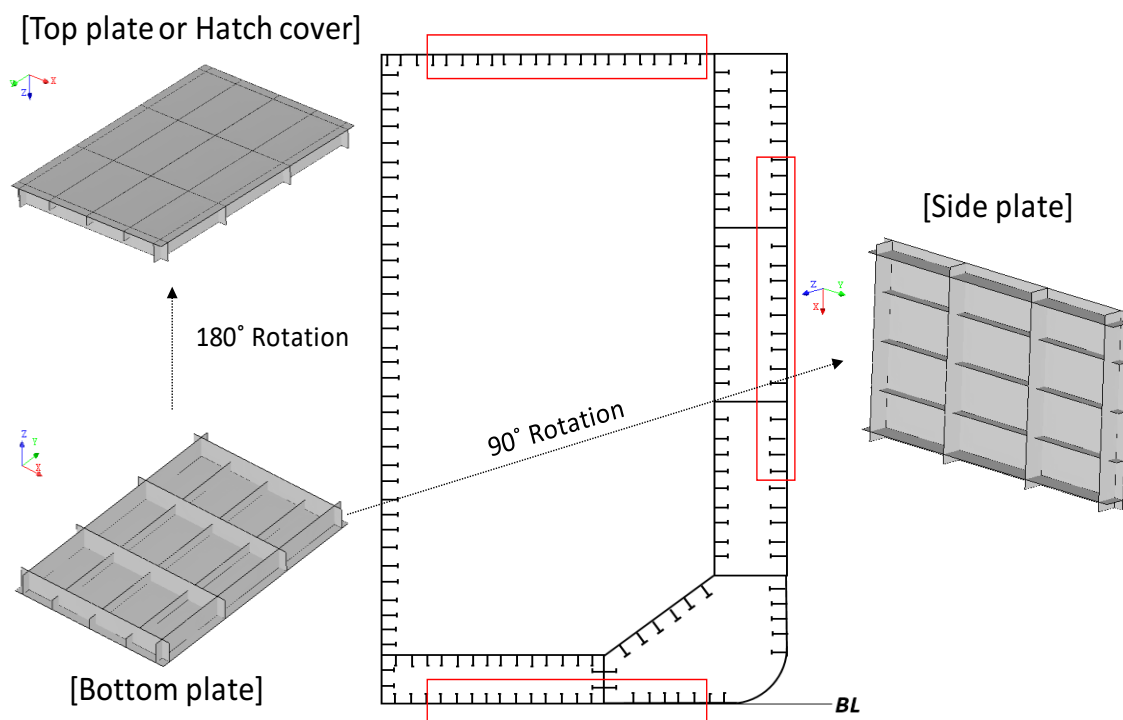


Figure 5.1 Change of the effect of the gravitational orientation on welded structures

### 5.2 Analysis model

To compare the effect of the gravity force on the numerical prediction of the optimal welding sequence of a welded structure, the general ship grillage structure which was introduced in the previous study is

introduced in the present study. HT20 steel is used to the structure as Table 1.2. Fig. 3.2 illustrates the dimension of the analysis model. CO<sup>2</sup> arc butt welding is used herein as Table 1.1. All the cross-section upper and bottom points were originally applied to MPC to assume tack welding and outline the complete structure before being in a full welding operation. A total of 29 welding lines are used, and three groups are categorized as longitudinal (1–5), transverse (6–9), and vertical (10–29).

### 5.3 Boundary condition of the rails considering the gravity force

Previous studies on the prediction of welding distortion using a numerical simulation did not consider the effect of the gravity force in the welding process. The magnitude of the gravity force and its influence on the structure depend on the dimension of the structure and the background condition of the welding work. Thus, the introduction of a boundary condition reflecting the real working condition is important to improve the numerical simulation analyzing the welding distortion. Previous studies generally introduced a simple boundary condition to control only the rigid body motion of the structures employed in the numerical simulations. Representatively, Figure 5.2 shows the simple boundary condition to constrain the motion of a general ship grillage structure. Based on the boundary condition, the gravity is applied to the structure prior to the beginning of the welding process. In Figure 5.2, the bottom plate of the general ship grillage structure is obviously deformed in the gravity direction, except at the position of the four corners, where fixed boundary conditions are given. The z-axis maximum displacement of the bottom plate is approximately 0.72 mm. In terms of the hazardous initial deflection in heavy industries, the shape of the deformation caused by the gravity and the magnitude of the z-axis maximum displacement are not negligible and are ideal for the considering real working environment.

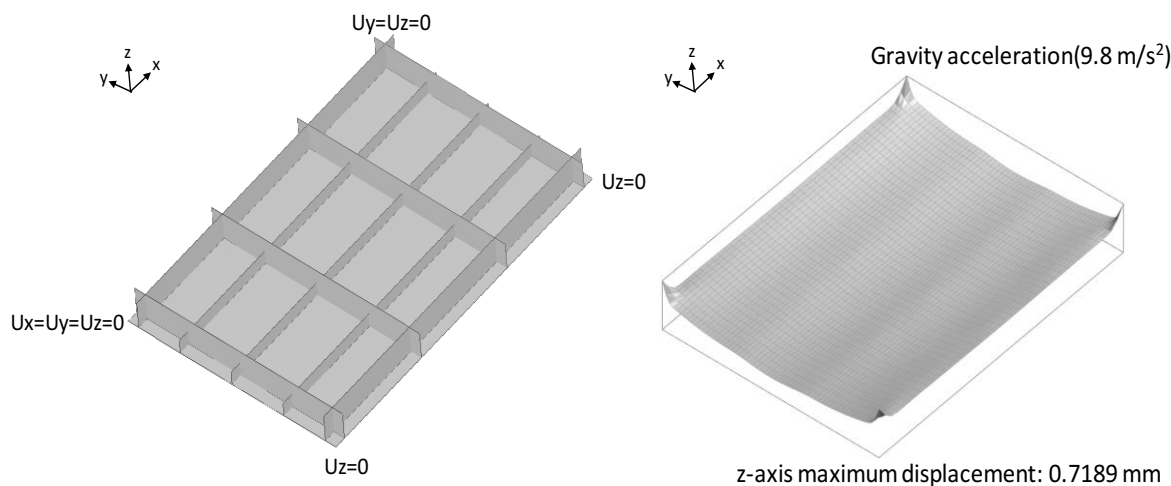


Figure 5.2 Effect of gravity force on the bottom plate under the simple boundary condition



Figure 5.3 Welding work environment in heavy industries

A bottom plate is positioned on the floor or rails when stiffeners are welded to the bottom plate, as shown in Figure 5.3 (PEMA, 2016). In particular, with the recent introduction of the automated robot welding method, rails are widely used to support a bottom plate for improving the productivity of the work process in heavy industries. In the present study, to reflect the real working condition when the bottom plate is positioned on rails, the rails are positioned behind the longitudinal stiffeners of the general ship grillage structure, as depicted in Figure 5.4. The interface element is introduced to define the mechanical relationship between the bottom plate and rails, which are considered as touching each other when processing the numerical simulation for the welding sequence. The interface element works as the boundary condition so that all the nodes of the bottom plate along the rails can move in any direction without restriction, except for the  $-z$  direction. In Figure 5.4, based on the newly introduced boundary condition, the  $z$ -axis maximum displacement of the bottom plate owing to the effect of gravity is approximately  $4.13\text{E-}7$  mm. It is a negligibly small size comparing to the previous  $z$ -axis maximum displacement ( $0.72$  mm) and could be considered as the ideal condition prior to beginning the welding process.

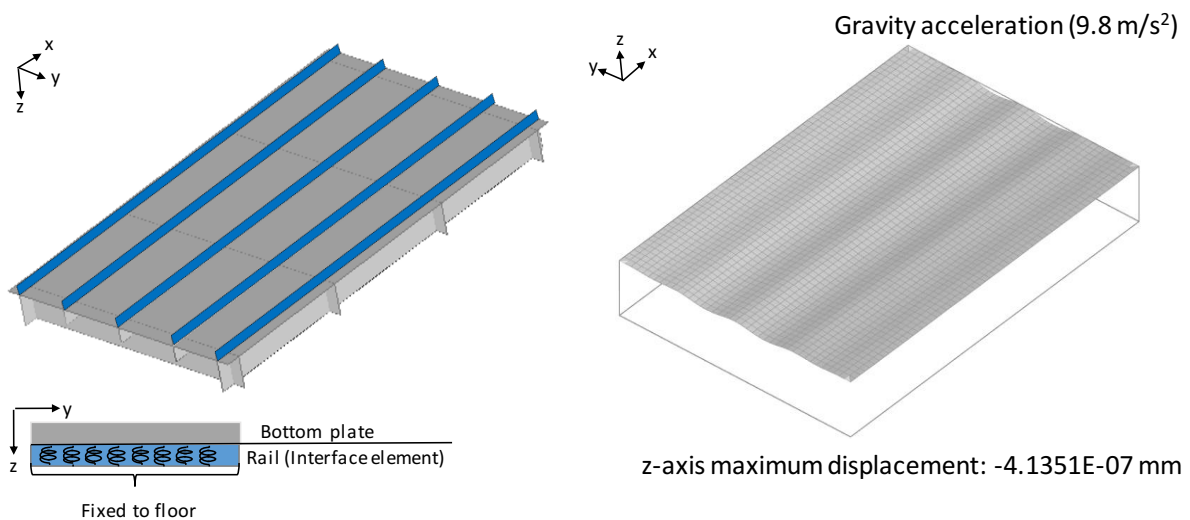


Figure 5.4 Effect of gravity on the bottom plate under the rail boundary condition

## 5.4 Effect of the gravity force under the rail boundary condition on welding sequence

Chapter 3 proposed a method to systemically order the welding sequence for a general ship grillage structure under the basic boundary condition as shown in Figure 5.2. In the present study, the proposed method to order the welding sequence systemically was carried out under the rail boundary condition considering the gravity force.

### 5.4.1 Effect of each welding line on the bottom plate

According to Chapter 3, the gap between the stiffeners and the bottom plate is measured when all the welding lines are respectively welded alone to analyze the effect of each welding line on the structure, as presented in Figure 5.5. In Figure 5.5, the newly proposed boundary condition successfully reduces the overall gap between the stiffeners and the bottom plate by 23% and 37% at welding lines 3 and 6, which present large gaps with the simple boundary condition. The rail boundary condition highly constraints deformation of the structure because a compression force is consistently applied to the stiffeners and the bottom plate and the rails prevent the bottom plate from deforming downward. However, in Figure 5.5, compared to the result of the simple boundary condition, the role ratio of each welding line among all welding lines to the overall gap under the rail boundary condition has a similar tendency.



Figure 5.5 Total gap between the welding lines and plate, after welding each line

### 5.4.2 Welding sequence

According to the method of the chapter 3 for systemically ordering the welding sequence, this study conducted 24 different welding sequences based on the data of the overall gap of each welding line, as presented in Tables 5.1 and 5.2. Category A classifies the welding lines into horizontal and vertical by their directions, as listed in Table 5.1. The horizontal welding lines consist of transverse and longitudinal welding lines. Category B divides the welding lines of the horizontal lines as longitudinal

and transverse welding lines for a deep analysis, as presented in Table 5.2. In Tables 5.1 and 5.2, ‘H’ denotes the preference of the first order of the welding line, which leads to a high value of the gap, and ‘L’ is the opposite.

Table 5. 1 Welding sequences of Category A

	Seque nce	Welding sequence preference			Welding sequence	
<b>Category A</b>	A-1	Horizo ntal	H	Vertical	H	6→9→7→8→3→2→4→5→1→20→19→24→23→15→16→14→17→22→25→18→21→27→28→11→12→26→29→10→13
	A-2		H		L	6→9→7→8→3→2→4→5→1→10→13→26→29→11→12→27→28→18→21→22→25→14→17→15→16→23→24→19→20
	A-3		L		H	1→5→4→2→3→7→8→6→9→20→19→24→23→15→16→14→17→22→25→18→21→27→28→11→12→26→29→10→13
	A-4		L		L	1→5→4→2→3→7→8→6→9→10→13→26→29→11→12→27→28→18→21→22→25→14→17→15→16→23→24→19→20
	A-5	Vertica l	H	Horizon tal	H	20→19→24→23→15→16→14→17→22→25→18→21→27→28→11→12→26→29→10→13→6→9→7→8→3→2→4→5→1
	A-6		H		L	20→19→24→23→15→16→14→17→22→25→18→21→27→28→11→12→26→29→10→13→1→5→4→2→3→7→8→6→9
	A-7		L		H	10→13→26→29→11→12→27→28→18→21→22→25→14→17→15→16→23→24→19→20→6→9→7→8→3→2→4→5→1
	A-8		L		L	10→13→26→29→11→12→27→28→18→21→22→25→14→17→15→16→23→24→19→20→1→5→4→2→3→7→8→6→9

Table 5. 2 Welding sequences of Category B

	Seque nce	Welding sequence preferences			Welding sequence			
<b>Category B</b>	B-1	Vertical	H	Longitudinal	Transverse	H	13→10→26→29→12→11→27→28→18→21→25→14→22→17→16→23→15→24→19→20→3→2→4→5→1→6→9→7→8	
	B-2					L	13→10→26→29→12→11→27→28→18→21→25→14→22→17→16→23→15→24→19→20→3→2→4→5→1→7→8→6→9	
	B-3					H	H	13→10→26→29→12→11→27→28→18→21→25→14→22→17→16→23→15→24→19→20→1→5→4→2→3→6→9→7→8
	B-4					H	L	13→10→26→29→12→11→27→28→18→21→25→14→22→17→16→23→15→24→19→20→1→5→4→2→3→7→8→6→9
	B-5					L	H	H

<b>Category B</b>	B-6		L		H	L	19→20→24→15→23→16→17→22→14→25→18→ 21→28→27→11→12→29→26→10→13→3→2→4 →5→1→7→8→6→9	
	B-7		L		L	H	19→20→24→15→23→16→17→22→14→25→18→ 21→28→27→11→12→29→26→10→13→1→5→4 →2→3→6→9→7→8	
	B-8		L		L	L	19→20→24→15→23→16→17→22→14→25→18→ 21→28→27→11→12→29→26→10→13→1→5→4 →2→3→7→8→6→9	
	B-9	Vertical	Transverse	Longitudinal	H	H	H	13→10→26→29→12→11→27→28→18→21→25→ 14→22→17→16→23→15→24→19→20→3→2→4 →5→13→6→9→7→8→3→2→4→5→1
	B-10				H	H	L	13→10→26→29→12→11→27→28→18→21→25→ 14→22→17→16→23→15→24→19→20→3→2→4 →5→1→5→4→2→3
	B-11				H	L	H	13→10→26→29→12→11→27→28→18→21→25→ 14→22→17→16→23→15→24→19→20→3→2→4 →5→7→8→6→9→3→2→4→5→1
	B-12				H	L	L	13→10→26→29→12→11→27→28→18→21→25→ 14→22→17→16→23→15→24→19→20→3→2→4 →5→7→8→6→9→1→5→4→2→3
	B-13				L	H	H	19→20→24→15→23→16→17→22→14→25→18→ 21→28→27→11→12→29→26→10→13→6→9→7 →8→3→2→4→5→1
	B-14				L	H	L	19→20→24→15→23→16→17→22→14→25→18→ 21→28→27→11→12→29→26→10→13→6→9→7 →8→1→5→4→2→3
	B-15				L	L	H	19→20→24→15→23→16→17→22→14→25→18→ 21→28→27→11→12→29→26→10→13→7→8→6 →9→3→2→4→5→1
	B-16				L	L	L	19→20→24→15→23→16→17→22→14→25→18→ 21→28→27→11→12→29→26→10→13→7→8→6 →9→3→2→4→5→1

### 5.4.3 Results and discussion of effect of gravity force under the rail boundary condition on welding sequence

The representative reference value to discuss the effect of gravity on the numerical prediction of welding displacement of the general ship grillage structure is the z-axis distance average. It is the average of the z-axis distance of all the bottom plate nodes from the z-axis displacement average as Eq. 3.1 to their original values as Eq. 3.2. To compare the z-axis distribution curves of welding displacement of the bottom plate, the values of two lines such as Line T (transverse) and Line L (longitudinal) are measured, as shown in Figure 5.6.

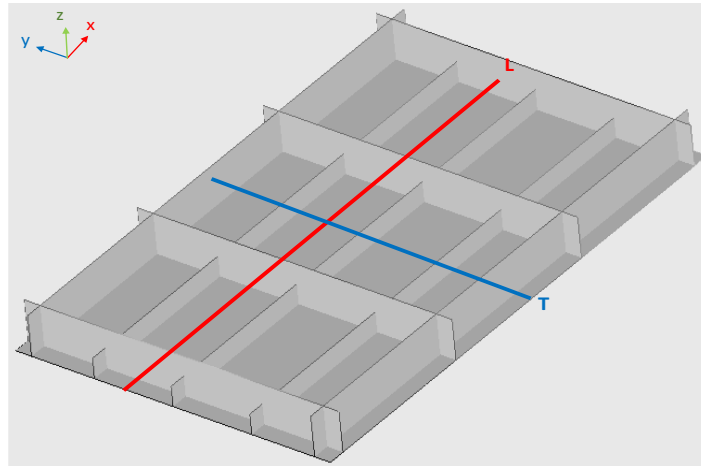


Figure 5.6 Measuring lines for the z-axis displacement distribution

Figure 5.7 shows the  $A_{distance}$  of different welding sequences of Category A under two different boundary conditions.  $A_{distance}$  in the simple boundary condition indicates the results of the chapter 3. The trend lines of  $A_{distance}$  with different welding sequences under the two different boundary conditions show a similar tendency in Figure 5.7. These results validate that the preference of welding vertical welding lines prior to starting the horizontal welding lines (longitudinal and transverse). This is because Sequences A-5, A-6, A-7 and A-8 in Category A under the rail boundary condition with the gravity force have smaller  $A_{distance}$  than sequences A-1, A-2, A-3 and A-4 and the results of the simple boundary condition. Comparing to these values, the newly proposed boundary condition leads to approximately 37.9%~54.1% reduction in  $A_{distance}$ . Although the bottom plate and rails touch each other under the gravity force during processing of the welding sequence in the newly proposed boundary, these considerably constraint the structure and lead to the difference. The gravity force of the structure mitigates significantly welding displacement without additional clamps for the restriction of its movement.

Figure 5.8 shows the  $A_{distance}$  of different welding sequences of Category B under two different boundary conditions. The trend lines of  $A_{distance}$  with different welding sequences under the two different boundary conditions show a similar tendency in Figure 5.8. As in Figure 5.7, the rail boundary condition results in 58.7%~ 67.4% reduction in  $A_{distance}$  of the welding sequences of Category B. Category B-10 has the lowest  $A_{distance}$  as 0.38 mm and 0.19 mm respectively under the two different boundary condition. Additionally, in view of the trend lines of  $A_{distance}$  of Category B, the relative efficiency for the reduction of welding displacements of each welding sequence under both boundary conditions is not changed. The welding sequences B-3, B-7, B-10, and B-14 in Category B show a relatively low  $A_{distance}$ . The common point of these four cases is the priority of the highest gap of transverse lines in their respective welding sequences. In terms of the preference for a welding sequence between the longitudinal and transverse welding lines after finishing vertical welding lines, these results also validate that assigning priority to the transverse welding lines which produce a relatively large

overall gap prior to the longitudinal welding lines, is beneficial for mitigating the welding distortion, which is the same as the study of the chapter 3.

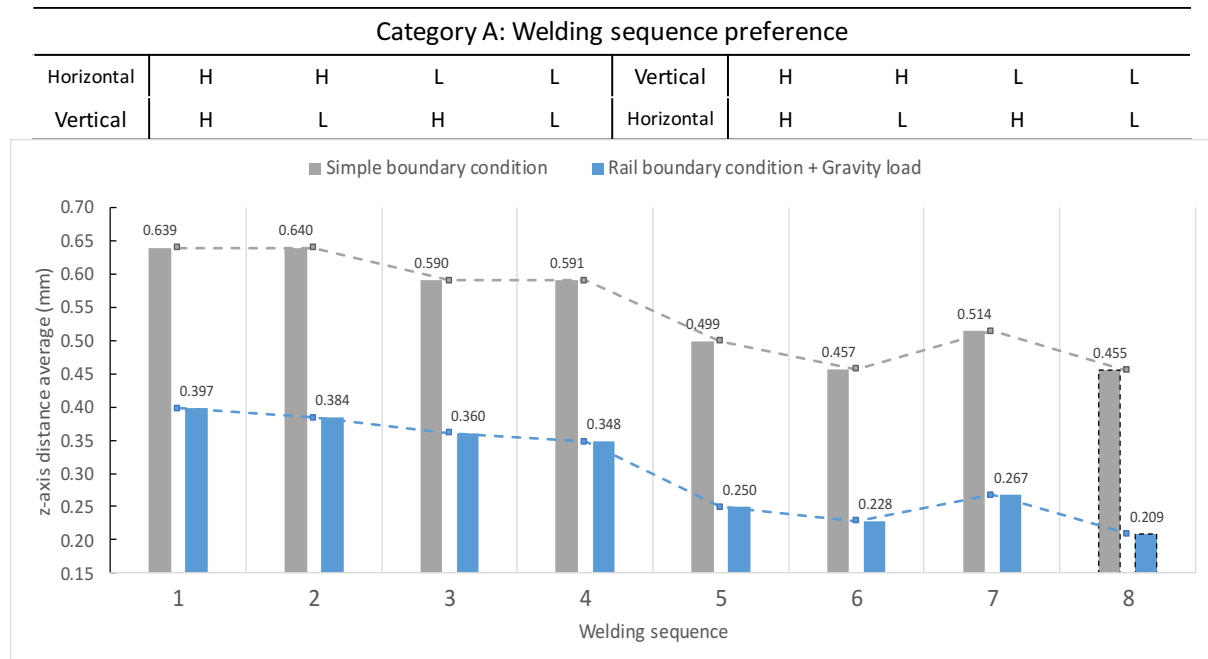


Figure 5.7  $A_{distance}$  of Category A under two different boundary condition

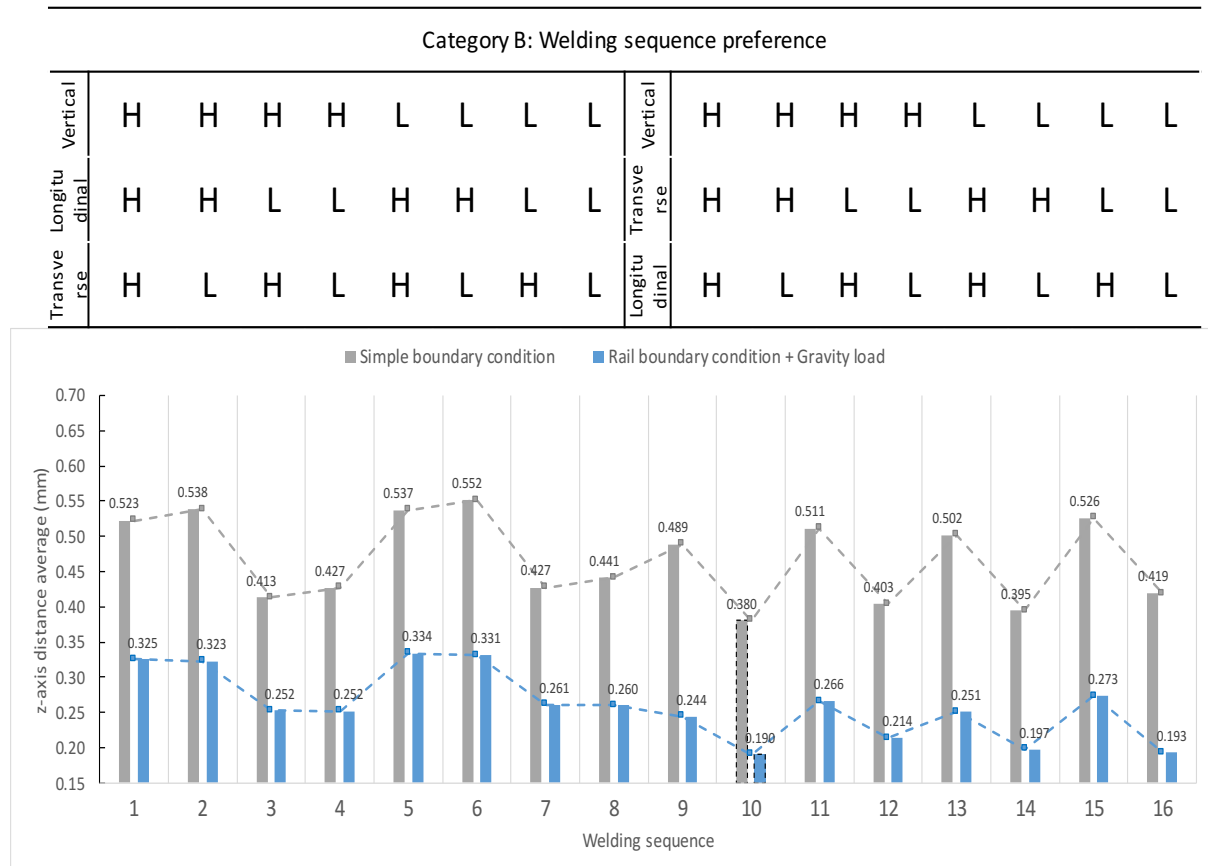


Figure 5.8  $A_{distance}$  of Category B under two different boundary condition

Figures 5.9 and 5.10 show the effect of the different boundary conditions on the z-axis displacement distribution of sequence B-10 in Category B along lines T and L. In Figure 5.9, it is observed that the buckling in the z-axis displacement distribution along line T increase when the simple boundary condition is applied. In the rail boundary condition with the gravity force, the previous tendency of the buckling feature is highly mitigated. Although there are no additional external constraints such as a jig and clamp to the rail boundary condition with the gravity force, the z-axis displacement distribution shows a different tendency compared to the simple boundary condition.

Owing to the angular distortion of welding, the general grillage structure is buckled to the upper direction. However, in 5.9, which shows the welding displacement along line L with gravity force, the buckling feature is highly mitigated. In Figure 5.10, the effect of the rail boundary condition with the gravity force on the mitigation of the z-axis displacement distribution at the central zone is clearly shown. However, the mitigation of each end section of the z-axis displacement is not relatively distinctive compared to the mitigation of the central zone.

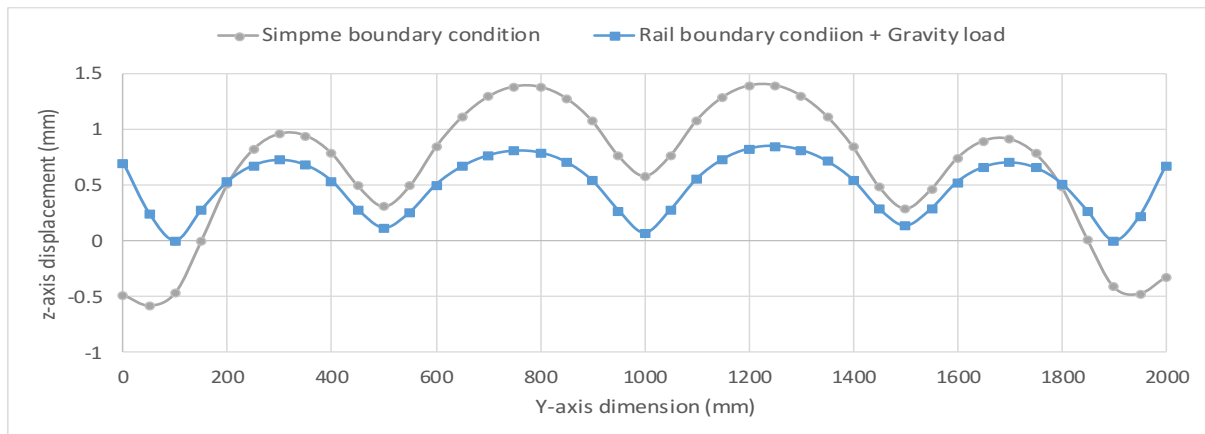


Figure 5.9 Z-axis displacement distribution along line T of Sequence B-10 under three different boundary conditions

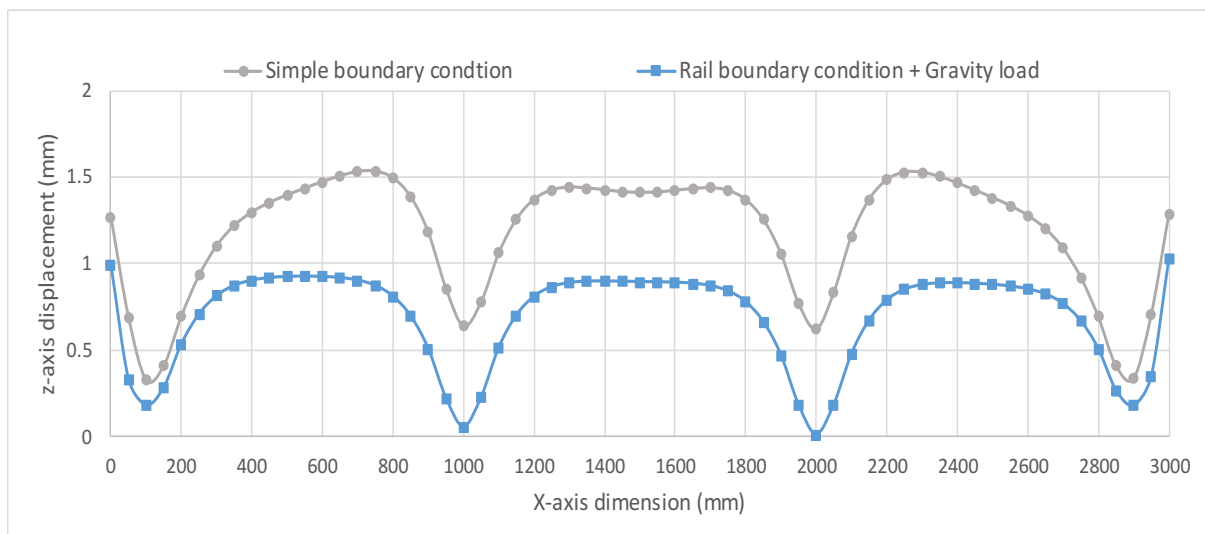


Figure 5.10 Z-axis displacement distribution along line L of Sequence B-10 under three different boundary conditions

## 5.5 Effect of the change in gravity direction on the numerical prediction of welding displacements

In heavy industries, several compartments are built separately before finally assembling them together according to the design plan. Generally, stiffeners are welded over the bottom plate to make the arc welding filler material flow well absorbed between the gaps of structures. Prior to assembling each compartment, the revision work for welding displacements under the final direction of the gravity is carried out, as shown Figure 5.11 (Abe, 2017). Thus, in the numerical prediction of welding displacements in the welding process, consideration of the change in direction of the gravity force with respect to the structure is technically essential. The present study examines the production process in heavy industries for building top and side plates. As depicted in Figure 5.1, turning of the general ship grillage structure by  $180^\circ$  and  $90^\circ$  after finishing welding of the stiffeners over the bottom plate for the final revision is numerically simulated. This allows validating the effect of the change in the gravity force on welding displacements. In the step of revision under the direction of the final plan, the general ship grillage structure is supposed to have simple supports at the four corners of the structure, as the simple boundary condition depicted in Figure 5.2, for allowing welders to revise the welding displacements under the structure.



Figure 5.11 Welding work process of a hatch cover

### 5.5.1 Results and discussion of effect of change of gravity direction on the numerical prediction of welding displacements

$A_{distance}$  as in Eq. 3.2 is representative for discussing the effect of the change in direction of the gravity force on welding displacements. In Figure 5.12,  $A_{distance}$  after reversing the structure by turning it  $180^\circ$ , is 0.212 mm, which leads to 25.4 % increase from 0.19 mm. In terms of the precise prediction of welding displacements, the value of 25.4 % is not a negligible impact factor. In other words, based on the result of the numerical prediction of welding displacement without considering the change in direction of the gravity force, the prediction of the additional production cost for the revision work would have a significant error. In Figure 5.12,  $A_{distance}$  after turning the structure  $90^\circ$  is 0.194 mm which leads to

2.1 % increase from 0.19 mm ( $A_{distance}$ ). Compared to the case of reversing the structure, the effect of the change in gravitational orientation in the case of turning it 90° is negligibly small because the dimension of the area affected by the gravity is greatly reduced from the whole plan of the bottom plate to the plan of the longitudinal stiffeners.

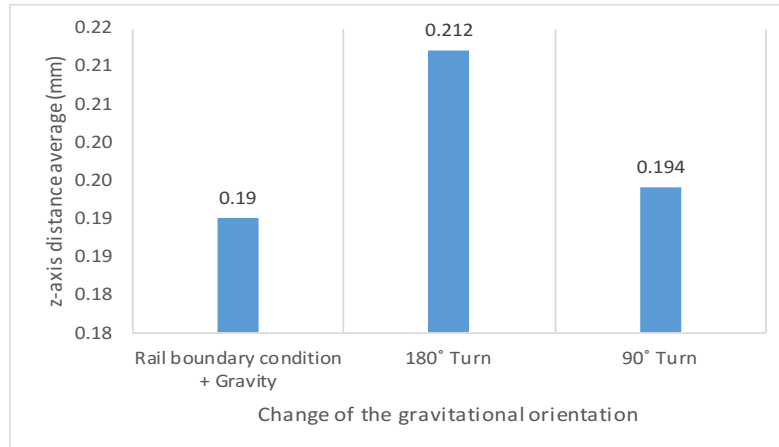


Figure 5.12  $A_{distance}$  with the change of the gravitational orientation

Figure 5.13 clearly shows the effect of reversing the general ship grillage structure on the distribution of welding displacements. Particularly, the buckling feature around the central zone obviously increases. Although the stiffness of the general ship grillage structure highly increases after finishing all the welding lines, the change in the direction of the gravity force has a considerable effect on welding displacements. However, it is difficult to recognize the effect of turning the side plate 90° on the distribution of welding displacements.

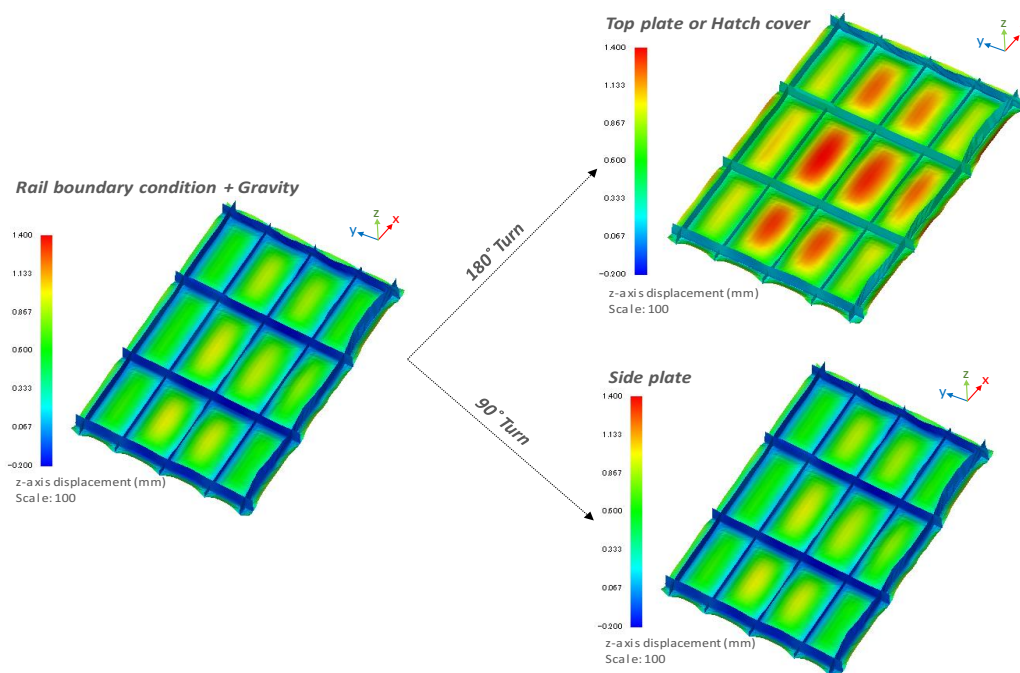


Figure 5.13 Z-axis displacement of Rail boundary condition + Gravitational orientation

## 5.6 Conclusion

In this study, the FEM approach is employed with the inherent strain, interface element and MPC to investigate the effect of the gravity force on the numerical prediction of welding displacements. This study proposes a new approach to reflect the real work environment in the numerical simulation, that is, the rail boundary condition using the interface element method. This research demonstrates the necessity of considering the gravity force in the numerical prediction of welding displacements for precisely predicting welding displacements in heavy industries. The conclusions of this research and suggestions are as follows:

1. Although the bottom plate and rails touch each other under the gravity force while processing the welding sequence under the rail boundary condition, these considerably constraint the structure, and therefore, significantly mitigate the welding displacement without additional clamps for the restriction of its movement. In other words, the numerical prediction of welding displacements without precisely reflecting the real work environment would lead to enormous errors in heavy industries.
2. In the rail boundary condition under the effect of the gravity force, the optimal welding sequence is to weld first vertically for improving the stiffness of the structure and then horizontally. It is preferable to begin the horizontal welding lines, which generate a direct heat effect on the bottom plate, as late as possible. Moreover, welding the transverse lines before the longitudinal lines is preferred for minimizing welding displacements. The conclusion is the same as that in the first study, which was validated according to the result of the simple boundary condition.
3. The change in direction of the gravity force according to the design plan has significant effects on the change in the distribution of welding displacements. Without consideration of these effects, the prediction of the additional production cost for the revision work could involve a substantial error. Thus, in the numerical prediction of welding displacements in the welding process, consideration of the change in direction of the gravity force with respect the structure is technically essential.

## **6. Systematic method for positioning clamps and strongbacks based on their influence on welding displacements**

### **6.1 Introduction**

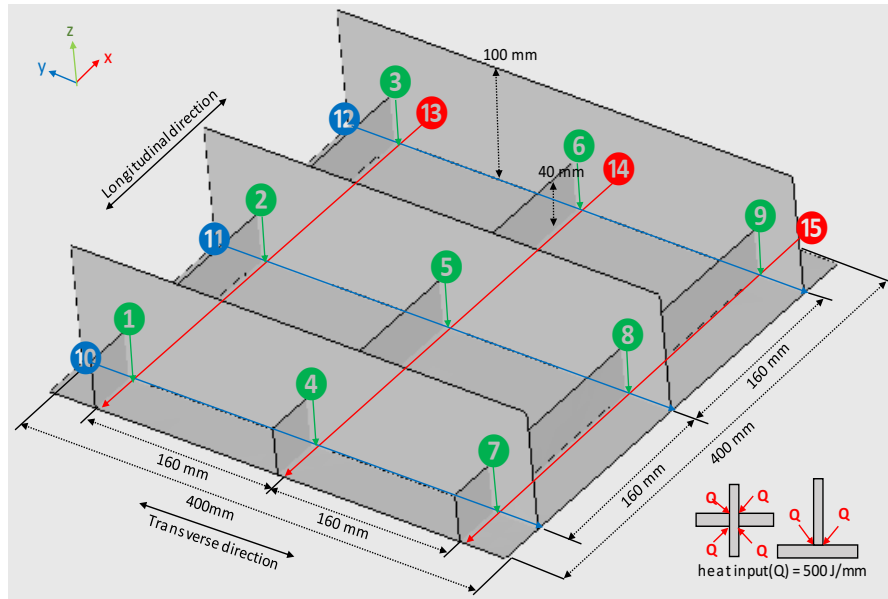
To control welding displacements, mitigation methods such as clamps and strongbacks are widely used in heavy industries. It can be easily concluded that providing for as many clamps and strongbacks as feasible on welded structures to minimize welding displacements is common knowledge, but this may not always be feasible due to restrictive work environments as well as cost factors and interference from other portions of the structure. Currently there is not a distinct system to efficiently position clamps and strongbacks at welded structures. Based on understanding of how clamps and strongbacks effect on the reduction of welding displacements, a systematic method to efficiently position them will enable improvements to the welding process. In the present study, several cases which have differently positioned clamps and strongbacks at welded structures were numerically simulated by the elastic FEM using inherent strain theory to investigate the influence of clamps and strongbacks on the reduction of welding distortions. According to the simulation data, the applicable systematic method for efficiently positioning clamps and strongbacks for minimizing welding deformations is proposed herein.

### **6.2 Analysis logic in the elastic FEM**

To reduce significant calculation time and be able to realize the sequence-based analysis, in-house developed code which based on the elastic FEM with the application of inherent strains is employed. Additionally, MPC and interface element are assigned along welding line to consider the effect of gap and misalignment in the welding sequence. In-house developed code has iteration logic system as Figure 3.1.

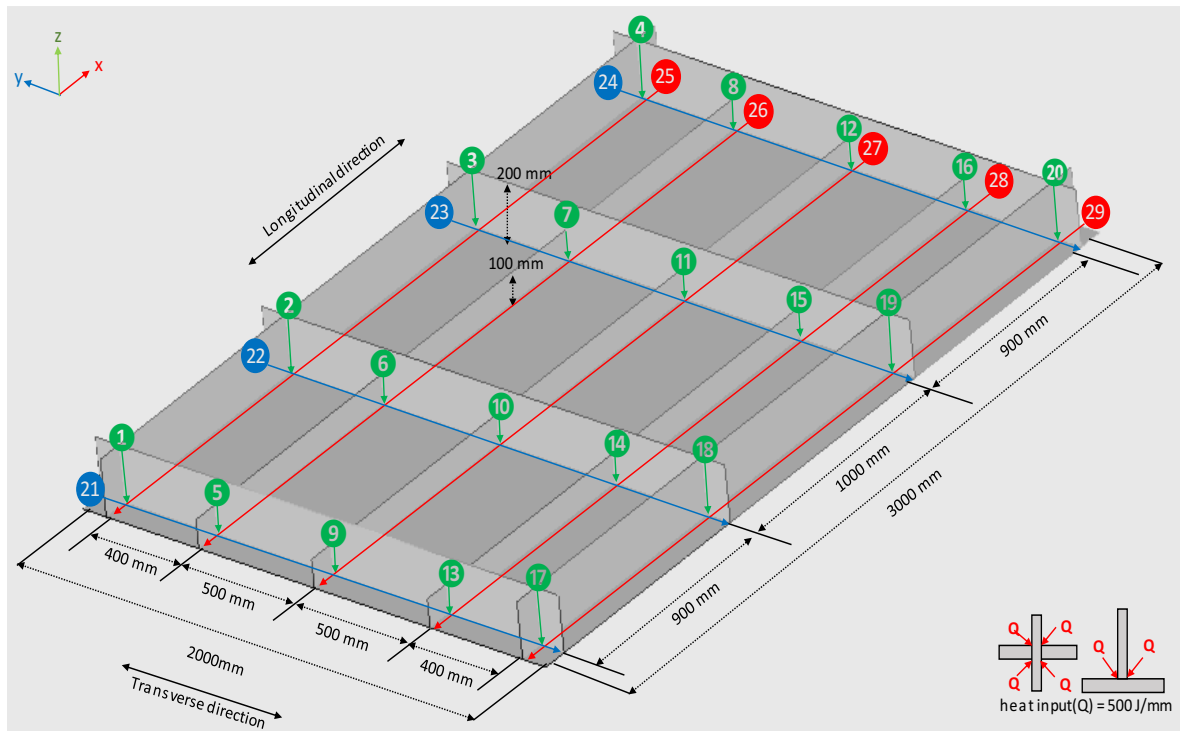
### **6.3 Analysis model**

A simple square-shaped grillage structure of 400 mm × 400 mm is employed as shown in Figure 5.1. Larger and smaller stiffeners are placed in transverse and longitudinal directions, respectively, to analyze the effects of the positions of clamps and strongbacks for preventing the structures from welding deformation. The length, height and thickness of stiffeners are also listed in Figure 6.1. Additionally, a general ship grillage structure is employed as Figure 6.2 for clearly validating the effects of these positions to welding deformation. The ship grillage structure of 3000 mm × 2000 mm is relatively large and has the different composition of stiffeners. The length, height and thickness of stiffeners are listed in Figure 6.2.



Part	Dimension (mm)
Bottom plate	400 × 400 × 10
Longitudinal stiffener (x-axis)	400 × 40 × 10
Transverse stiffener (y-axis)	400 × 100 × 10

Figure 6. 1 Square Shape Grillage Structure (400 mm × 400 mm)



Part	Dimension (mm)
Bottom plate	3000 × 2000 × 10
Longitudinal stiffener (x-axis)	3000 × 200 × 10 3000 × 100 × 10
Transverse stiffener (y-axis)	2000 × 200 × 10

Figure 6.2 General Ship Grillage Structure (3000 mm × 2000 mm)

The welding sequence of all weld lines is schematically drawn by circled numbers in Figure 6.1 and Figure 6.2. The vertical welds are finished first, and the transverse welds and longitudinal welds are sequentially performed according to the third chapter. Table 1.1 shows the arc butt welding condition. The cross points at both ends of welding lines are tack-welded prior to the full welding of the structure.

## 6.4 Effect of Additional Clamps and Efficient Positioning of Clamps to reduce Welding Displacements of the Square-Shaped Grillage Structure

During welding process, clamps are widely used to hold the structures in place. Basically, Clamps are positioned at the points where larger displacements are expected along the edge of welded structures for improving their performances. In the numerical simulation, clamps are defined by completely fixing the nodes in all axial directions. First, the basic clamping condition that clamps four corners of the bottom plate are applied to the structure. This simulation is noted as Case A-1, and shown in Figure 6.3. where yellow circles indicate the basic clamps. Additional clamps are basically positioned at nodes which have the highest displacement along each edge of Case A-1. To study the effects of the relationship between the stiffener size and the additional clamp position on the welding displacements, three cases are simulated. These cases are indicated as Cases A-2, A-3 and A-4 as shown in Figure 6.4.

A-1: Basic clamps at the corners of bottom plate marked by yellow circles

A-2: Additional clamps along the longitudinal edges marked by blue circles

A-3: Additional clamps along the transverse edges marked by red circles

A-4: Additional clamps along both of the longitudinal and transverse edges

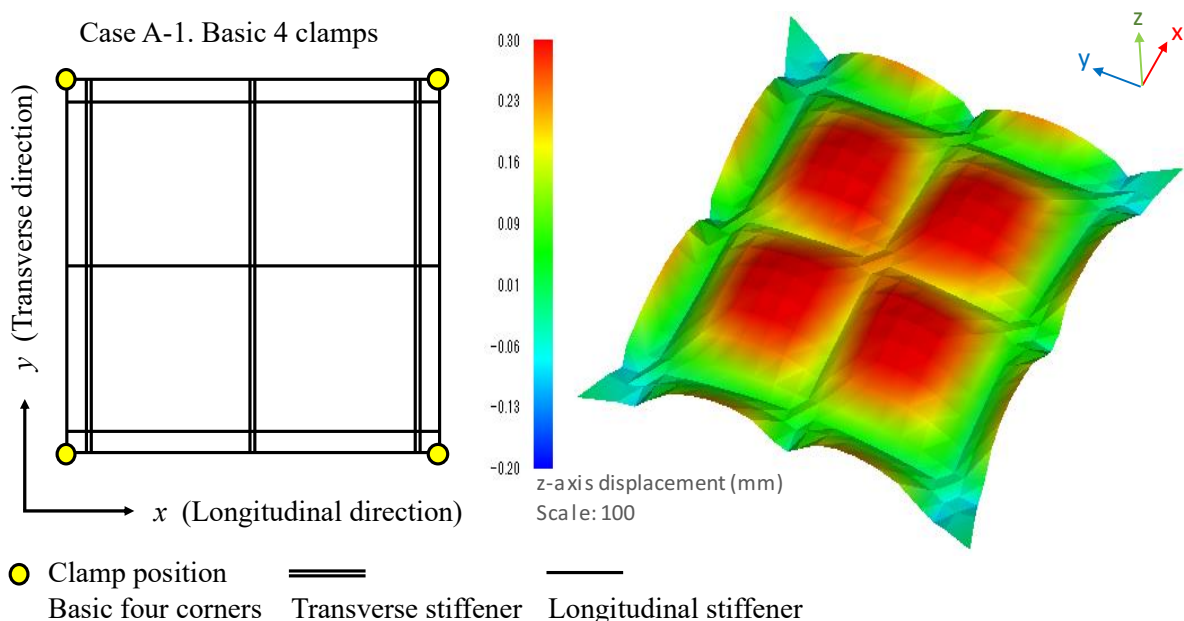


Figure 6.3 Z-axis displacement of the bottom plate of Case A-1

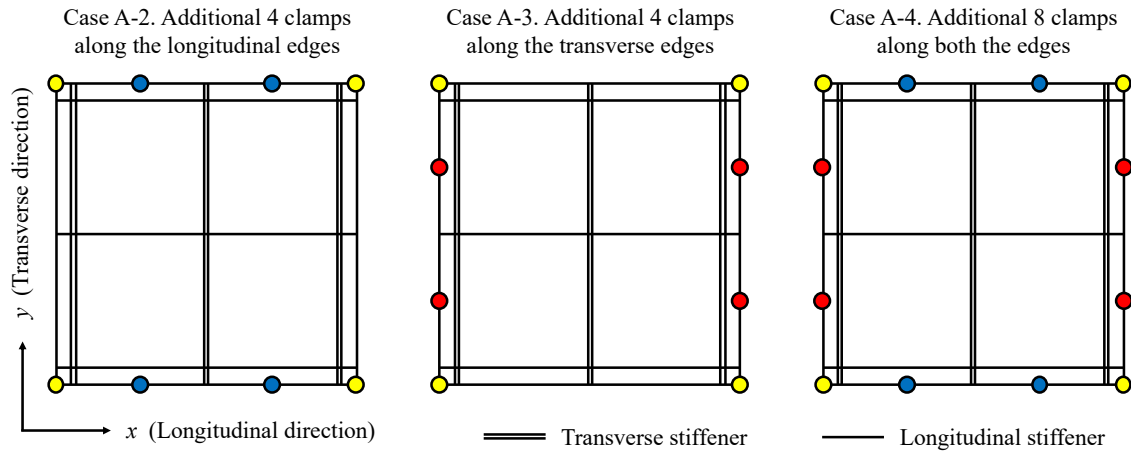


Figure 6.4 Additional clamping cases (Square shape grillage structure 400 mm × 400 mm)

### 6.4.1 Results and Discussion of the Effect of Clamping on the Square-Shaped Grillage Structure

$Z_{average}$  (Eq. 3.1) calculating the average absolute value of the z-axis nodal displacement of the bottom plate is used to see the overall effect of the additional clamps. The z-direction displacement distributions of the bottom plate along the selected two lines, ST (Transverse) and SL (Longitudinal), are compared to analyze the effects of clamp positions precisely. These lines are indicated by red lines in Figure 6.5. Additionally, the displacement along the lines of TS (Transverse stiffener) and LS (Longitudinal stiffener) of the square-shaped grillage structure are measured to analyze the effect of differently positioned clamps on stiffeners. They are shown by blue lines in Figure 6.5.

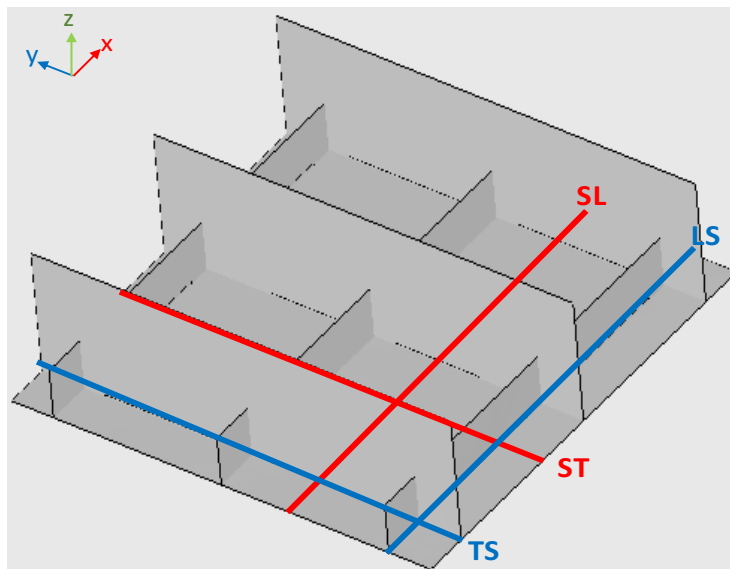


Figure 6.5 Measuring line for the displacement distribution of the square-shaped grillage structure

Figures 6.6 and 6.7 show the results of four cases A-1 ~ A-4 using different clamping schemes to hold the side edges of the square-shaped grillage structure. It is observed in Figure 6.6 that adding more

clamps (Cases A-2, A-3 and A-4) results in 42.7 ~ 55.1% reduction in  $Z_{average}$  compared to Case A-1. Figure 6.7 shows the z-axis displacement distributions of the bottom plate under these clamping schemes. It is noted that severe buckled features appear at the centers of the stiffened plates in Case A-1. Adding more clamps to the side edges of the bottom plate helped to reduce the large displacements along edges and the buckled features. It should be emphasized that  $Z_{average}$  and the z-axis displacement of the bottom plate of Case A-2 are smaller than those of Case A-3, even though the same total number of clamps have been used in both cases. Case A-4 gives the smallest  $Z_{average}$  as expected since all edges are clamped.

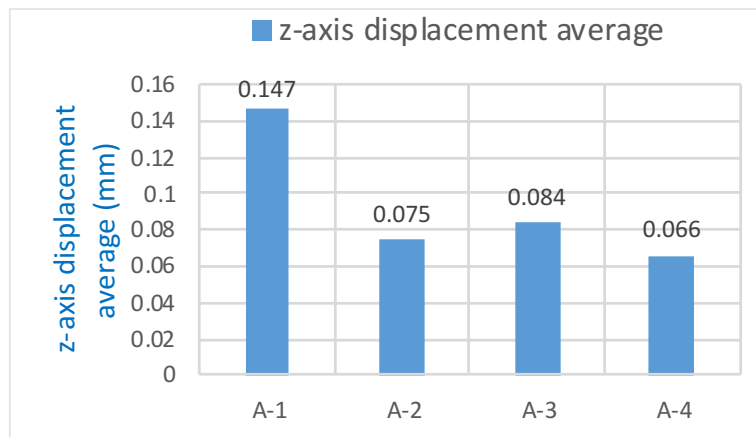


Figure 6.6  $Z_{average}$  of Cases A-1, A-2, A-3 and A-4

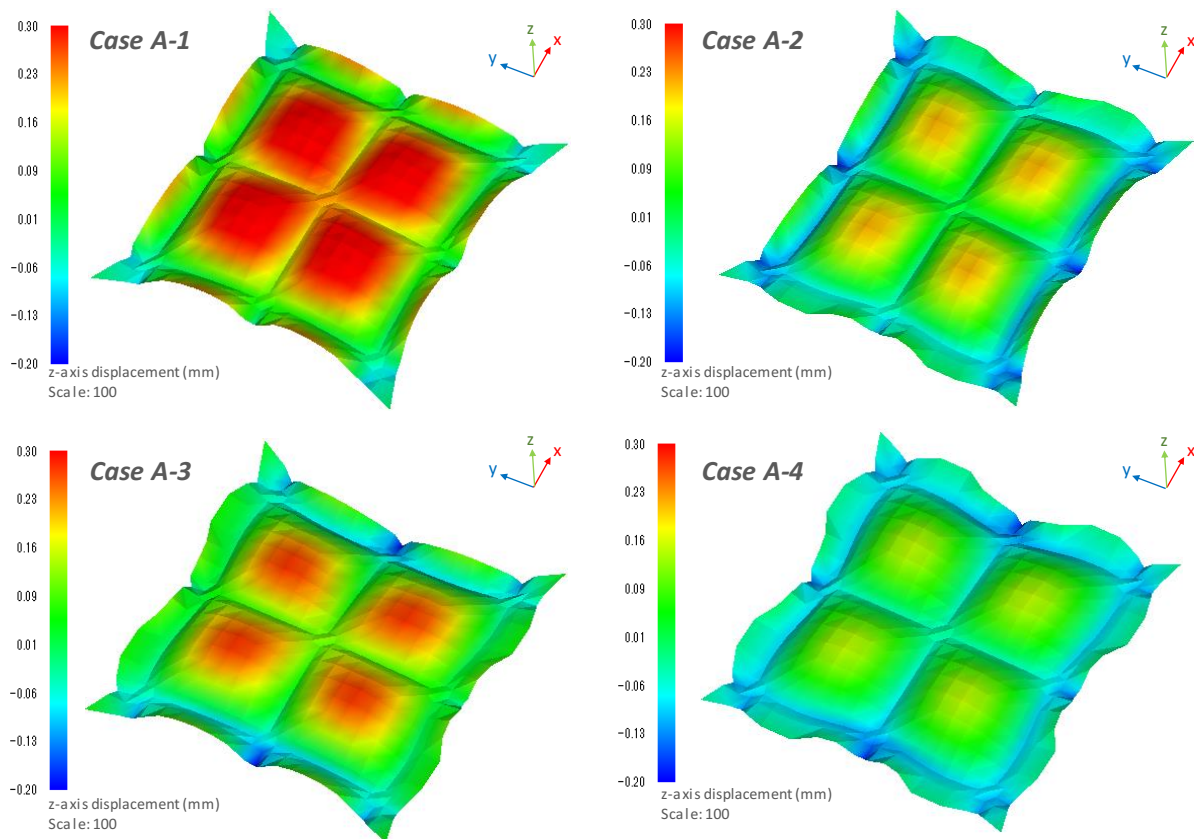


Figure 6.7 Z-axis displacement of the bottom plate of Case A-1, A-2, A-3 and A-4

The z-axis displacement distributions along ST and SL are plotted in Figures 6.8 and 6.9, respectively. These figures clearly show the difference in the efficacies of clamps between Cases A-2 and A-3. The distances of the reduction of Cases A-2, A-3 and A-4 from Case A-1 on line ST are 0.1515 mm, 0.0773 mm and 0.1574 mm which are measured at the highest point of the buckling curve of Case A-1 as shown in Figure 6.8. Comparing to Case A-4 which produces the maximum reduction in the z-axis displacement, the efficiencies of Cases A-2 and A-3 for reducing the buckling curve is discussed. In Case A-2, the effect of the additional clamps at longitudinal edges on the reduction of the buckling feature along line ST (96.3%) is higher than SL (83.1%). On the other hand, the additional clamps at transverse edges work more effectively along line SL (67.8%) than ST (49.1%) in Case A-3. Comparing the z-axis displacement distributions along ST and SL for Case A-2, significant differences are observed not only in the displacement value but also in the angle of the displacement curve at the ends of these lines. The displacement curve starts from 0 mm with small slope along ST in Figure 6.8 since additional clamp is given at this end point, while a relatively large displacement and slope are seen at the end of SL in Figure 6.9.

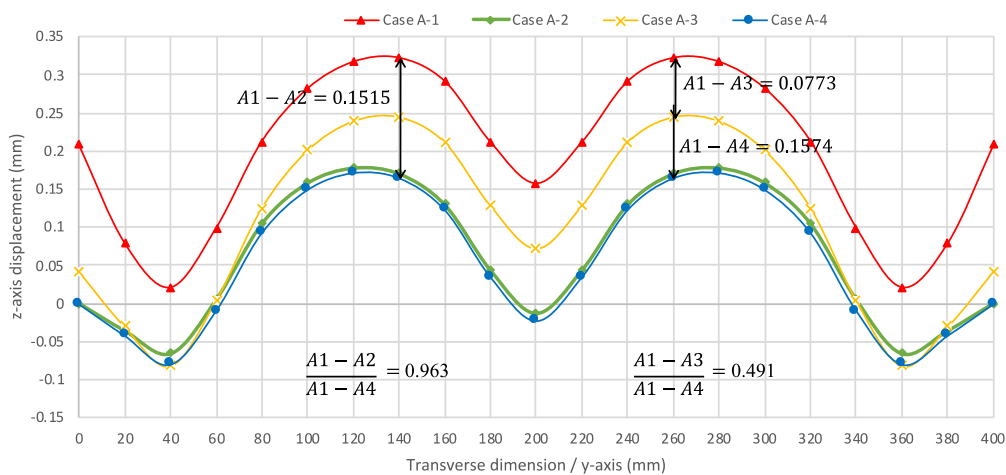


Figure 6.8 Z-axis displacement distribution of ST

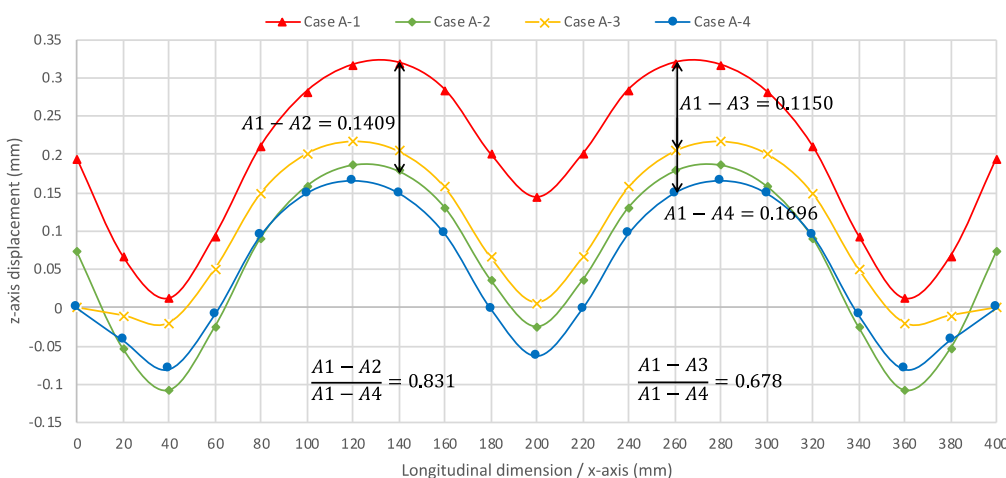


Figure 6.9 Z-axis displacement distribution of SL

Figure 6.10 shows the relationships between the displacements measured lines and clamp positions. Since the additional clamps of Case A-2 are located at both ends of line ST (A2-ST), they are effective to mitigate the buckling feature deformation along this line resulting in the large reduction efficiency of 96.3%. On the other hand, this clamp condition for SL (A2-SL) can't mitigate the buckling feature deformation along line SL directly, so the efficiency of reducing displacement is down to 83.1%. The same kind of relationship is seen in Case A-3 such that the additional clamps at transverse edges worked more effectively along line SL (A3-SL) than ST (A3-ST) since these clamps are located at both ends of line SL. So, it is noted that additional clamps show their high performance in the direction perpendicular to the edge which they are applied.

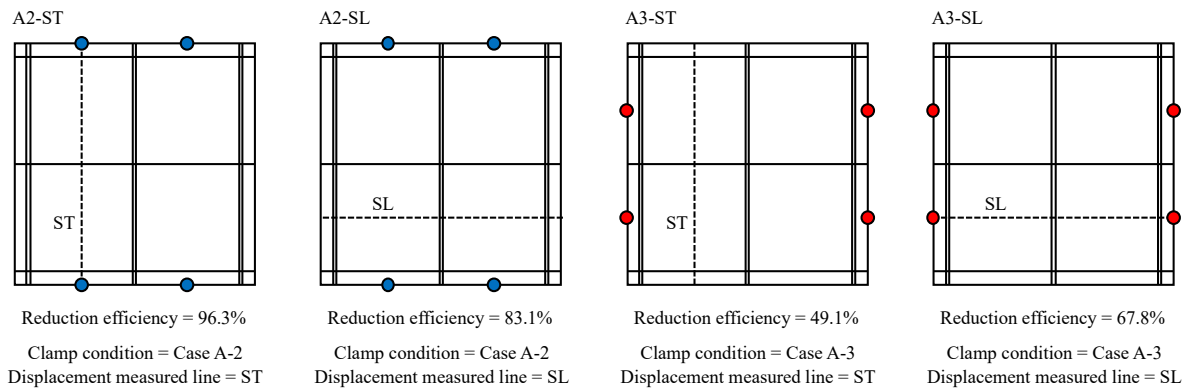


Figure 6.10 Displacement reduction efficiency of clamp position with respect to displacement measured line

Though the relationship between clamp position and stiffener direction of ST in Case A-2 and that of SL in Case A-3 are the same, the displacement reduction efficiencies are different such as 96.3% and 67.8% (A2-ST and A3-SL in Figure 6.10). The structural difference in the longitudinal and transverse directions is only stiffener size. But, the size difference itself doesn't make so large difference in the z-axis displacements along ST and SL since the displacements on these lines for Case A-1 are almost the same as shown in Figures 6.8 and 6.9. This fact indicates the importance of the combination of the stiffener size and the clamp position.

In order to analyze the effects of the additional clamps with respect to the stiffener size, the z-axis displacement distributions on the lines where stiffeners are located are plotted in Figures 6.11 and 6.12. TS and LS indicate the lines of transverse and longitudinal stiffeners, respectively. Although there is little difference between the displacement distributions on TS and LS for Case A-1 having basic 4 clamps, there exist significant differences for Cases A-2 and A-3 having additional clamps in different sides. In Case A-2, additional clamps on the longitudinal edges directly let the transverse stiffeners as close to a straight line (A2-TS in Figure 6.11). Since the longitudinal stiffeners are weaker than the transverse stiffeners, the longitudinal stiffeners follow the deformation created by the transverse stiffeners resulting in its relatively flat deformation (A2-LS in Figure 6.12). In Case A-3, additional clamps on the transverse edges make the longitudinal stiffeners relatively flat (A3-LS). But, the

longitudinal stiffeners aren't strong enough to prevent the transverse stiffeners from deforming resulting in the large displacement of TS (A3-TS). This is the reason why Case A-2 decreases the welding deformation more than Case A-2, and hence, it is recommended that the additional clamps are placed along the plate edges perpendicular to the larger stiffener direction.

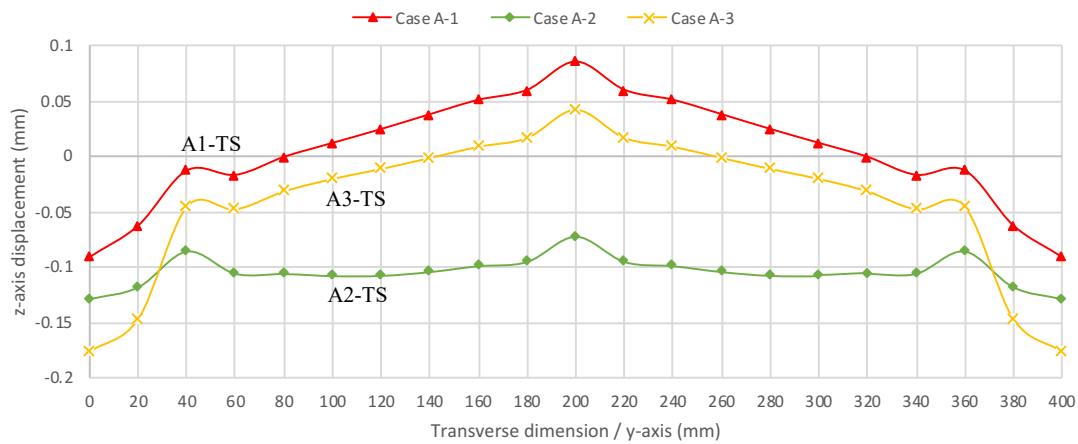


Figure 6.11 Z-axis displacement distribution of TS

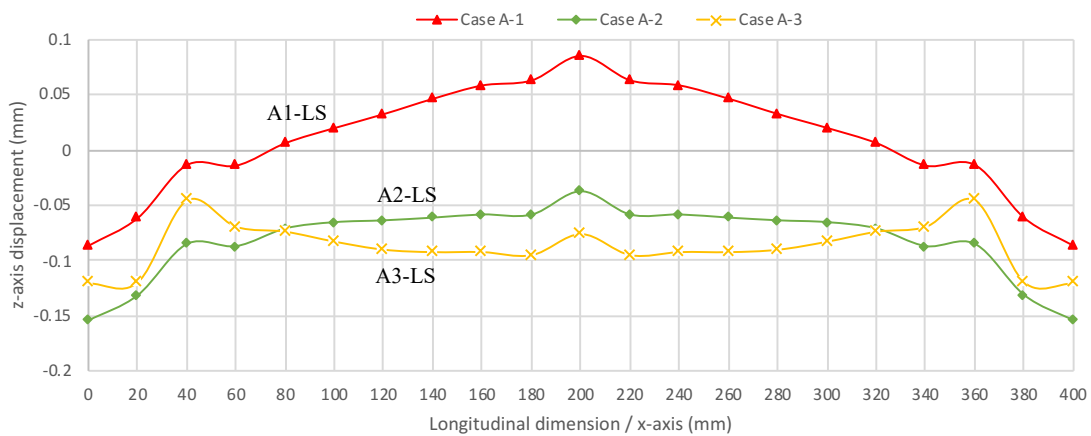


Figure 6.12 Z-axis displacement distribution of LS

According to the above results and discussions, the systematic method for optimally clamping under limited work environment condition to maximize their efficacy for minimizing welding displacements is proposed as Figure 6.13.

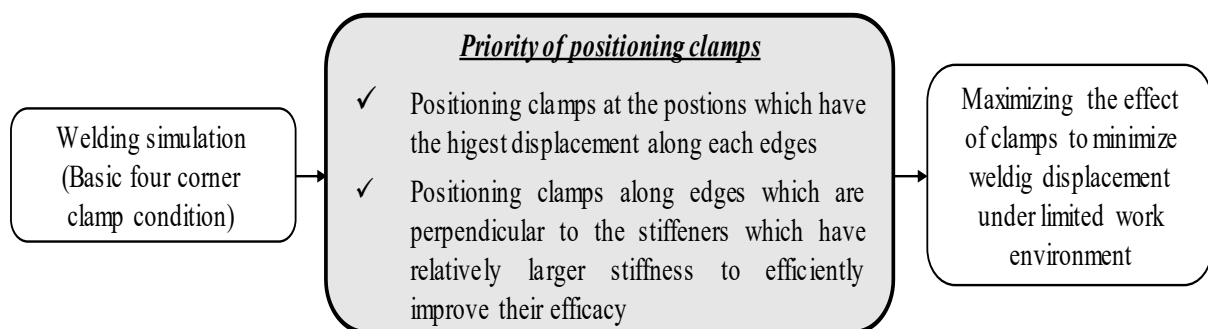


Figure 6.13 Systematic method to optimally position clamps under limited work environment

## 6.5 The Effect of Strongbacks and Efficient Positioning of Strongbacks to Minimize Welding Displacements of the Square-Shaped Grillage Structure

To minimize the welding displacements, strongbacks are temporarily installed on a structure as stiffeners during fabrication. The positioning of these strongbacks is critical, and different results can be obtained depending on their placement on the structure. Therefore, a method to optimally position strongbacks that minimizes welding displacements is essential, especially for welding applications in building ships and offshore structures. Figure 6.14 shows the z-axis displacement distribution in Case A-1 in the top view and the lines on which strongbacks to be positioned. These lines pass over the area where the largest displacements have been found. Four strongbacks are attached along these lines to strengthen the stiffness in each direction, and the relationship between the positioning strongback and the stiffener size is investigated.

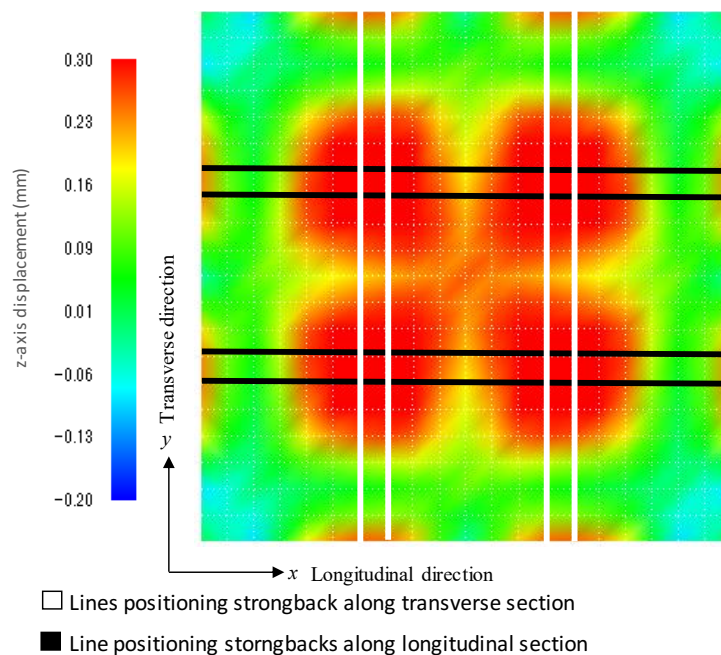


Figure 6.14 Lines positioning strongbacks of the square shaped grillage structure

### 6.5.1 Results and Discussion of the Effect of Strongbacks on the Square-Shaped Grillage Structure

To compare the effect of strongback positioning on the welding displacements of the square-shaped grillage structure,  $Z_{average}$  is introduced. The z-direction displacement distributions of the bottom plate along the selected two lines, ST and SL shown in Figure 6.5, are compared to analyze the effect of strongback positioning for the square-shaped grillage structure precisely.

Three cases B-1, B-2 and B-3 using different length of strongbacks along the longitudinal direction are simulated as shown in Figure 6.15. These cases are as follows:

- B-1: Strongback legs are positioned at the maximum points of the displacement curve
- B-2: Strongback legs are positioned outside of the minimum points of the displacement curve
- B-3: Strongback legs are positioned inside of the minimum points of the displacement curve

$Z_{average}$  of these cases are compared in Figure 6.16 where large reduction mitigation is obtained in Case B-3.  $Z_{average}$  is reduced 37.4% (from 0.147 mm to 0.092 mm) by setting the strongback legs at the positions of  $x = 40 \sim 60$  mm and  $340 \sim 360$  mm. On the other hand, strongbacks of Cases B-1 and B-2 are not so effective since their reductions of  $Z_{average}$  are only 2.7% and 5.4%, respectively. The z-axis displacement curves of them are shown in Figure 6.15 where the result of analysis without strongback (Case A-1) is also plotted. Case B-1 shows that the presence of the strongbacks has a slight impact on reducing the welding displacements of the center area as can be seen by the two displacement curves with and without strongbacks. In Case B-2, it is observed that there is no impact on the welding displacements in the inner zone (the area between the strongback legs), but there is a decrease in the welding displacement in the outer zone. In Case B-3, it is seen that there is a substantial reduction in the welding displacements in the inner zone and a slight increase in the outer zone.

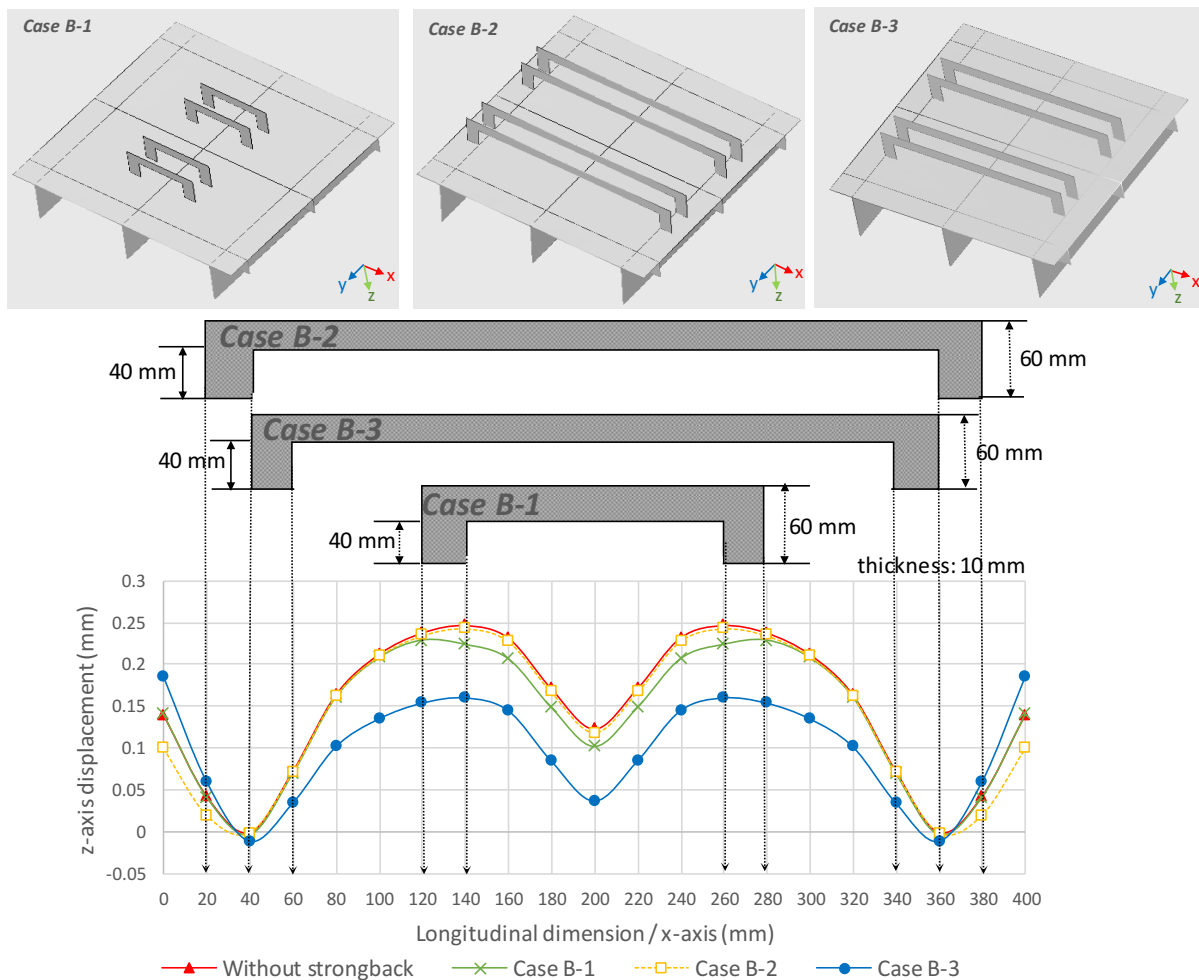


Figure 6.15 Positions of strongbacks and z-axis displacement curves of SL in Cases B-1, B-2 and B-3

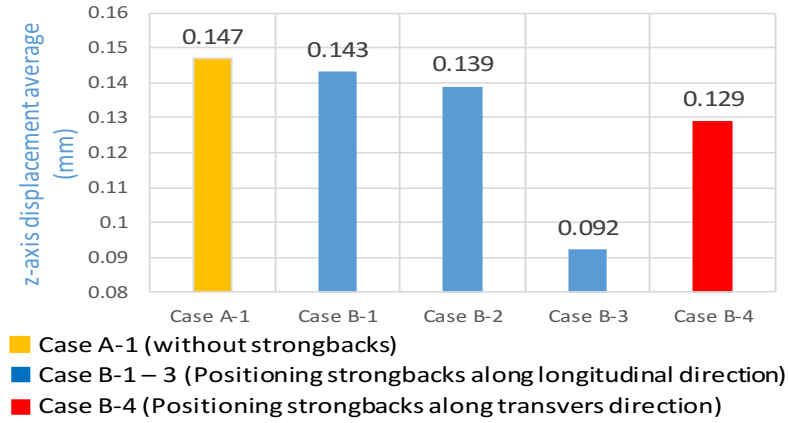
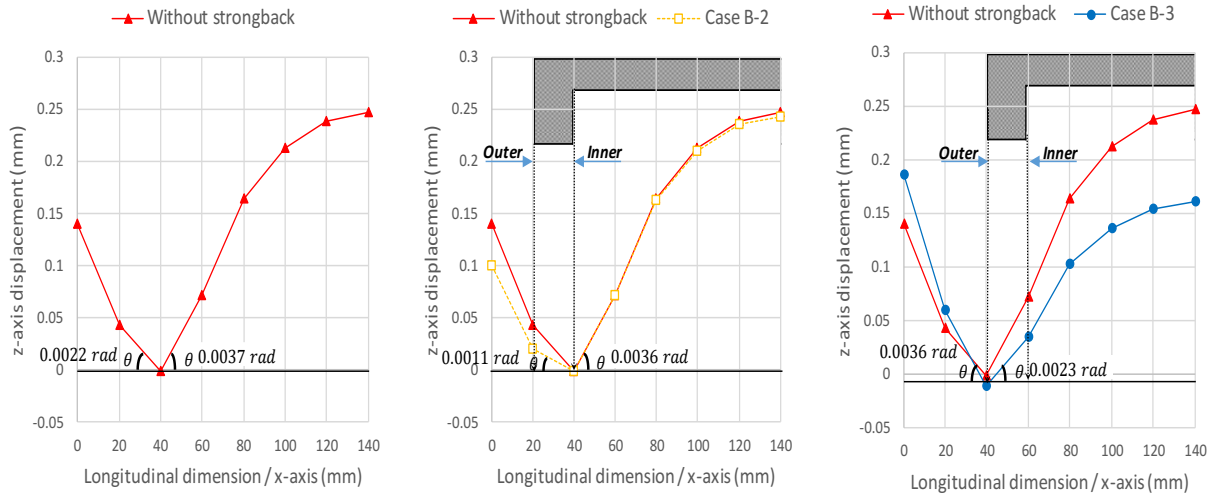


Figure 6.16  $Z_{average}$  of the square-shaped grillage structure with differently positioned strongbacks

To thoroughly discuss the results of z-axis displacement curves of Cases B-2 and B-3, Figure 6.17 is introduced. In Case B-3, the additional strongback leads to the reduction of the angular displacement of 0.0014 rad (38 %) in the inner zone resulting in the descent of the curve. However, this strongback effects on the increase of the angular displacement of 0.0014 rad (64 %) in the outer zone. In Case B-2, the additional strongback leads to the reduction of the angular displacement of 0.0011 rad (50 %) in the outer zone as similar to Case B-3, but small increase of the angular displacement of 0.000043 rad (1 %) in the inner zone is observed. The reason for the small change of angular displacement in the inner zone is that the inner part connects to the center of the structure which has the high stiffness, and it leads to mitigate the increase of the angular displacement. The large stiffener located just inner side of the leg also disturbs the angular change in the inner zone.



Strongback leg position (x-axis)	20 ~ 40 mm		40 ~ 60 mm	
Without strongbacks	0.0022 rad	Angular Difference from 0.0022 rad	0.0037 rad	Angular Difference from 0.0037 rad
Case B-2	0.0011 rad	0.0011 rad (50 % ↓)	0.0036 rad	0.000043 rad (1 % ↑)
Case B-3	0.0036 rad	0.0014 rad (64 % ↑)	0.0023 rad	0.0014 rad (38 % ↓)

Figure 6.17 Effect of strongback on z-axis displacement curves in Case B-2 and B-3

It is expected that strongbacks make the slope of the plate flat at the positions where their legs are attached. Hence, it is tried to use the angular deformation (the slope of the z-axis displacement) without strongbacks for determining the locations of the strongbacks. Figure 6.18 shows the angular deformation by welding without strongbacks (Case A-1). The strongback legs of Cases B-1 and B-3 are positioned where the angular deformations are 0.0004 rad and 0.0037 rad, respectively. Three additional numerical simulations with strongbacks at the positions whose angular deformations of 0.0046 rad, 0.0024 rad and 0.0013 rad are carried out to see the relationship between the angular deformation of Case A-1 and welding displacement. The results of them are shown in Figure 6.19 in which the horizontal axis indicates the x coordinates of the positions of the strongback legs. A green dashed line shows the angular deformation without strongback, while a blue solid line shows the  $Z_{average}$  in the cases with strongbacks. A negative correlation between the angular deformation and the  $Z_{average}$  observed. It is clearly seen that the efficiency of the strongback is the highest in the case that its legs are placed at the zone where the largest angular deformation is observed before attaching strongback.

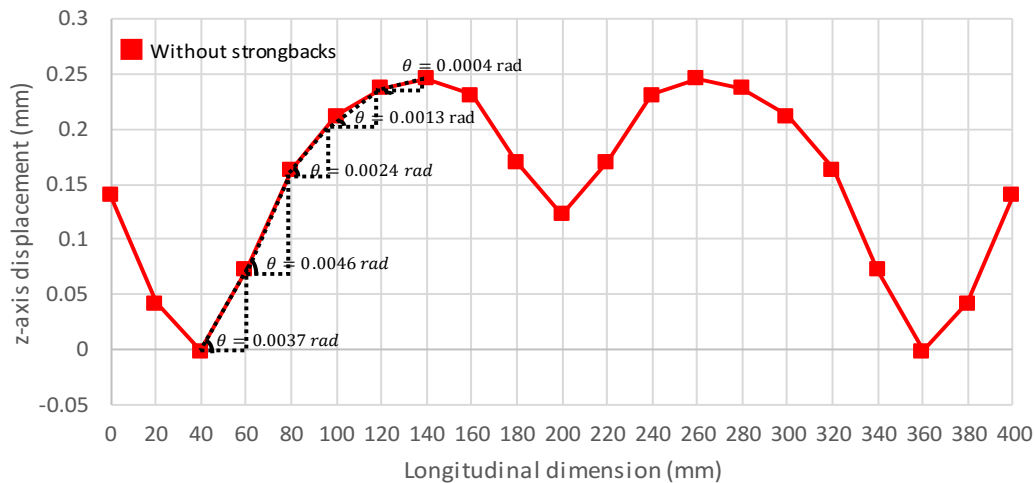


Figure 6.18 Angle of each section (40 ~ 140 mm) of the displacement distribution curve without strongbacks

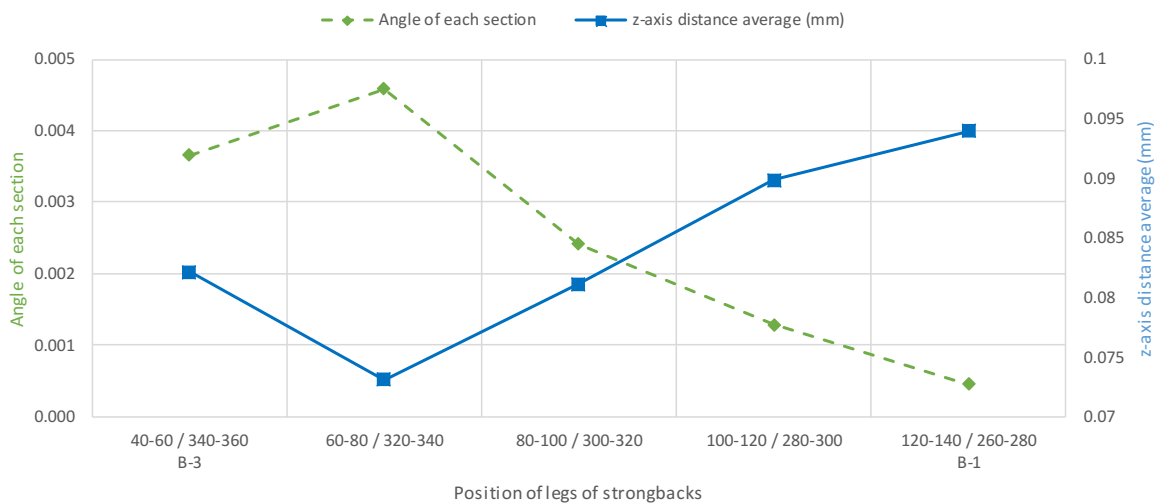


Figure 6.19  $Z_{average}$  for the square shape grillage structure obtained for each of the five strongbacks positions based on the angle of the displacement curve

In Case B-4, the strongbacks are positioned along the transverse direction as shown in Figure 6.20. Their legs are attached at the inside of the minimum points of the displacement curve as similar to Case B-3 that is the most effective in the previous simulations. The tendency of the displacement curve in Case B-4 is somewhat similar to those obtained in Case B-3, with a reduction in welding displacement in the inner zone and a rise in the outer zone; however, the results obtained in Case B-3 are clearly superior to Case B-4. This is due to the fact that the high stiffness of the transverse stiffeners reduces the effect of placed strongbacks in Case B-4.

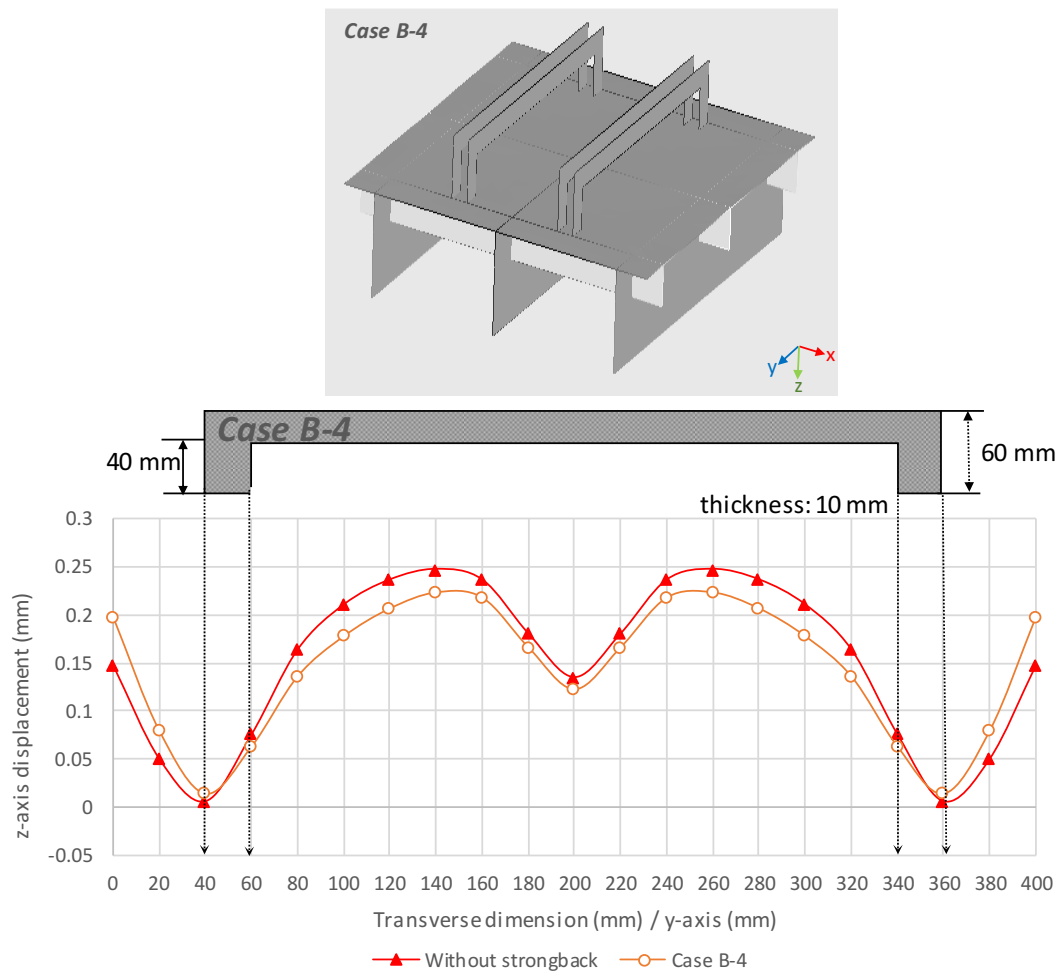


Figure 6.20 Position of strongbacks and z-axis displacement curve of ST in Case B-4

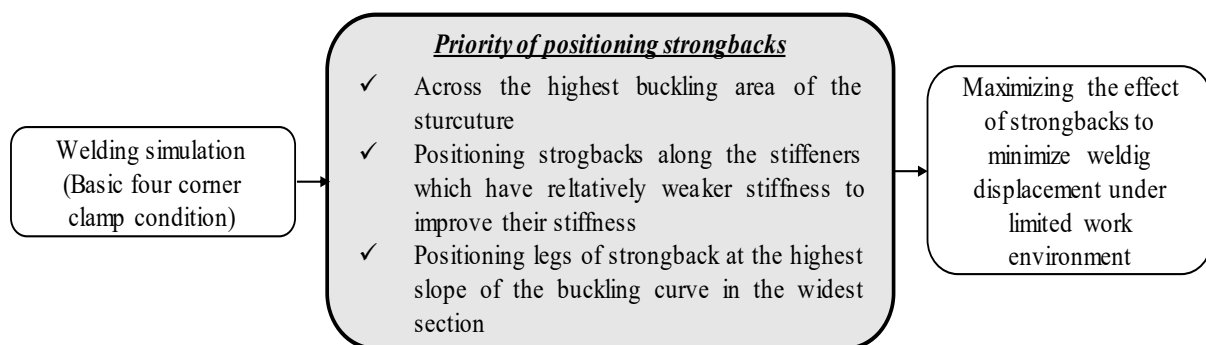


Figure 6.21 Systematic method to optimally position strongbacks under limited work environment

According to above results and discussions, the systematic method for optimally positioning strongbacks under limited work environment condition to maximize their efficacy for minimizing welding displacements is proposed as Figure 6.21.

## 6.6 The Effect of Additional Clamping along Strongbacks on the Square-Shaped Grillage Structure

In Case B-3, the two legs of strongbacks are positioned inside of the location indicated by the minimum points of the displacement curve to provide large mitigation in the welding displacement in the inner zone; however, this led to an increase in the welding displacements in the outer zone. To address this increase in welding displacement in the outer zone, additional clamping is provided as Case B-3+ in Figure 6.22.  $Z_{average}$  is 0.053 mm which is 63.8% reduction from A-1, while  $Z_{average}$  of Case B-3 is 0.092 mm which is 37.4% reduction from A-1. Hence, an optimal combination of clamps and strongbacks is also effective in reducing the welding displacements.

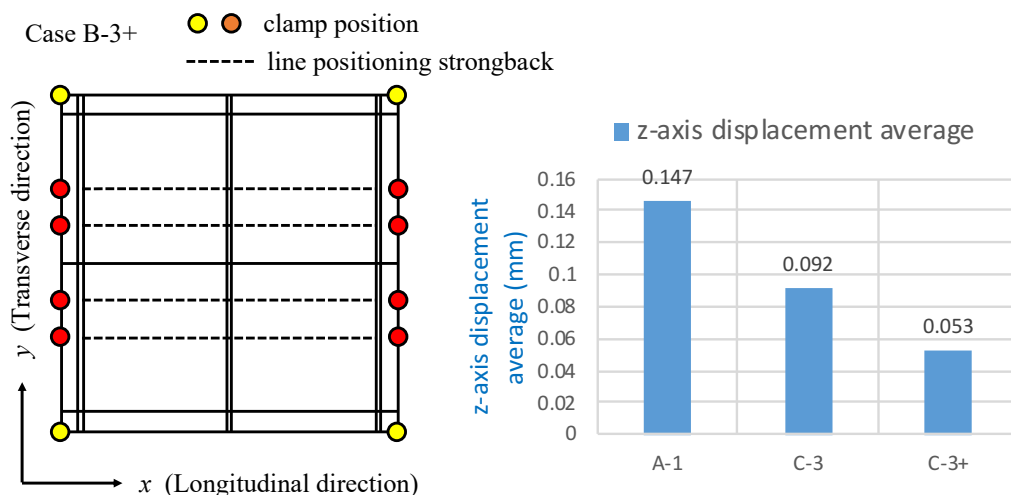


Figure 6.22 Combining clamps and strongbacks in Case B-3+ and  $Z_{average}$

## 6.7 Validation of Systematic Method to Efficiently Position Clamps for the reduction of Welding Displacements of the General Ship Grillage Structure under Limited Work Environment

First, the basic clamping condition that clamps four corners of the bottom plate is applied to the general ship grillage structure. It is noted as Case C-1 and shown in Figure 6.23 where yellow circles indicate the basic clamps. Additional clamps are basically positioned at nodes which have the highest displacement along each edge based on the results of these basic clamping conditions. Additional 6 clamps are positioned along longitudinal edges as C-2 in Figure 6.24 according to the systematic method proposed in chapter 4 since transverse stiffeners are stronger than longitudinal stiffeners. But, the difference of the moment of inertia of area between the longitudinal and transverse sections is not so

large. Case C-3 with additional 8 clamps is used for comparing the effectivity of clamp positioning though the number of additional clamps is more than Case C-2.

C-1: Basic clamps at the corners of bottom plate marked by yellow circles

C-2: Additional 6 clamps along the longitudinal edges marked by blue circles (by the proposed method)

C-3: Additional 8 clamps along the transverse edges marked by red circles

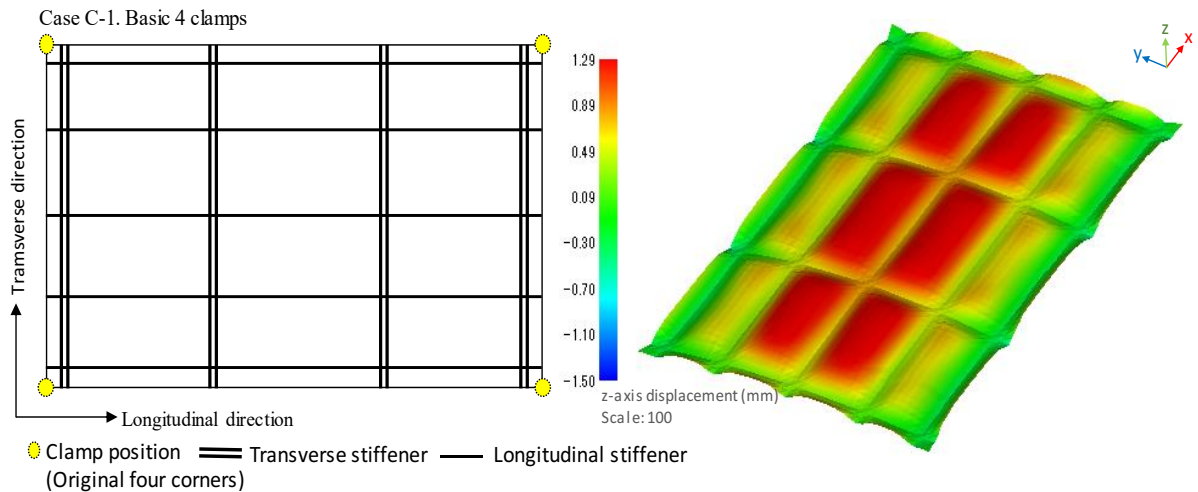


Figure 6.23 Z-axis displacement of the bottom plate of Case C-1

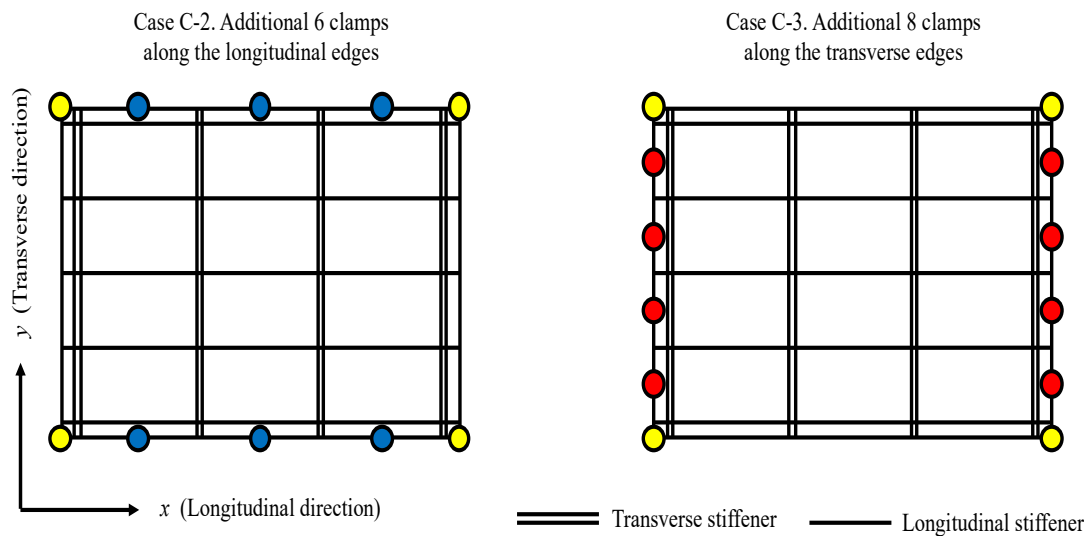


Figure 6.24 Additional clamping cases (General ship grillage structure 3000 mm × 2000 mm)

### 6.7.1 Results and Discussion of the Effect of Clamping on the General Ship Grillage Structure

$Z_{average}$  is used to see the overall effect of the additional clamps on the welding displacements of the general ship grillage structure. Two lines, GT (Transverse) and GL1 (Longitudinal), are selected to analyze the effects of clamp positions as Figure 6.25.

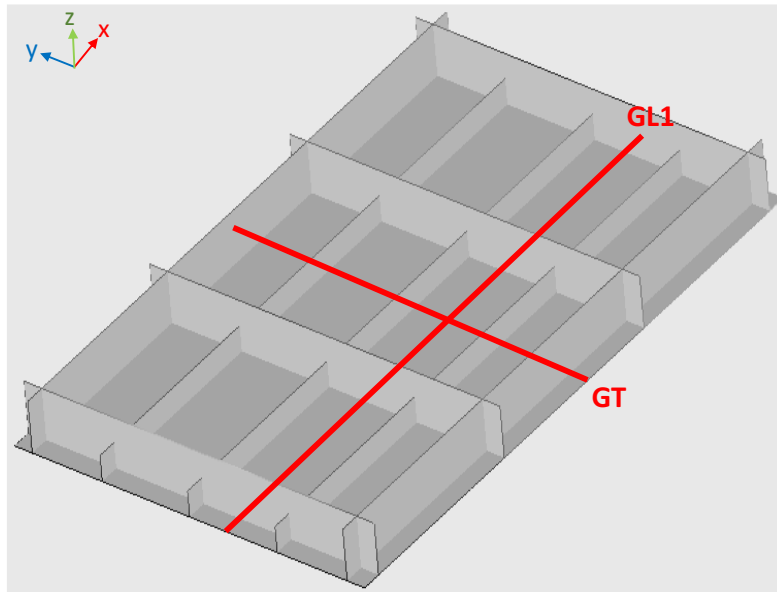


Figure 6.25 Measuring line for the displacement distribution of the general ship grillage structure GT and GL1

Figures 6.26 shows  $Z_{average}$  for the three Cases C-1, C-2 and C-3 obtained for the general ship grillage structure. Case C-2 whose clamping positions are determined by the proposed method reduces  $A_{displacement}$  from 0.650 mm to 0.397 mm, while  $Z_{average}$  of Case C-3 is 0.454 mm. So, the proposed clamping method works well for the general ship grillage structure, even though Case C-2 has disadvantage in the number of clamps.

In Figure 6.27, Case C-2 shows that the additional 6 clamps on the longitudinal edges mitigate buckling feature deformation at both of the longitudinal edges and the center of bottom plate. Case C-3, whose reduction of  $Z_{average}$  is 30.2%, shows that the additional 8 clamps on the transverse edges successfully mitigate local z-axis displacement of transverse edges but the reduction of the center buckled feature deformation is less than Case C-2. Focusing on the edges of plate, Case C-2 suppresses the z-axis displacement, but Case C-3 generates a large displacement in the negative direction along longitudinal edges.

Figures 6.28 and 5.29 show the z-axis displacement distributions of Cases C-1, C-2 and C-3 along the lines of GT and GL1, respectively. Case C-2 based on the proposed method shows the good performance along both lines except for the end points of GL1 where the additional clamps are given in Case C-3.

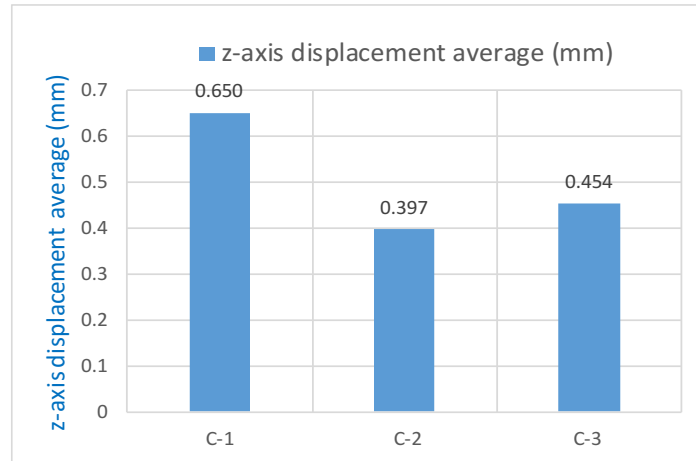


Figure 6.26  $Z_{average}$  of the general ship grillage structures

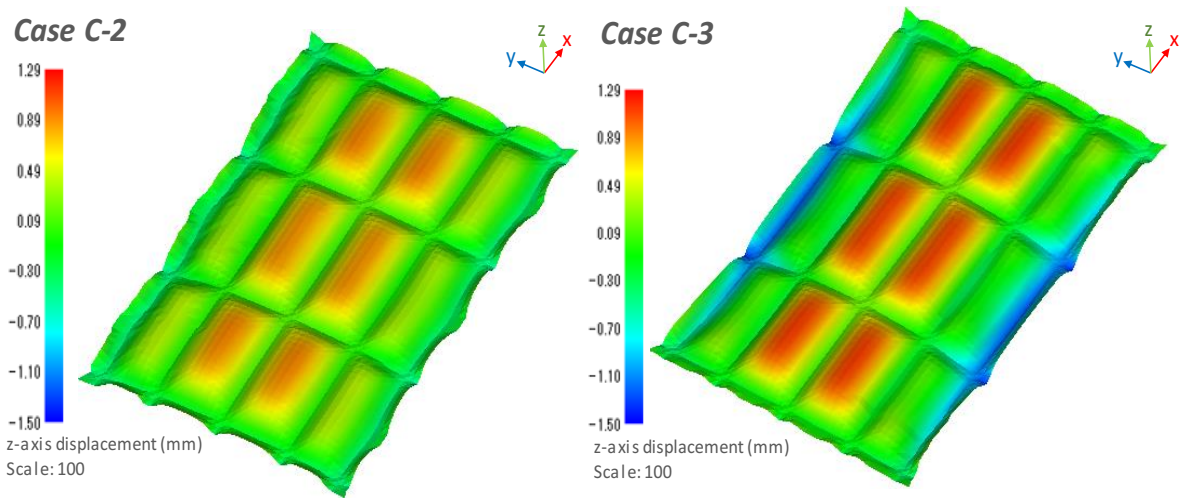


Figure 6.27 Z-axis displacement of the bottom plate of Case C-2 and C-3

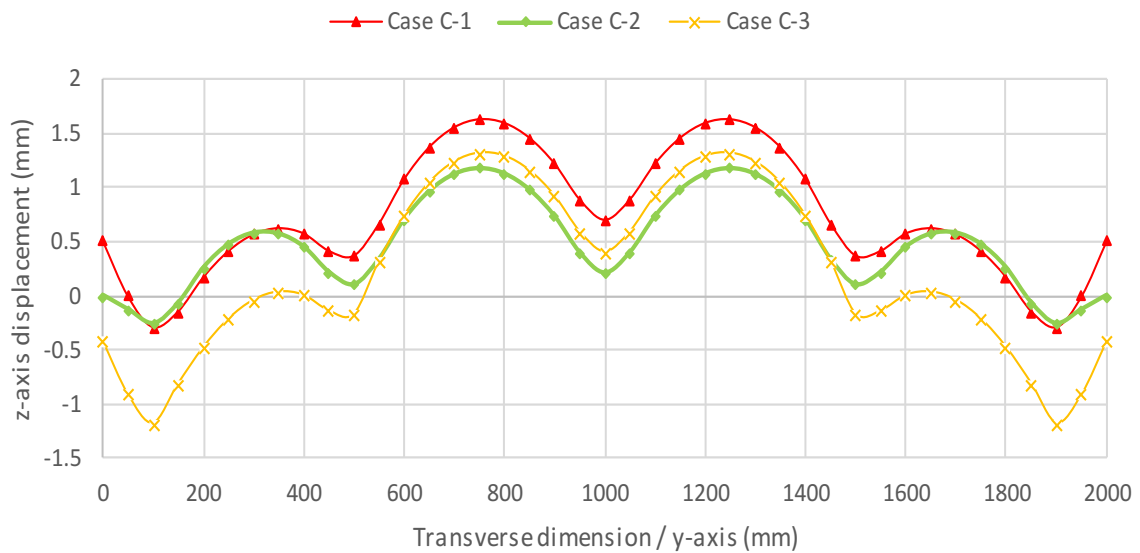


Figure 6.28 Z-axis displacement distribution of GT

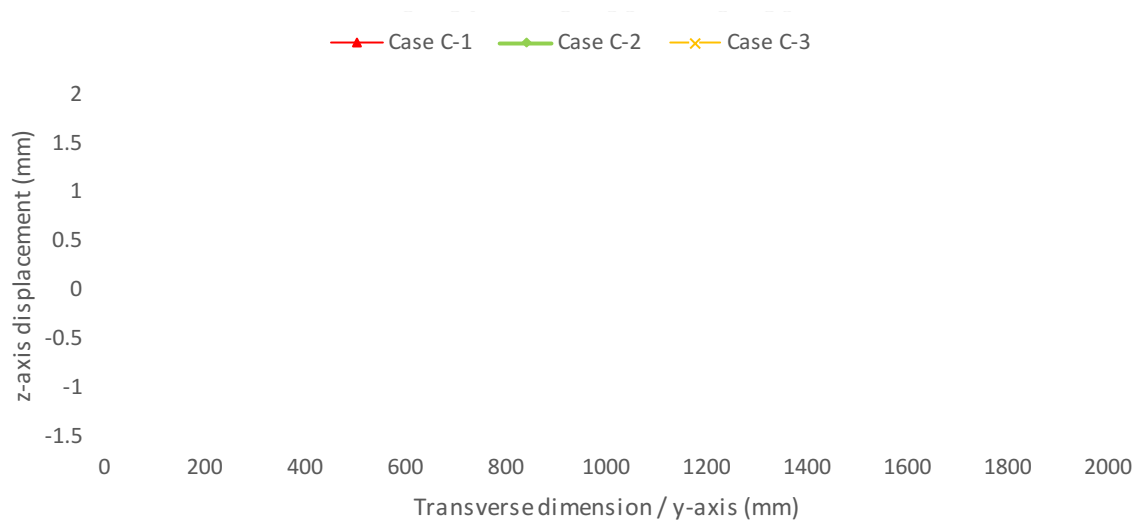


Figure 6.29 Z-axis displacement distribution of GL1

## 6.8 Validation of Systematic Method to Efficiently Position Strongbacks for the reduction of Welding Displacements of the General Ship Grillage Structure under Limited Work Environment

Figure 6.30 shows the distribution of z-direction displacement of Case C-1 in the top view. Three strongbacks along the transverse direction and the longitudinal direction are positioned, respectively, as shown in Figure 6.31 such that they across the highest displacement zones of each section of the general ship grillage structure to minimize the global welding displacements. The efficiency of the directions of the strongbacks is evaluated.

D-1: Strongback legs are positioned at the maximum slope of the displacement curve along the transverse direction

D-2: Strongback legs are positioned at the maximum slope of the displacement curve along the longitudinal direction (by the proposed method)

Case D-2 has the strongback position according to the method proposed in chapter 6.7 since the longitudinal stiffeners are weaker than transverse stiffeners. Since three strongbacks are used for both cases to give the same condition to two cases, the layout of strongbacks in Case D-2 may not be the best.

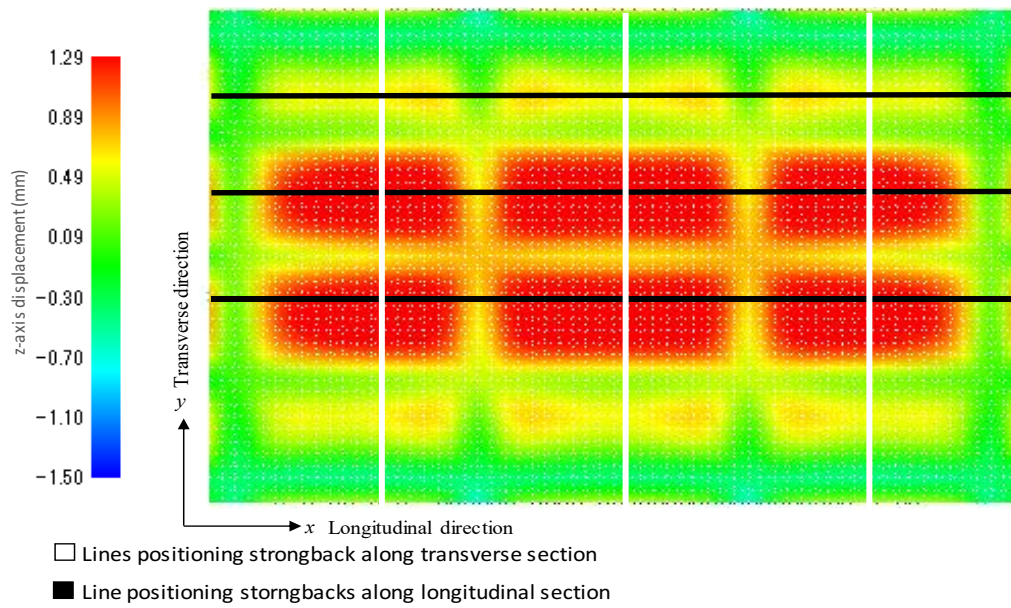


Figure 6.30 Lines positioning strongbacks of the general ship grillage structure

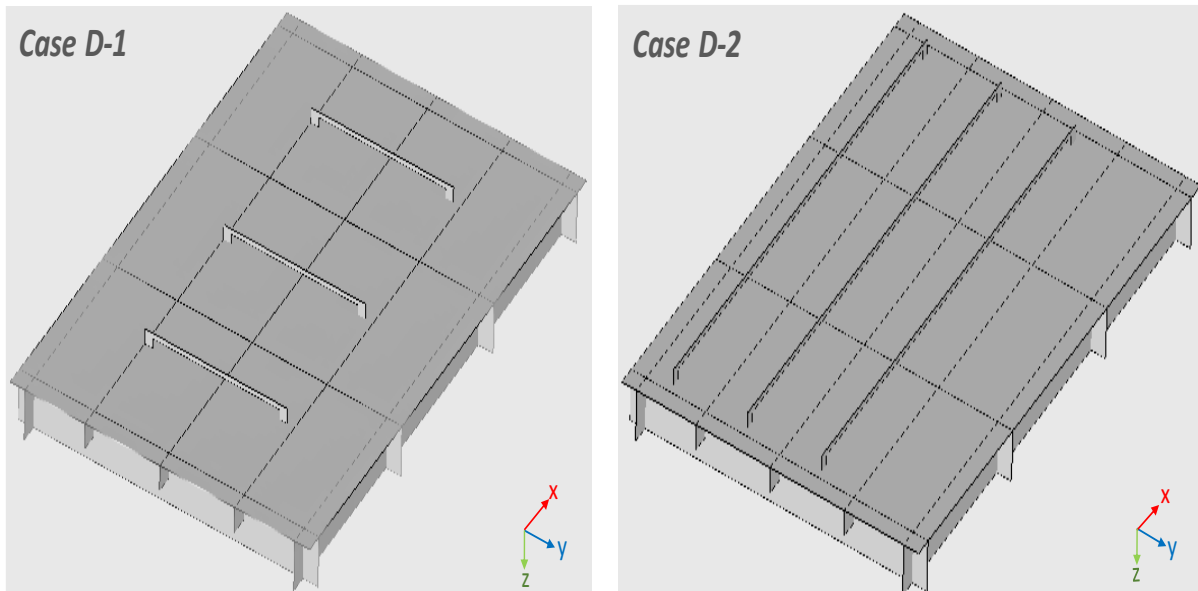


Figure 6.31 Strongbacks positioning in Cases D-1 and D-2

### 6.8.1 Results and Discussion of the Effect of Strongbacks on the General Ship Grillage Structure

$Z_{average}$  is used to see the overall effect of the additional strongbacks on the welding displacements. The z-direction displacement distributions of the bottom plate along the selected two lines, GT (Transverse) and GL2 (Longitudinal) shown in Figure 6.32, are used to analyze the effects of strongback positions.

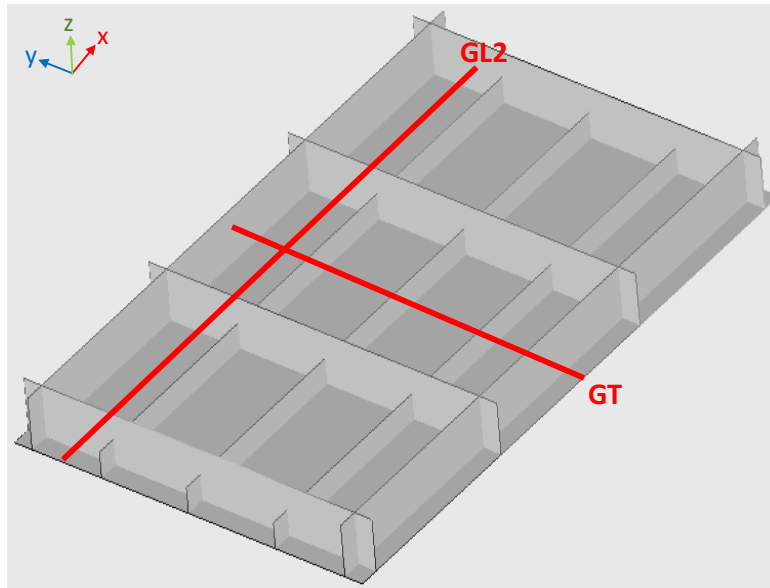


Figure 6.32 Measuring line for the displacement distribution of the general ship grillage structure GT and GL2

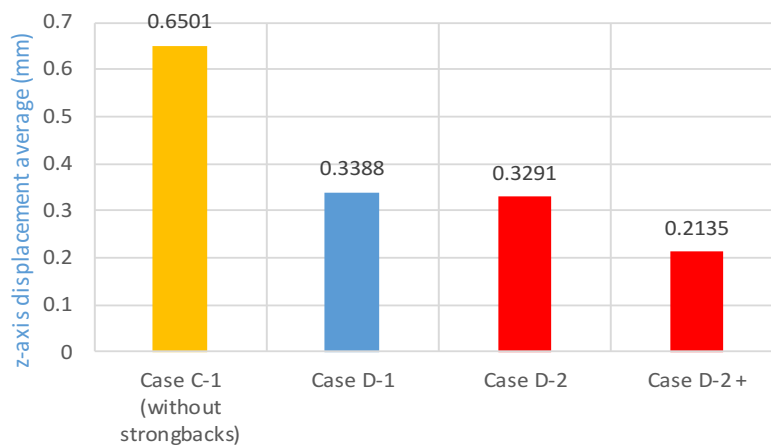


Figure 6.33  $Z_{average}$  of the general ship grillage structures with differently positioned strongbacks.  $Z_{average}$  of Cases D-1 and D-2 are 0.339 mm and 0.329 mm, respectively, as shown in Figure 6.33. So, Case D-2 based on the proposed method shows better performance than Case D-1 just a little bit. Figures 6.34 and 6.35 show the positions of strongbacks and the z-axis displacements along GT and GL2, respectively. It is clearly shown that the strongbacks in both cases are very effective to mitigate the welding deformations along both lines in the inner zones of their legs. Case D-2 has the disadvantage such that the number of strongbacks and the number of sections between stiffeners don't match, while one strongback is set for each high displacement area in Case D-1. Despite this unfavorable condition,  $Z_{average}$  of Case D-2 is smaller than D-1. So, the effectivity of the proposed method for reducing welding deformation by strongbacks is seen in the general ship grillage structure.

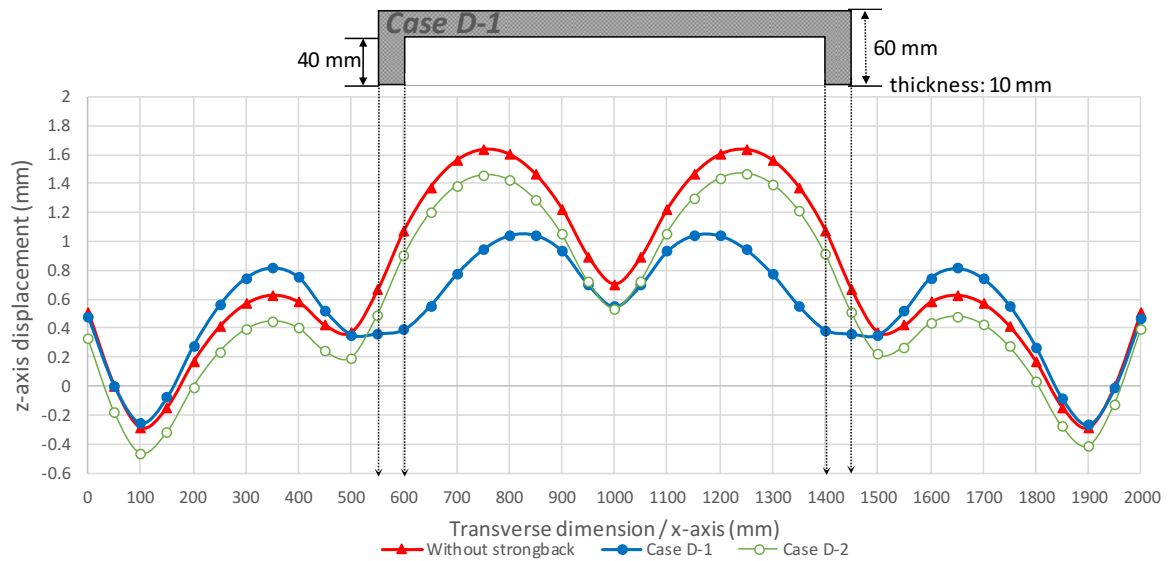


Figure 6.34 Positions of strongbacks and z-axis displacement curve of Cases D-1 and D-2 along GT

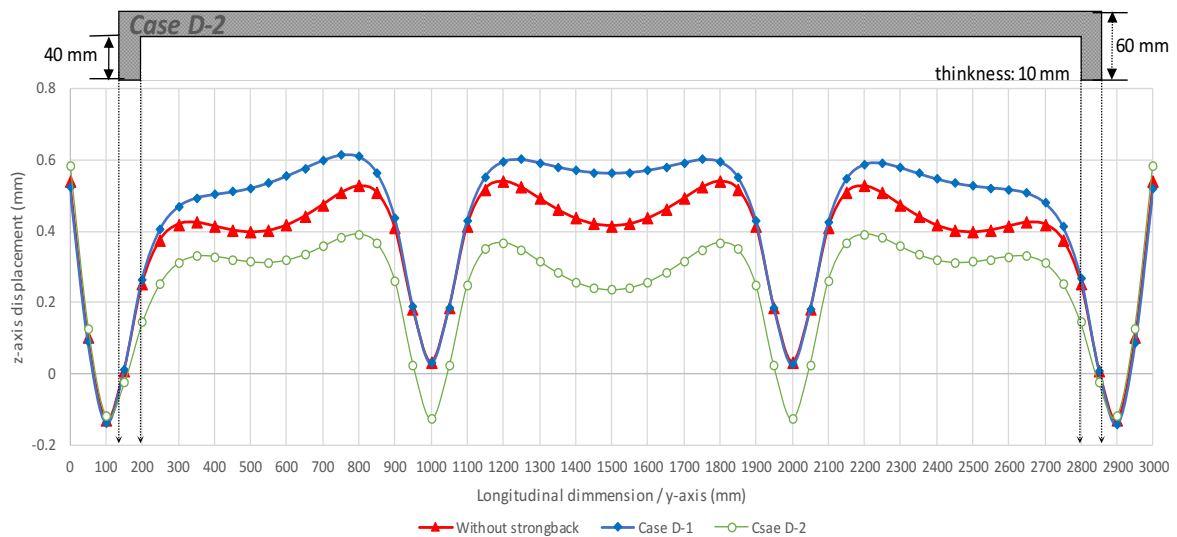


Figure 6.35 Positions of strongbacks and z-axis displacement curve of Cases D-1 and D-2 along GL2

## 6.9 Validation of the effect of additional clamping along strongbacks on the General Ship Grillage Structure

To validate the efficacy of the combination of clamps with strongbacks in the general ship grillage structure. Case D-2+ is created by adding clamps along the edges near the ends of strongbacks in Case D-2. Figure 6.36 shows that the z-axis displacement distribution curve of Case D-2+ close the zero line, and the overall welding displacement has been greatly reduced.  $Z_{average}$  is 0.2135 mm, which is 64.9% of Case D-2. Hence, an optimal combination of clamps and strongbacks is very effective in reducing the welding displacements.

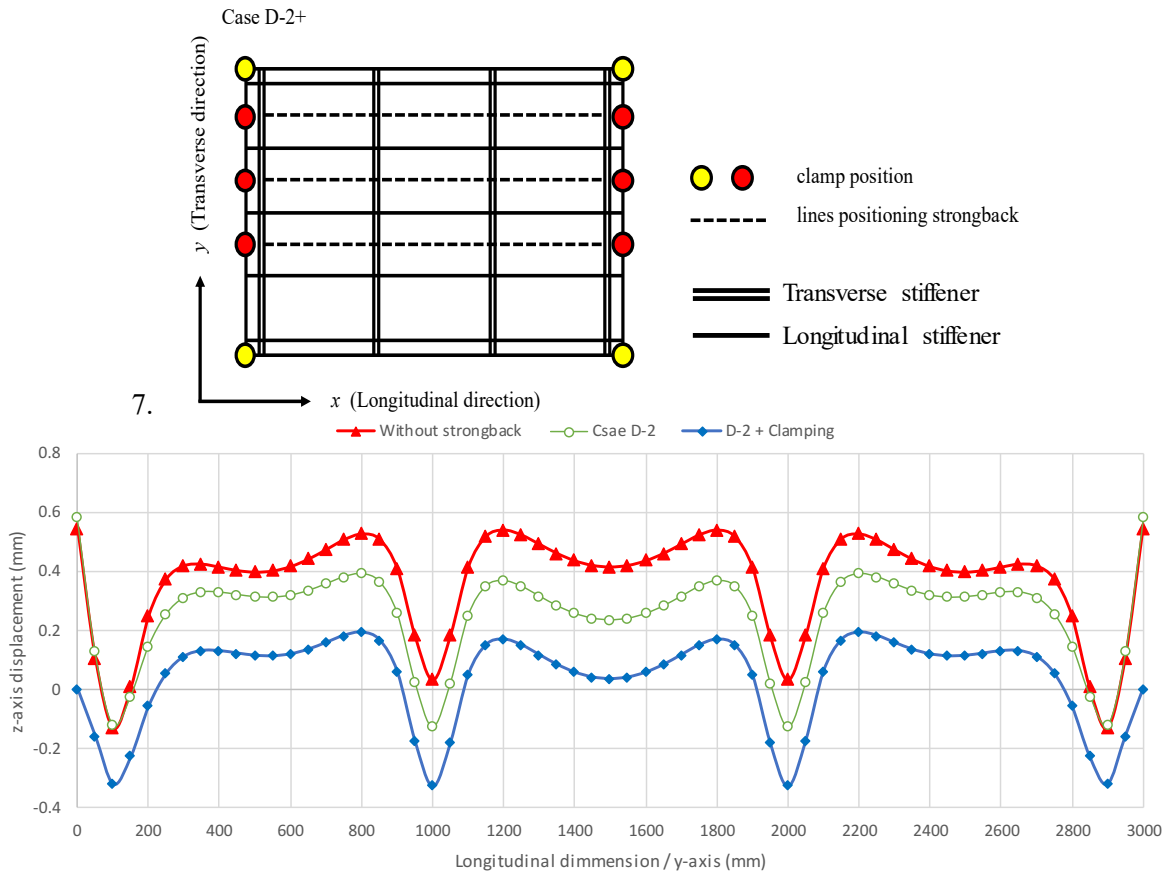


Figure 6.36 Combining clamps and strongback and z-axis displacement curves of Case D-2+ along GL2

## 6.10 Conclusion

In the present study, the systematic method to optimally position clamps and strongbacks that results in minimal welding displacements was proposed. Several cases were numerically simulated using the theory of inherent strain, interface-element method, and MPC to study the effect of clamps and strongbacks and help identify the optimal placements for these external constraints. This study contributes to the understanding of the role of clamps and strongbacks in welding displacement reduction. The conclusions are:

1. Positioning additional clamps obviously reduce  $Z_{average}$ . In particular, the efficiency of additionally positioned clamps highly depends on the relationship between the size of stiffeners (placed in both of the longitudinal and transverse directions) and the position of additional clamps.
2. Based on positioning clamps at the highest displacement points along edges of the welded structure, clamps along edges perpendicular to the stiffeners which have relatively larger stiffness efficiently improve their role to mitigate welding displacement.
3. Strongbacks lead to the reduction of  $Z_{average}$  by influencing the displacement distribution curve.

4. Positioning legs of strongbacks at the largest slope section of the displacement distribution curve maximizes the efficiency of strongbacks for minimizing welding displacements.
5. The extension of the area influenced by the strongback to mitigate the z-axis displacement curve is limited by the stiffeners. Thus, positioning strongbacks at the widest section which isn't separated by stiffeners improves their efficacy.
6. The efficiency of strongbacks becomes relatively weaker when they are placed along the stiffest section of the structure as the transverse section herein.
7. Combining optimally positioned clamps and strongbacks along the same line is effective in minimizing welding displacements.

## 7. Conclusion and Future Works

This thesis studied on the improvement of welding process of ship grillage structures by elastic FEM using inherent strain theory. The systemic methods for optimally ordering and grouping of welding sequences and positioning clamps and strongbacks for minimizing welding displacements were proposed in this thesis. This chapter summarizes the main points of each study and recommend future work for their improvement.

### 7.1 Conclusions

**Chapter 3** proposed the method for systemically ordering welding sequence which results in the minimum of welding displacements of the bottom plate of the ship grillage structure. The main point of this chapter is deciding the priority of welding lines based on their structural characteristic. Initially welding vertical lines which do not make the direct thermal effect on the bottom plate improves the total strength of the structure without the substantial increase of welding displacements of the bottom plate. The priority for a weld sequence between the longitudinal and transverse welding lines which require heat effect directly on the bottom plate; the welding group of transverse welding lines that produce a relatively higher gap prior to the longitudinal welding lines are beneficial in mitigating distortion.

**Chapter 4** proposed the method for optimally grouping welding sequence which proposed in the previous chapter in order to reflect the simultaneous welding. Even if the optimized welding sequence is employed to build a structure, a wrongly grouped simultaneous welding sequence leads to a higher displacement for the structure. Based on understanding the role of each welding line, an optimally grouped welding sequence is essential. Vertical welding lines should first be welded before welding transverse and longitudinal welding lines. Additionally, firstly welding group of vertical lines which are positioned at the center of the structure is preferred for obtaining sufficient stiffness of the center area. Welding transverse and longitudinal lines together after finishing the vertical welding lines produce a palliative effect on reducing the final welding displacement.

**Chapter 5** demonstrated the necessity of the consideration of the gravity force in numerical prediction of welding displacements to be able to precisely predict welding displacements in heavy industries. In the rail boundary condition under the effect of the gravity force, the optimal welding sequence is same as the conclusion of the previous study of Chapter 3 which was validated according to the result of the simple boundary condition. The change of the direction of the gravity force according to the design plan highly effects on the change of the distribution of welding displacements. Without the consideration of these effects, the prediction of the additional production cost for the revision work could have high error.

Thus, in the numerical prediction of welding displacements in the welding process, the consideration of the change of the direction of the gravity force to the structure is technically essential.

**Chapter 6** proposed the applicable systemic method for optimally positioning clamps and strongbacks for minimizing welding displacements under limited work environments. The efficiency of additionally positioned clamps highly depends on the relationship between the size of stiffeners (placed in both of the longitudinal and transverse directions). Thus, clamps along edges perpendicular to the stiffeners which have relatively larger stiffness efficiently improve their role to mitigate welding displacement. Positioning legs of strongbacks along the relatively weak section of the structure and at the largest slope section of the displacement distribution curve maximizes the efficiency of strongbacks for minimizing welding displacements. Moreover, combining optimally positioned clamps and strongbacks along the same line is effective in minimizing welding displacements.

## 7.2 Future Works

Studies that have been conducted show good results but still need further works for the improvement of proposed methods and experimental validation.

- In order to improve the widely applicable system of optimally ordering welding lines, study of various standards of welding lines to characterize different structures is necessary.
- The experiments is necessary for the validation and improvement of the results of numerical calculation.
- The addition of residual stress in the comparison of the effect of proposed methods on the structure is necessary in the future study.

## References

- Abe, R., 2017, A study on the accuracy control and measurement of hull structure using 3D Measurement Technique (Doctoral thesis), Hiroshima University
- Deng, D., Murakawa, H., 2008. FEM prediction of buckling distortion induced by welding in thin plate panel structures. *Comput. Mater. Sci.* <https://doi.org/10.1016/j.commatsci.2008.01.003>
- Deng, D., Murakawa, H., Liang, W., 2007. Numerical simulation of welding distortion in large structures. *Comput. Methods Appl. Mech. Eng.* <https://doi.org/10.1016/j.cma.2007.05.023>
- Deng, D., Murakawa, H., Ueda, Y., 2004. Theoretical prediction of welding distortion considering positioning and gap between parts. *Int. J. Offshore Polar Eng.*
- Jung, G., 2004. Fundamental Studies on the Relationship Between Plastic Strains and Angular Distortion in Fillet Welded T-Joints. <https://doi.org/10.1063/1.1766693>
- Kunihiko, Satoh, Terasaki, T., 1976. Effect of Welding Conditions on Residual Stresses Distributions in Welded Structures Materials. *J. JAPAN Weld. Soc.* <https://doi.org/10.2207/qjjws1943.45.150>
- Liang, W., Deng, D., 2018. Influences of heat input, welding sequence and external restraint on twisting distortion in an asymmetrical curved stiffened panel. *Adv. Eng. Softw.* <https://doi.org/10.1016/j.advengsoft.2017.11.002>
- Liang, W., Deng, D., Sone, S., Murakawa, H., 2005. Prediction of welding distortion by elastic finite element analysis using inherent deformation estimated through inverse analysis. *Weld. World.* <https://doi.org/10.1007/BF03266500>
- Luo, Y., Murakawa, H., Ueda, Y., 1997. Prediction of welding deformation and residual stress by elastic FEM based on inherent strain (Report I). *Trans. JWRI.*
- Ma, N., Huang, H., 2017. Efficient Simulation of Welding Distortion in Large Structures and Its Reduction by Jig Constraints. *J. Mater. Eng. Perform.* <https://doi.org/10.1007/s11665-017-3000-4>
- Ma, N., Huang, H., Murakawa, H., 2015. Effect of jig constraint position and pitch on welding deformation. *J. Mater. Process. Technol.* <https://doi.org/10.1016/j.jmatprotec.2015.02.022>
- Ma, N., Huang, H., Yin, X., Guo, N., 2016. Welding distortion and inherent deformation under temporary tacking and its released states. *Sci. Technol. Weld. Join.* <https://doi.org/10.1080/13621718.2015.1123443>
- Ma, N., Tateishi, J., Hiroi, S., Kunugi, A., Huang, H., 2017. Fast Prediction of Welding Distortion of

- Large Structures using Inherent Deformation Database and Comparison with Measurement. Q. J. JAPAN Weld. Soc. <https://doi.org/10.2207/qjws.35.137s>
- Ma, Ninshu, Wang, J., Okumoto, Y., 2016. Out-of-plane welding distortion prediction and mitigation in stiffened welded structures. *Int. J. Adv. Manuf. Technol.* <https://doi.org/10.1007/s00170-015-7810-y>
- Michaleris, P., Debiccari, A., 1997. Prediction of welding distortion. *Weld. J.* <https://doi.org/10.1016/j.jmatprotec.2007.10.009>
- Murakawa, H., Deng, D., Ma, N., Wang, J., 2012. Applications of inherent strain and interface element to simulation of welding deformation in thin plate structures. *Comput. Mater. Sci.* <https://doi.org/10.1016/j.commatsci.2011.06.040>
- PEMA, 2016. Pema welding automation company, <https://pemamek.com/case/seaspans-vancouver-shipyard-selects-pema-welding-automation-solutions/>
- Shadkam, S., Ranjbarnodeh, E., Iranmanesh, M., 2018. Effect of sequence and stiffener shape on welding distortion of stiffened panel. *J. Constr. Steel Res.* <https://doi.org/10.1016/j.jcsr.2018.07.010>
- SMITH, C., Davidson, P., CHAPMAN, J., 1988. STRENGTH AND STIFFNESS OF SHIPS' PLATING UNDER IN-PLANE COMPRESSION AND TENSION. *R. Inst. Nav. Archit. Trans.*
- Ueda, Y., Murakawa, H., Ma, N., 2012. Welding Deformation and Residual Stress Prevention, *Welding Deformation and Residual Stress Prevention.* <https://doi.org/10.1016/C2011-0-06199-9>
- Ueda, Y., Yuan, M.G., 2008. Prediction of Residual Stresses in Butt Welded Plates Using Inherent Strains. *J. Eng. Mater. Technol.* <https://doi.org/10.1115/1.2904240>
- Ueda, Y., Yuan, M.G., Mochizuki, M., Umezawa, S., Enomoto, K., 1993. Experimental verification of a method for prediction of welding residual stresses in T joints using inherent strains 4th report: Method for prediction using source of residual stress. *Weld. Int.* <https://doi.org/10.1080/09507119309548506>
- Wang, J., Rashed, S., Murakawa, H., Luo, Y., 2013. Numerical prediction and mitigation of out-of-plane welding distortion in ship panel structure by elastic FE analysis. *Mar. Struct.* <https://doi.org/10.1016/j.marstruc.2013.09.003>
- Wang, J., Yuan, H., Ma, N., Murakawa, H., 2016. Recent research on welding distortion prediction in thin plate fabrication by means of elastic FE computation. *Mar. Struct.* <https://doi.org/10.1016/j.marstruc.2016.02.004>
- Wang, J., Zhao, H., Zou, J., Zhou, H., Wu, Z., Du, S., 2017. Welding distortion prediction with elastic

FE analysis and mitigation practice in fabrication of cantilever beam component of jack-up drilling rig. Ocean Eng. <https://doi.org/10.1016/j.oceaneng.2016.11.059>

White, J.D., Leggatt, R.H., Dwight, J.B., 1980. WELD SHRINKAGE PREDICTION. Weld. Met. Fabr.

Japan Shipbuilding Research Association (2000), 'Japan Shipbuilding Research Association No. 237 Research Subcommittee (SR237): Research on Advanced Machine Accuracy Management Technology (Total Joint Report)', Japan Shipbuilding Research Association.